Western Australian School of Mines: Minerals, Energy, and Chemical Engineering

Fuels and Energy Technology Institute

Biochar Gasification Mechanism

Muhammad Asif Akhtar

This thesis is presented for the Degree of
Doctor of Philosophy
of
Curtin University

February 2020

Declaration

To the best of my knowledge and belief this thesis contains no material previously published by any other person except where due acknowledgment has been made.

This thesis contains no material which has been accepted for the award of any other degree or diploma in any university.

Signature: -- [redacted] -- (Muhammad Asif Akhtar)

Date: 19/02/2020

Copyright

I warrant that I have obtained, where necessary, permission from the copyright owners to use any third-party copyright material reproduced in the thesis (e.g. questionnaires, artwork, unpublished letters), or to use any of my own published work (e.g. journal articles) in which the copyright is held by another party (e.g. publisher, co-author).

Signature: --  ------ (Muhammad Asif Akhtar)

Date: 19/02/2020

Dedication

To My Beloved Mother

To My Beloved Father (Late)

To My Beloved Siblings

And

To My Beloved Aunty

who passed away during my Ph.D.

Abstract

Gasification-based technologies are at the core of many low emission technologies for the utilisation of low-rank fuels including biomass. The overall conversion rate of gasification depends on the heterogeneous biochar-gas reactions, which are the slowest reactions in the gasification process. The biochar-O_2 and biochar-H_2O reactions are fundamental reactions during the gasification process. The active sites in the biochar are formed and consumed continuously as gasification progresses in O_2 and H_2O and can give rise to the kinetic compensation effects.

This study aims to gain insights into the reaction mechanisms from the kinetic compensation effects ($lnA_{app} = mE_{app} + c$) of the gasification of biochar using 0.4% O_2, 15% H_2O, 2% H_2O, 0.4% O_2 + 15% H_2O and 0.4% O_2 + 2% H_2O (others is Ar). The biochar was produced in situ in a fluidised-bed reactor from the Australian mallee wood in two particle size ranges of 0.80-1.0 mm and 2.0-3.3 mm. The overall biochar gasification rate and the product formation rates of CO, CO_2, and H_2 were calculated by continuously monitoring the product gas stream with a quadrupole mass spectrometer. The kinetic parameters i.e. the apparent activation energy (E_{app}) and the apparent pre-exponential factors (lnA_{app}) of char gasification and the formation of CO, CO_2 and H_2 were calculated by the Arrhenius plots. The char structural properties were investigated using FT-Raman and X-ray photoelectron spectroscopies (XPS).

The phenomenon of the kinetic compensation effects was observed during the char gasification and for the formation of the products. The kinetic compensation effects together with structural properties of char provided further insights into the char gasification mechanisms. The results from this study contribute to a better understanding of the biochar gasification mechanisms and to the development of green bioenergy technologies.

Keywords: Kinetic compensation effect; Biochar gasification; Carbon release kinetics; Carbon active sites; Mallee wood.

Table of Contents

List of Figures

List of Tables

Nomenclature

Abbreviations

AAEM	Alkali and alkaline earth metallic
QMS	Quadrupole mass spectrometer
Ar	Argon
wt.	Weight
MFC	Mass flow controller
UHP	Ultra-high purity
KCE	Kinetic compensation effect
XPS	X-ray photoelectron spectroscopy
R.S.F	Relative sensitivity factor
IR	Infrared absorption spectroscopy
FT-IR	Fourier-transform infrared spectroscopy
FC	Fixed carbon
VM	Volatile matter
M	Moisture
daf	Dry and ash-free
eV	Electronvolt
WP	Weisz-Prater
TPD	Temperature-programmed desorption

NMR	Nuclear magnetic resonance spectroscopy

Symbols

m/z	Ratio of mass (amu) to charge number
U_{mf}	Velocity of minimum fluidisation (m/s)
U	Superficial gas velocity (m/s)
N_{Re}	Reynold number
d_p	Average diameter of the zircon (bed) particles (m)
N_{Ga}	Galileo number
g	Acceleration due to gravity (9.8 m^2/s)
Q	Volumetric flow rate of the fluidising gas (m^3/s)
T_{amb}	Ambient temperature (K)
P	Atmospheric pressure (bar)
R	Gas constant (0.0831 bar L $mol^{-1}K^{-1}$)
r_{CO}	Rate of CO formation (s^{-1})
r_{CO_2}	Rate of CO_2 formation (s^{-1})
r_{H_2}	Rate of H_2 formation (s^{-1})
r_C	Rate of char consumption (s^{-1})
W_i	Moles of species '*i*' remaining (mol)
x	Conversion
y	Gas-phase mole fraction

A_{app}	Apparent pre-exponential factor (s^{-1})
E_{app}	Apparent activation energy (kJ mol^{-1})
E_T	True activation energy (kJ mol^{-1})
C_{Ab}	Concentration of a gasifying agent (A) in the bulk gas-phase (mol/m^3)
C_{AS}	Concentration of a gasifying agent (A) on the char external surface (mol/m^3)
C_A	Concentration of a gasifying agent (A) in the interior pores of char (mol/m^3)
ΔH_i°	Enthalpy of activation in the standard state of species *'i'* (kJ mol^{-1})
ΔS_i°	Entropy of activation in the standard state of species *'i'* (kJ/mol. K)
ΔH_i	Enthalpy changes of species *'i'* (kJ mol^{-1})
ΔS_i	Entropy changes of species *'i'* (kJ/mol. K)
k_C	Mass-transfer coefficient (mol/m^2. s)
KBr	Potassium bromide

Greek Letters

η	Effectiveness factor
$\emptyset_1$	Thiele modulus
μ_f	Viscosity of the fluidising gas mixture (kg/m.s)

ρ_f	Density of the fluidising gas mixture (kg/m^3)
ρ_s	Density of the solid (bed) material (kg/m^3)
δ	Boundary layer thickness (m)

List of Publications included as part of the Thesis

- Akhtar M.A., Zhang S, Shao X, Dang H, Liu Y, Li T, et al. Kinetic compensation effects in the chemical reaction-controlled regime and mass transfer-controlled regime during the gasification of biochar in O_2.Fuel Process Technol 2018;181:25–32. **https://doi.org/10.1016/j.fuproc.2018.09.009**

- Akhtar M.A., Zhang S, Li C.-Z. Mechanistic insights into the kinetic compensation effects during the gasification of biochar in H_2O. Fuel 2019;255:115839. **https://doi.org/10.1016/j.fuel.2019.115839**

- Akhtar M.A., Li C.-Z. Mechanistic insights into the kinetic compensation effects during the gasification of biochar: Effects of the partial pressure of H_2O. Fuel 2020;263:116632. **https://doi.org/10.1016/j.fuel.2019.116632**

- Akhtar M.A., Li C.-Z. Some discussions into the reaction mechanisms from the kinetic compensation effects of the gasification of biochar in O_2, H_2O, and their mixtures (plan to submit in Fuel).

Conference/Symposium Presentations

- Muhammad Asif Akhtar, Shu Zhang, Chun-Zhu Li, Mechanistic insights into the kinetic compensation effects during the gasification of biochar in H_2O, The 6th International Symposium on Gasification and its Applications (ISGA-6), October 25-28, 2018 Chengdu, Sichuan Province, China.

- Akhtar M. Asif, Zhang Shu, Li Chun-Zhu, Mechanistic insights into the nature of carbon active sites during the gasification of biochar in O_2 and H_2O atmospheres, ACS Student Conference 2018, 6-7 December 2018, University of Sydney, Australia.

- M. A. Akhtar., S. Zhang, C.-Z. Li. Probing the char gasification mechanisms through quantifying the changes in char structure and surface property: the importance of particle size, 5th Annual Symposium 2017, Fuels and Energy Technology Institute, Curtin University, Perth, Australia.

Acknowledgements

"*In the name of Allah, the Most Gracious, the Most Merciful. All the praises and thanks be to Allah, the Lord of all the Worlds".* (The Quran, 1:1-2)

I would like to acknowledge the University of Engineering and Technology (UET) Lahore, (Pakistan) and Curtin University (Australia) for providing financial support for my Ph.D. studies. I also acknowledge funding from the Australian Government through ARENA's Emerging Renewables Programs and the Australian Research Council DP180101788.

It has been a real privilege and an honour working with Prof. Chun-Zhu Li for my Ph.D. I thank him for his comprehensive and constructive feedback, guidance, and suggestions throughout the experimental and thesis write-up stage that has contributed to the success of this research. His superb insights, suggestions and keen observations have invaluably empowered me to see through the core issues in my research. I thank him for his unlimited efforts to resolve all the challenges I faced during my research.

I would also like to thank Prof. Shu Zhang for his suggestions and discussions on research methodology during the initial stage of my Ph.D. I also thank my friend and colleague Dr. Qasim Imtiaz for his insightful discussions on the kinetics. A sincere thanks also go to Mr. Nathan Nie (from Scitek Australia) for his technical support on the mass spectrometer in the initial stage of the experimentation.

A special thanks to Ms. Angelina Rossiter for providing her technical support for the consumables. A heartfelt thanks to Ms. Tasneem Dawood and Ms. Lana McQueen for providing their support on the administrative tasks. My special appreciation to Safer Community Team of Curtin University for facilitating me in after-hours escorts. I really appreciate the Safer Community Team for doing a great job.

I would also extend my sincere thanks to my friend and colleague Dr. H. M. Zaheer Aslam for looking after my scholarship and study leave matters at UET, Lahore, Pakistan.

Lastly, my deep gratitude to my family, special friends, and colleagues for their continuous encouragement, motivation, and moral support throughout my Ph.D. tenure.

Muhammad Asif Akhtar

1.0 Chapter

Introduction

1.1 Bioenergy as an alternate resource of energy

Energy is an essential component that affects the living standard and economic development of a country. The world population will reach around 9.2 billion people in 2040 [1] and this will result in a significant increase in the global energy demand. Oil supplies around 34% of the total world energy consumption followed by coal and natural gas [2], which shows that oil is the leading fuel of the world.

Despite the share of coal in primary energy supply and power generation is declining, it still supplies 28% of the total world energy consumption [2]. Whereas, the consumption of natural gas is increasing and the increase in 2018 was about 4.6%, which shows the switch from coal to natural gas [3]. Fossil fuels supply about 85% of the global energy demand [2]. All the energy-related activities based on fossil fuels are unsustainable environmentally and economically. The energy data for 2018 shows that the energy demand and carbon emissions both have been increasing rapidly over the past years [3]. This requires a paradigm shift from carbon-rich fossil fuels to renewable sources of energy to address environmental concerns as well as to gain energy independence for long-term sustainability.

Renewable energy is the fastest growing energy source with 4% growth only in 2018 and contributes over 25% of the global power output [4]. It is expected that renewables will provide almost 30% of power demand in 2023 [3]. Bioenergy is the largest renewable energy source, which accounts for around 9% of the global primary energy supply [3]. According to the World Energy Council [5], "Bioenergy includes traditional biomass (forestry and agricultural residues), modern biomass and biofuels. It represents the transformation of organic matter into a source of energy, whether it is collected from natural surroundings or specifically grown for the purpose".

The energy supply in Australia heavily relies on fossil fuels and about 85% of electricity production is from coal and natural gas [6]. The energy from renewable sources (hydro, solar and wind) has a share of only 15% in electricity generation [6]. Western Australia (WA) can develop large mallee biomass resources and around 30 million trees have been grown in the WA wheat belt to control dryland salinity since the early 1990s [7]. Mallee trees have small harvesting cycle with low production cost and if adopted, this wheat belt in WA has the potential to provide around 10 million

tonnes (on dry basis) of biomass annually [8]. The mallee tree belongs to lingocellulosic biomass and its use for bioenergy does not threaten the food supply. In fact, by helping to combat the dryland salinity, planting mallee trees help to improve the overall food production. Therefore, a huge opportunity is available to produce mallee-based bioenergy for long-term sustainability and economic development of WA.

1.2 Significance of gasification

Gasification is the thermochemical conversion of carbonaceous materials (either in liquid or solid form) at elevated temperature through their reactions with gasifying agents (O_2, H_2O or CO_2) into valuable synthesis gas. The gasification process produces a gas mixture with a higher hydrogen to carbon (H/C) ratio by adding hydrogen and stripping away carbon from the feedstock [9]. Low-grade fuels for instance coal, peat, lignite and biomass show huge potential for gasification due to their high reactivity [10]. The gasification-based technology is versatile in terms of feedstock flexibility and in terms of variety of the products formed [10,11]. The synthesis gas produced can be used for the production of a wide range of products. Figure 1-1 illustrates the overview of the gasification-based products [10].

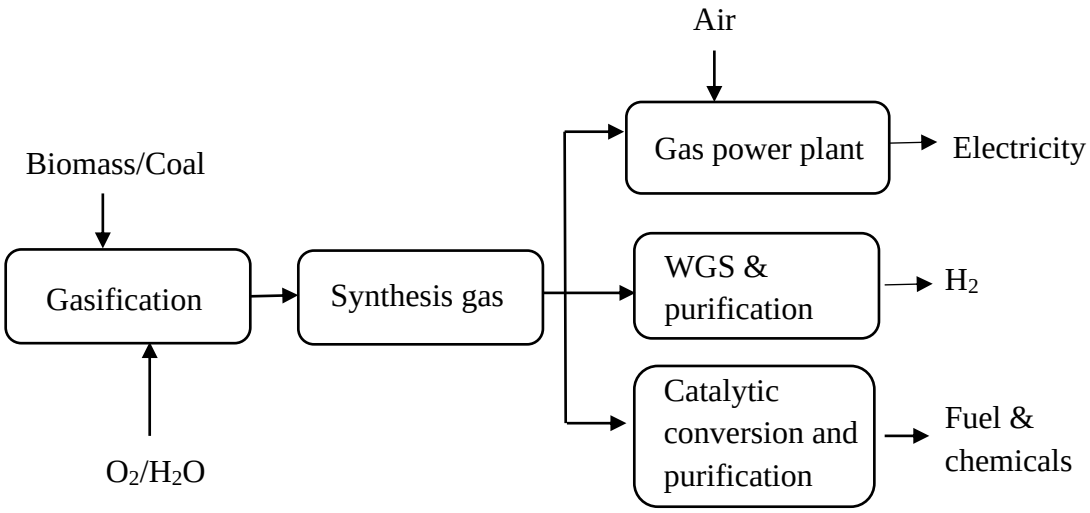

Figure 1-1 Overview of the gasification-based products.

The gasification consists of two major steps [10]. The first step is termed as pyrolysis or devolatilisation, which produces volatiles and char through the thermal decomposition of the solid fuel. The pyrolysis breaks down large molecules of the solid fuel thermally into gaseous, vapour and solid components [9]. The second step includes the reforming of volatiles and the gasification of solid residue (char). The pyrolysis and reforming of volatiles are much faster [10] than the gasification of char which is the slowest step and affects the gasification efficiency. The steps involved in gasification can be represented by Figure 1-2.

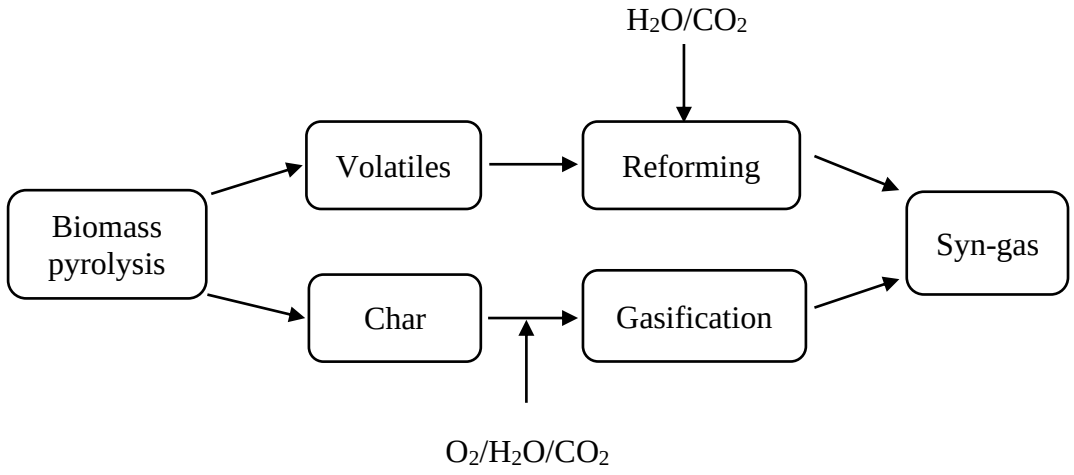

Figure 1-2 Steps involved in the gasification process.

Thermodynamically, low-rank fuels, e.g. brown coal and biomass, have the potential to be gasified at a lower temperature than the high-rank fuels [10]. This also suggests that low-rank fuels can better recuperate the thermal energy at low temperatures into chemical energy than the high-rank fuels. Low-rank fuels have alkali and alkaline earth metallic species (AAEM) dispersed even at the atomic scale [12]. Because of their catalytic effects, the reactivity of low-rank fuels is much higher than that of high-rank fuels. These AAEM species also have catalytic effects during the gasification of char [13–16], which is a promising aspect of low-rank fuel gasification. Some of the common reactions [12] involved during the char gasification are enlisted below:

Char-steam reactions:

$$C(s) + H_2O(g) \rightleftharpoons CO(g) + H_2(g) \qquad \text{(R 1-1)}$$

$C(s) + 2H_2O(g) \rightleftharpoons CO_2(g) + 2H_2(g)$ (R 1-2)

Oxidation:

$C(s) + 0.5O_2(g) \longrightarrow CO(g)$ (R 1-3)

$C(s) + O_2(g) \longrightarrow CO_2(g)$ (R 1-4)

$CO(g) + 0.5O_2(g) \longrightarrow CO_2(g)$ (R 1-5)

Boudouard reaction:

$C(s) + CO_2(g) \rightleftharpoons 2CO(g)$ (R 1-6)

Hydrogasification:

$C(s) + 2H_2(g) \rightleftharpoons CH_4(g)$ (R 1-7)

Methanation reactions:

$CO(g) + 3H_2(g) \longrightarrow CH_4(g) + H_2O(g)$ (R 1-8)

$CO_2(g) + 4H_2(g) \longrightarrow CH_4(g) + 2H_2O(g)$ (R 1-9)

Water-gas shift reaction

$CO(g) + H_2O(g) \rightleftharpoons CO_2(g) + H_2(g)$ (R 1-10)

Steam-Reforming reaction

$CH_4(g) + H_2O(g) \rightleftharpoons CO(g) + 3H_2(g)$ (R 1-11)

1.3 Mass-transfer effects during char gasification

The char-gas reactions are heterogeneous reactions and their kinetics can be controlled by one or more of the following steps [17,18]:

- Mass transfer of the gasifying agent from the bulk gas-phase through the boundary layer to the external surface of the char particle

- Diffusion of the gasifying agent from the particle external surface to the active sites of the internal char surface
- Adsorption of the gasifying agent on the char surface
- Reaction on the char surface
- Desorption of the products from the surface of char
- Diffusion of the products from the internal char surface to the external surface of the char particle
- Mass transfer of the products from the external char surface to the bulk gas-phase

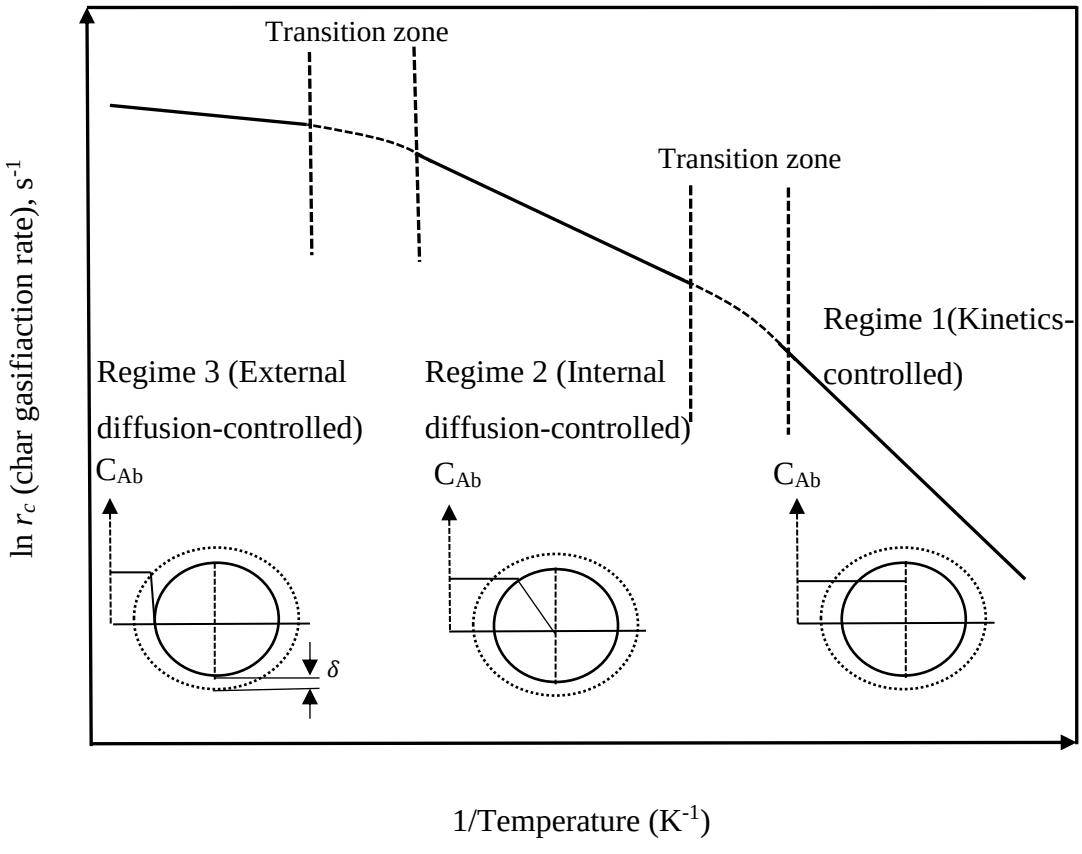

Figure 1-3 Temperature regimes during the biochar-gas reactions

The overall rate of the char gasification is equivalent to the rate of the slowest step during gasification. The dependency of the char-gas reactions on temperature can be well understood by Figure 1-3. Figure 1-3 also shows how the concentration of a gasifying agent A (C_A) changes with temperature and can be divided into three regimes:

- Regime 1 (Kinetics-controlled regime)
- Regime 2 (Internal diffusion-controlled regime)
- Regime 3 (External diffusion-controlled regime)

In regime 1, the rate of char gasification is controlled by the intrinsic chemical kinetics of the char-gas reactions and is, therefore, independent of the gas velocity inside the reactor and the particle diameter. The observed kinetic parameters i.e. the apparent activation energy and the apparent pre-exponential factor represent the intrinsic properties of the char and the nature of the reaction. As the diameter of the particle decreases, Thiele modulus ($\emptyset_1$) also decreases and the effectiveness factor (η) is increased. The effectiveness factor is a measure of how far the gasifying agent is diffusing into the char particle. The effectiveness factor is nearly unity i.e. $\eta \approx 1$ in regime 1. The concentration of the gasifying medium (C_A) from the bulk gas-phase to the interior pores of the char particle is uniform or the concentration gradient is so small that a uniform concentration (C_A) can be assumed. The observed activation energy (E_{app}) is equal to the true activation energy (E_T) of the char-gas reaction.

In regime 2, the concentration of the gasifying agent from the char external surface (C_{AS}) to the interior pores of the char reduces so that C_A is less than C_{AS} where C_A is the concentration of the reactant gas in the interior pores. Under such circumstances, the gasification takes place near the external surface of the char and the active sites inside the deep char matrix become starved to reactant gas and stay unreacted. Weisz-Prater (WP) criterion [18] is used to determine whether internal mass-transfer effects are limiting the reaction or not. WP criterion can be represented as:

$$C_{WP} = \frac{\text{Actual reaction rate}}{\text{A diffusional rate}}$$

or

$$C_{WP} = \eta \emptyset_1^2 \qquad (Eq. 1-1)$$

For the larger char particles, it takes longer for the gas to diffuse into the interior pores as compared to the reaction time and, consequently, the reaction is limited by the gas diffusion. Alternatively, when the temperature is high enough, the reaction rates are also high so that the reactant gas does not have enough time to diffuse inside the char pores and reaction can still become diffusion-limited. Under both conditions $C_{WP} \gg 1$. The observed activation energy (E_{app}) in this regime is related to the true activation energy as:

$$E_{app} = \frac{1}{2} E_T \qquad (Eq. 1-2)$$

In regime 3 (high-temperature regime), the transport of the gasifying agent from the bulk gas-phase through the boundary layer of thickness i.e. δ to the external surface of the char particle becomes the slowest step (external diffusion). The rate in this regime can be written as:

$$\text{Rate} = k_C(C_{Ab} - C_{AS}) \qquad (Eq. 1-3)$$

where k_C represents the mass-transfer coefficient, C_{Ab} is the concentration of any gasifying agent in the bulk gas-phase and C_{AS} is the concentration on the char external surface. k_C depends on the hydrodynamic conditions i.e. gas-phase velocity and the particle diameter. In this regime, the concentration of the gasifying agent reduces on the char surface such that $C_{AS} < C_{Ab}$. The lower gas-phase velocities and bigger particle sizes increase the boundary layer thickness surrounding the char particle and, consequently, the external diffusion limitations. The activation energies are quite low and the effectiveness factor i.e. η is $\ll 1$ in this regime.

It is very important to understand the role of these mass-transfer limitations and their effects on char-gas reactions. Understanding of these mass-transfer effects not only aids to determine the true kinetics-controlled regime but also provides a basis for predicting a true mechanism of the char gasification.

1.4 Kinetic compensation effects (KCEs)

KCE is the linear relationship between the kinetic parameters of the Arrhenius equation i.e. the apparent activation energy (E_{app}) and the apparent pre-exponential factors (A_{app}). For the KCE, the change in one Arrhenius parameter is offset by a simultaneous (compensatory) change in the other parameter. The linear relationships between enthalpy changes (ΔH_i) and entropy changes (ΔS_i) or between enthalpy of activation (ΔH_i°) and entropy of activation (ΔS_i°) in their standard states are also named as the compensation effects or enthalpy-entropy compensation. These can be expressed [19–23] as:

$$lnA_{app} = mE_{app} + c \qquad (\text{Eq. } 1-4)$$

$$\Delta H_i = m\Delta S_i + c \qquad (\text{Eq. } 1-5)$$

$$\Delta H_i^\circ = m\Delta S_i^\circ + c \qquad (\text{Eq. } 1-6)$$

where 'm' and 'c' are constants.

The linear relationship between lnA_{app} and E_{app} was initially reported [24] by Constable in 1925 during the hydrogenation of ethanol using copper films at 500-673 K. Cremer also investigated [25] the hydrogenation of ethanol using different compositions of catalyst at constant temperature and confirmed Eq. 1-4. Later in 1949, this was known as Constable-Cremer relation [26] first and then as the "Compensation effect" [27] which is now commonly used.

Different relationships [23] are possible between E_{app} and A_{app}. E_{app} and A_{app} can increase or decrease linearly in the same direction and this type of behavior is the normal compensation effect. E_{app} and A_{app} can also vary in the opposite direction and is regarded as an anti or negative compensation effect. There is also a possibility that either E_{app} is constant with increasing A_{app} or A_{app} is constant with changing E_{app}. Under both conditions, no compensation effect is observed.

The observation of the KCE has been quite common during the heterogeneous catalytic reactions when either the catalyst is modified or the reactants are changed [28–30].

There are many other instances reported which follow Eq. 1-4. For example, the KCE was reported for the reactions (homogeneous), which take place in solutions [31]. Similarly, food chemistry [32], the decomposition of $CaCO_3$ [33], ionic hydration [34], reactions on electrodes [35], liquid or gas chromatography [36,37], hydrogenolysis of alkanes [38], Langmuir adsorption [39], the oxidation of metals [40,41] and crystal melting [42] etc. all follow Eq. 1-4. This shows that the compensation behaviour is not limited to heterogeneous reactions only and it has been observed in many other processes. This also suggests that the KCE does not depend only on the catalyst and the reactant but there is some other factor, which affects the activation energy and the pre-exponential factor.

The various theories of compensation behaviour have been proposed for heterogeneous catalytic reactions. One group of authors [24,43,44] suggested that the catalyst surface consists of groups of energetically different sites requiring different activation energy on each group of sites. The overall rate constant can be written as:

$$k = \sum A_i \exp\left(-\frac{E_i}{RT}\right) \qquad (\text{Eq. } 1-7)$$

This composite reaction, which does not strictly follow the Arrhenius equation could cause the KCE.

The first explanation [24] of the KCE came from Constable, who explained the decrease in E_{exp} and A_{exp} with increasing temperature by assuming Gaussian distribution of active sites and the proportionality constant in the $lnA_{exp} - E_{exp}$ plot was named as the distribution constant. Cremer and Sosnowsky [45,21,22] also discussed the concept of active-site distribution for the KCE.

Other authors suggested [46,21,22] that compensation during heterogeneous catalytic reactions could be due to the enthalpy-entropy compensation during chemisorption. The enthalpy (ΔH_i) and entropy (ΔS_i) change during chemisorption of a molecule to a free site on a solid surface, can be expressed [46] in the form of a linear correlation as:

$$\Delta H_i = \frac{\Delta S_i}{R} + b \qquad (\text{Eq. } 1-8)$$

In these reactions, ΔH_i and ΔS_i terms increase the activation energy and the frequency factor of the reaction respectively and the compensation behaviour can be expected.

The simulation studies [47,48] have also given some evidence about the interaction of adsorbate molecules and suggested that such interactions can change the surface potential-energy of adsorbate-substrate and, therefore, alter the activation energy and pre-exponential factors in the rate constant. The simulation results also confirmed that the surface coverage could cause the KCE. Ertl [21]correlated the distribution of the active site with the surface coverage during the decomposition of N_2O and reported that E_{app} increased with increasing O_2 coverage.

Various other explanations [19,21-23] of the kinetic compensation behaviour include the dependency of the active-sites concentration on temperature, catalyst doping, surface diploes, lateral interactions of the adsorbed species and the changes in the state of the transition complex from an immobile state to mobile state as a function of temperature, etc.

1.5 Thesis objectives

The char gasification reactions are critical to understand the gasification process. During the gasification process, the rate of char gasification is much slower than the rate of pyrolysis of biomass and plays a vital role in the design of a gasifier. The char-O_2, char-CO_2 and char-H_2O reactions are considered fundamental reactions during the gasification process.

Many mechanistic studies indicate that the char properties change [49–58] as the gasification is progressed in O_2 and H_2O. The char conversion can significantly affect the kinetics of char gasification. Similarly, the temperature and particle size are also important variables, which can significantly affect the extent of diffusion limitations, and, consequently, the gasification behaviour. The intrinsic kinetics is required in terms of the products (CO, CO_2, CH_4, and H_2) formed to understand the gasification reaction mechanisms and for the designing of a gasifier.

The KCEs can be quite important to determine the reaction mechanisms, particularly those of the heterogeneous reactions. As mentioned in section 1.3, there are several steps either separately or in combination, which can affect the activation energy and pre-exponential factors and can lead to false kinetics and misinterpretation. Therefore, it is very important to establish the true kinetics-controlled regime before predicting the reaction mechanism. Once the true kinetics-controlled regime is established then the phenomenon of the KCEs can provide useful insights into the reaction mechanism. The activation energy in the kinetics-controlled regime shows the intrinsic properties of the reactants. Whereas, the pre-exponential factor indicates the active sites population. The rate constant, in turn, is the product of the intrinsic properties of the reactants and the active sites population.

In the true kinetics-controlled regime, the '*m*' and '*c*' can be the characteristic and distinct values which indicate the reaction pathways of the given char-gas heterogeneous reaction or alternatively changing values of '*m*' and '*c*' indicate the change in the controlling mechanism of the reaction. Therefore, variations in the '*m*' and '*c*' values or in other words the factors affecting the '*m*' and '*c*' values can be very helpful in understanding the mechanism of any char-gas reaction.

Our previous studies [59,60] reported and explained the KCE for the char-O_2 reaction at low temperature, wherein, the char was produced from the brown coal. It is important to understand how the presence of the mass-transfer effects would affect the kinetics of the char-O_2 reaction and the nature/extent of the KCEs. The extents of the KCEs are indicated by the kinetic parameters including the activation energy and the pre-exponential factor as well as the '*m*' and '*c*' values. The mass-transfer effects become prominent when the reaction temperature is increased for any given particle size or when the particle size is increased in any given temperature range. Therefore, there is a need for a comprehensive study for the char-O_2 reaction over a broad range of temperature conditions as well as including different particle sizes to investigate the extent of the KCEs.

There is still no agreement in the literature on the formation of CO_2 during the char-H_2O reaction. Some studies [61–63] consider that water-gas-shift reaction mainly dominates in the formation of CO_2 while other studies believe [64–66] that CO and

CO_2 both are primary products of the char-H_2O reaction. The temperature also affects the equilibrium of the water-gas-shift reaction as well as the extent of diffusion limitations. It is fundamentally important to understand the formation kinetics of CO, CO_2 and H_2 as well as the char consumption kinetics to gain insights into the formation mechanisms of CO, CO_2 and H_2 during the char-H_2O reaction. It is still unclear how the KCEs of char consumption as well as the formation of CO, CO_2 and H_2 will change during the char-H_2O reaction, which needs to be explored.

In addition to this, the partial pressure of gasifying agent particularly H_2O is very important because steam gasification produces synthesis gas (CO + H_2) mixture. The quality of synthesis gas is also an important consideration during the char-H_2O reaction. The change in the partial pressure of H_2O would also change the local gas concentration around the char particle and can affect the rates of active site formation and consumption as well as the formation rates of CO, CO_2, and H_2, which is a significant aspect to investigate during the char-H_2O reaction. Further, it is still unknown how the KCEs of char gasification as well as the formation of CO, CO_2 and H_2 change when the partial pressure of H_2O is changed.

The higher gasification rates are desired for the higher overall efficiency during the gasification. The char-O_2 reaction is a necessary reaction during gasification, which oxidises carbon through exothermic reactions and supplies energy to drive the endothermic char-H_2O reaction, which produces valuable synthesis gas. It is very important to understand how the gasification proceeds in the mixture of O_2 and H_2O. It is possible that O_2 and H_2O compete for the same active sites and can inhibit each other or char-O_2 and char-H_2O reactions take place in parallel. There is also a likelihood that char gasification has synergistic effects in the mixture of O_2 and H_2O. It would also be important to know how the KCEs of char gasification and the formation of CO, CO_2 and H_2 change during steam gasification in the presence of oxidising agent i.e. O_2. The partial pressure of H_2O can also play a significant role during the biochar gasification in O_2 and H_2O mixture. Therefore, the specific objectives of the thesis can be outlined as follows:

- The thesis will focus on the char-O_2 reaction and investigate the behaviour of the kinetic compensation effects in the different temperature regimes using different particle sizes i.e. 0.80-1.0 mm and 2.0-3.3 mm.

- The mechanism of the char-H_2O reaction will be investigated by considering the kinetics of CO, CO_2, H_2 formation and char consumption as well as the kinetic compensation effects for 0.80-1.0 mm and 2.0-3.3 mm particle sizes.

- The mechanism of the char-H_2O reaction will be examined under different partial pressures of H_2O with the aid of kinetic compensation effects.

- The thesis will also explore the char-O_2 and char-H_2O reaction mechanisms in the mixture of O_2 and H_2O.

1.6 Thesis outline

The thesis consists of seven chapters. The overview of each chapter is mentioned as below:

Chapter 1 is the introduction of the thesis. The significance of gasification and the role of mass-transport during heterogeneous reactions has been discussed. The important phenomenon of the kinetic compensation effect and its various proposed explanations are briefly mentioned followed by the thesis objectives.

Chapter 2 begins with the sample preparation procedure, feed analysis, design of experiment and the description of the experimental setup. This is followed by the calculation methods used to determine the rates. The different characterisation methods/techniques including the FT-Raman and XPS spectroscopies, which have been employed to characterise the char structures and surface properties are also outlined.

Chapter 3 evaluates the kinetic compensation effects during the char-O_2 reaction in 0.4% O_2-Ar in the kinetics-controlled, mixed and the diffusion-controlled regimes. The effects of particle size and char conversion on the kinetic compensation effects are also discussed in these regimes.

Chapter 4 explores the mechanism of char gasification in 15% H_2O-Ar and discusses the kinetic compensation effects of the product components (CO, CO_2, and H_2) as well as char gasification in the kinetics-controlled and mixed regimes for 0.80-1.0 mm and 2.0-3.3 mm particle sizes.

After the char gasification in 15% H_2O-Ar, the mechanism of char-H_2O reaction in 15% H_2O-Ar and 2% H_2O-Ar has been investigated in Chapter 5. This chapter also discusses the formation of CO, CO_2, and H_2 in 15% H_2O-Ar and 2% H_2O-Ar.

Chapter 6 is devoted to biochar gasification in 0.4% O_2-Ar, 15% H_2O-Ar, 0.4% O_2 +15% H_2O-Ar and 0.4% O_2 + 2% H_2O-Ar and presents how the reaction pathways and the kinetic compensation effects vary in these gasification atmospheres.

Lastly, chapter 7 summarises/concludes the thesis and outlines recommendations for future research work.

1.7 References

[1] BP Energy Outlook 2018. doi:10.1088/1757-899X/342/1/012091.

[2] BP Statistical Review of World Energy. 67th edition, June 2018:1–56.

[3] International Energy Agency. Global Energy & CO_2 Status Report. 2018:1–15.

[4] International Energy Agency. Renewables 2018. doi:10.1787/re_mar-2018-en.

[5] World Energy Resources report, World Energy Council 2016. https://www.worldenergy.org

[6] Department of the Environment and Energy, Australian Government 2019. https://www.energy.gov.au/government-priorities/energy-supply (last accessed on 24/09/2019).

[7] Bartle J, Cooper D, Olsen G, Carslake J. Acacia species as large-scale crop plants in the Western Australian wheatbelt. Conserv Sci West Aust 2002;4:96–108.

[8] Wu H, Fu Q, Giles R, Bartle J. Production of mallee biomass in Western Australia: Energy balance analysis. Energy and Fuels 2008;22:190–8. doi:10.1021/ef7002969.

[9] Basu P. Biomass Gasification and Pyrolysis. Elsevier; 2010. doi:10.1016/C2009-0-20099-7.

[10] Li C.-Z. Importance of volatile-char interactions during the pyrolysis and gasification of low-rank fuels - A review. Fuel 2013;112:609–23. doi:10.1016/j.fuel.2013.01.031.

[11] Li C.-Z. Special issue - Gasification: A route to clean energy. Process Saf Environ Prot 2006;84:407–8. doi:10.1205/psep.ed.0606.

[12] Li C.-Z. Advances in the science of Victorian Brown Coal. 2004. doi:10.1016/B978-0-08-044269-3.X5000-6.

[13] Takarada T, Tamai Y, Tomita A. Reactivities of 34 coals under steam gasification. Fuel 1985;64:1438–42. doi:10.1016/0016-2361(85)90347-3.

[14] Miura K, Hashimoto K, Silveston PL. Factors affecting the reactivity of coal chars during gasification, and indices representing reactivity. Fuel 1989;68:1461–75. doi:10.1016/0016-2361(89)90046-X.

[15] Kannan MP, Richards GN. Gasification of biomass chars in carbon dioxide: dependence of gasification rate on the indigenous metal content. Fuel 1990;69:747–53. doi:10.1016/0016-2361(90)90041-N.

[16] Hashimoto K, Miura K, Ueda T. Correlation of gasification rates of various coals measured by a rapid heating method in a steam atmosphere at relatively low temperatures. Fuel 1986;65:1516–23. doi:10.1016/0016-2361(86)90327-3.

[17] Levenspiel O. Chemical Reaction Engineering, 3rd Edition. 1999. doi:10.1016/0009-2509(64)85017-X.

[18] Fogler H.S. Elements of Chemical Reaction Engineering. 4th Edition 2006. Prentice Hall.

[19] Liu L, Guo QX. Isokinetic relationship, isoequilibrium relationship, and enthalpy-entropy compensation. Chem Rev 2001;101:673–95. doi:10.1021/cr990416z.

[20] Koga N. A review of the mutual dependence of Arrhenius parameters evaluated by the thermoanalytical study of solid-state reactions: The kinetic compensation effect. Thermochim Acta 1994;244:1–20. doi:10.1016/0040-6031(94)80202-5.

[21] Bond GC, Keane MA, Kral H, Lercher JA. Compensation phenomena in heterogeneous catalysis: General principles and a possible explanation. Catal Rev 2000;42:323–83. doi:10.1081/CR-100100264.

[22] Bligaard T, Honkala K, Logadottir A, Norskov JK, Dahl S, Jacobsen CJH. On the Compensation Effect in Heterogeneous Catalysis. J Phys Chem B 2003;107:9325–31. doi:10.1021/jp034447g.

[23] G.C. Bond. Catalysis by Metals, Academic Press, London and New York 1962.

[24] Constable F.H., The mechanism of cataystic decomposition, Proc.Roy.Soc. London, 1925;108:355.

[25] Cremer E, Z. About the catalytic behaviour of rare earth oxides, Phys. Chem 1929;144:231.

[26] Patat. F, Z. On the question of compensation effect in catalytic reactions, Elektrochem 1949;53:216.

[27] Cremer. E, Z. For the absolute determination of the speed of heterogeneous reactions, Elektrochem 1949;53:269.

[28] Shufen Li and Yuanlin Cheng. Catalytic gasification of gas-coal char in CO_2. Fuel 1995;74:456–8.

[29] Kwon TW, Kim JR, Kim SD, Park WH. Catalytic steam gasification of lignite char. Fuel 1989;68:416–21. doi:10.1016/0016-2361(89)90261-5.

[30] Dhupe AP, Gokarn AN, Doraiswamy LK. Investigations into the compensation effect at catalytic gasification of active charcoal by carbon dioxide. Fuel 1991;70:839–44. doi:10.1016/0016-2361(91)90192-D.

[31] R. A. Fairdough, C. N. Hinshelwood J. The functional relation between the constants of the Arrhenius equation. Solvent effects in the formation of quaternary ammonium salts, Chem. Soc 1937;538:1573.

[32] Borea PA, Varani K, Gessi S, Gilli P, Dalpiaz A. Receptor binding thermodynamics as a tool for linking drug efficacy and affinity. Farmaco 1998;53:249–54. doi:10.1016/S0014-827X(98)00017-2.

[33] J. Zsako, H. E. Arz, J . Kinetic analysis of thermogravimetric data: VII. Thermal decomposition of calcium carbonate, Therm. Anal 1974;6:651.

[34] Schmid R, Miah AM, Sapunov VN. A new table of the thermodynamic quantities of ionic hydration: Values and some applications (enthalpy-entropy

compensation and Born radii). Phys Chem 2000;2:97–102. doi:10.1039/a907160a.

[35] Appleby AJ. Electrocatalysis and Fuel Cells. Catal Rev 1971;4:221–44. doi:10.1080/01614947108075490.

[36] Morin N, Guillaume YC, Peyrin E, Rouland JC. Retention mechanism study of imidazole derivatives on a β-cyclodextrin-bonded stationary phase. Thermal Analysis Contributions. Anal Chem 1998;70:2819–26. doi:10.1021/ac980194p.

[37] Zhou L-M, Nie M-Y, Wang Q-H, Zhu D-Q, Shen H-Q. Enthalpy-entropy compensation effect in gas chromatographic enantiomeric separation. Chinese J Chem 2010;17:363–76. doi:10.1002/cjoc.19990170409.

[38] Properties VIC, Bond GC. Characterization of the standard platinum/silica catalyst Europt- 1 1988;41:313–35.

[39] Sugihara G, Shigematsu DS, Nagadome S, Lee S, Sasaki Y, Igimi H. Thermodynamic study on the Langmuir adsorption of various bile salts including taurine and glycine conjugates onto graphite in water. Langmuir 2000;16:1825–33. doi:10.1021/la990358c.

[40] Ignacio MG. Molecular Composition , Solid state structure and properties of industrial waxes and peptide inclusion materials by 2017.

[41] Saleh JM, Matloob MH. Oxidation of titanium, tantalum, and niobium films by oxygen and nitrous oxide. J Phys Chem 1974;78:2486–9. doi:10.1021/j100617a014.

[42] D. Mondieig, P. Espeau, L. Robles, Y. Haget, H. A. J. Oonk, M. A. CuevasDiarte, J. Chem. Soc. Faraday Trans 1997;93:3343.

[43] Bond GC, Webb G, Wells PB, Winterbottom JM. Patterns of behavior in catalysis by metals. J Catal 1962;1:74–84. doi:10.1016/0021-9517(62)90011-8.

[44] K. J. Laidler, “Catalysis” (P. H. Emmett, ed.) 1954; 1:224. Reinhold, New York.

[45] Cremer E. The compensation effect in heterogeneous catalysis. Adv Catal 1955;75-91.

[46] D. H. Everett. The thermodynamics of adsorption. Part III. Analysis and discussion of experimental data, Trans. Faraday Soc 1950;46:957.

[47] Fichthorn KA, Balan PG. Non-Arrhenius behavior in the initial rate of a catalytic-surface reaction: Theory and Monte Carlo simulation. J Chem Phys 1994;101:10028–37. doi:10.1063/1.467991.

[48] Kang HC, Jachimowski TA, Weinberg WH. Role of local configurations in a Langmuir-Hinshelwood surface reaction: Kinetics and compensation. J Chem Phys 1990;93:1418–29. doi:10.1063/1.459151.

[49] Zhang S, Min Z, Tay HL, Wang Y, Dong L, Li C.-Z. Changes in char structure during the gasification of mallee wood: Effects of particle size and steam supply. Energy and Fuels 2012;26:193–8. doi:10.1021/ef2011589.

[50] Zhang S, Hayashi JI, Li C.-Z. Volatilisation and catalytic effects of alkali and alkaline earth metallic species during the pyrolysis and gasification of Victorian brown coal. Part IX. Effects of volatile-char interactions on char-H_2O and char-O_2 reactivities. Fuel 2011;90:1655–61. doi:10.1016/j.fuel.2010.11.008.

[51] Tay H-L, Kajitani S, Wang S, Li C.-Z. A preliminary Raman spectroscopic perspective for the roles of catalysts during char gasification. Fuel 2014;121:165–72. doi:10.1016/j.fuel.2013.12.030.

[52] Tay HL, Kajitani S, Zhang S, Li C.-Z. Effects of gasifying agent on the evolution of char structure during the gasification of Victorian brown coal. Fuel 2013;103:22–8. doi:10.1016/j.fuel.2011.02.044.

[53] Tay HL, Kajitani S, Zhang S, Li C.-Z. Inhibiting and other effects of hydrogen during gasification: Further insights from FT-Raman spectroscopy. Fuel 2014;116:1–6. doi:10.1016/j.fuel.2013.07.066.

[54] Li T, Zhang L, Dong L, Li C.-Z. Effects of gasification atmosphere and temperature on char structural evolution during the gasification of Collie sub-

bituminous coal. Fuel 2014;117:1190–5. doi:10.1016/j.fuel.2013.08.040.

[55] Keown DM, Hayashi J-I, Li C.-Z. Drastic changes in biomass char structure and reactivity upon contact with steam. Fuel 2008;87:1127–32. doi:10.1016/j.fuel.2007.05.057.

[56] Guo X, Tay HL, Zhang S, Li C.-Z. Changes in char structure during the gasification of a Victorian brown coal in steam and oxygen at 800 °C. Energy and Fuels 2008;22:4034–8. doi:10.1021/ef800528c.

[57] Bayarsaikhan B, Hayashi J, Shimada T, Sathe C, Li C, Tsutsumi a, et al. Kinetics of steam gasification of nascent char from rapid pyrolysis of a Victorian brown coal. Fuel 2005;84:1612–21. doi:10.1016/j.fuel.2005.02.008.

[58] Asadullah M, Zhang S, Min Z, Yimsiri P, Li C.-Z. Importance of biomass particle size in structural evolution and reactivity of char in steam gasification. Ind Eng Chem Res 2009;48:9858–63. doi:10.1021/ie901214z.

[59] Wu H, Li X, Hayashi JI, Chiba T, Li C.-Z. Effects of volatile-char interactions on the reactivity of chars from NaCl-loaded Loy Yang brown coal. Fuel 2005;84:1221–8. doi:10.1016/j.fuel.2004.06.037.

[60] Yip K, Ng E, Li C.-Z, Hayashi JI, Wu H. A mechanistic study on kinetic compensation effect during low-temperature oxidation of coal chars. Proc Combust Inst 2011;33:1755–62. doi:10.1016/j.proci.2010.07.073.

[61] Yip K, Tian F, Hayashi JI, Wu H. Effect of alkali and alkaline earth metallic species on biochar reactivity and syngas compositions during steam gasification. Energy and Fuels 2010;24:173–81. doi:10.1021/ef900534n.

[62] Pereira P, Somorjai GA, Heinemann H. Catalytic steam gasification of coals. Energy and Fuels 1992;6:407–10. doi:10.1021/ef00034a009.

[63] Fushimi C, Araki K, Yamaguchi Y, Tsutsumi A. Effect of heating rate on steam gasification of biomass. 2. Thermogravimetric-mass spectrometric (TG-MS) analysis of gas evolution. Ind Eng Chem Res 2003;42:3929–36. doi:10.1021/ie0300575.

[64] Wigmans T, Elfring R, Moulijn JA. On the mechanism of the potassium carbonate catalysed gasification of activated carbon: the influence of the catalyst concentration on the reactivity and selectivity at low steam pressures. Carbon 1983;21:1–12. doi:10.1016/0008-6223(83)90150-1.

[65] Wang J, Jiang M, Yao Y, Zhang Y, Cao J. Steam gasification of coal char catalyzed by K_2CO_3 for enhanced production of hydrogen without formation of methane. Fuel 2009;88:1572–9. doi:10.1016/j.fuel.2008.12.017.

[66] Li J, van Heiningen ARP. Kinetics of gasification of black liquor char by steam. Ind Eng Chem Res 1991;30:1594–601. doi:10.1021/ie00055a027.

2.0 Chapter

Experimental

2.1 Biomass Sample Preparation

The Australian mallee wood was used in this study. The feedstock was prepared by following the procedures outlined elsewhere [1]. The freshly harvested wood was debarked and air-dried. It was then milled using a Fritsch laboratory cutting mill (Model Pulverizette 15) and sieved to get 4.0-5.6 mm particle size range. The samples of two different particle size ranges of 0.80-1.0 mm and 2.0-3.3 mm were prepared

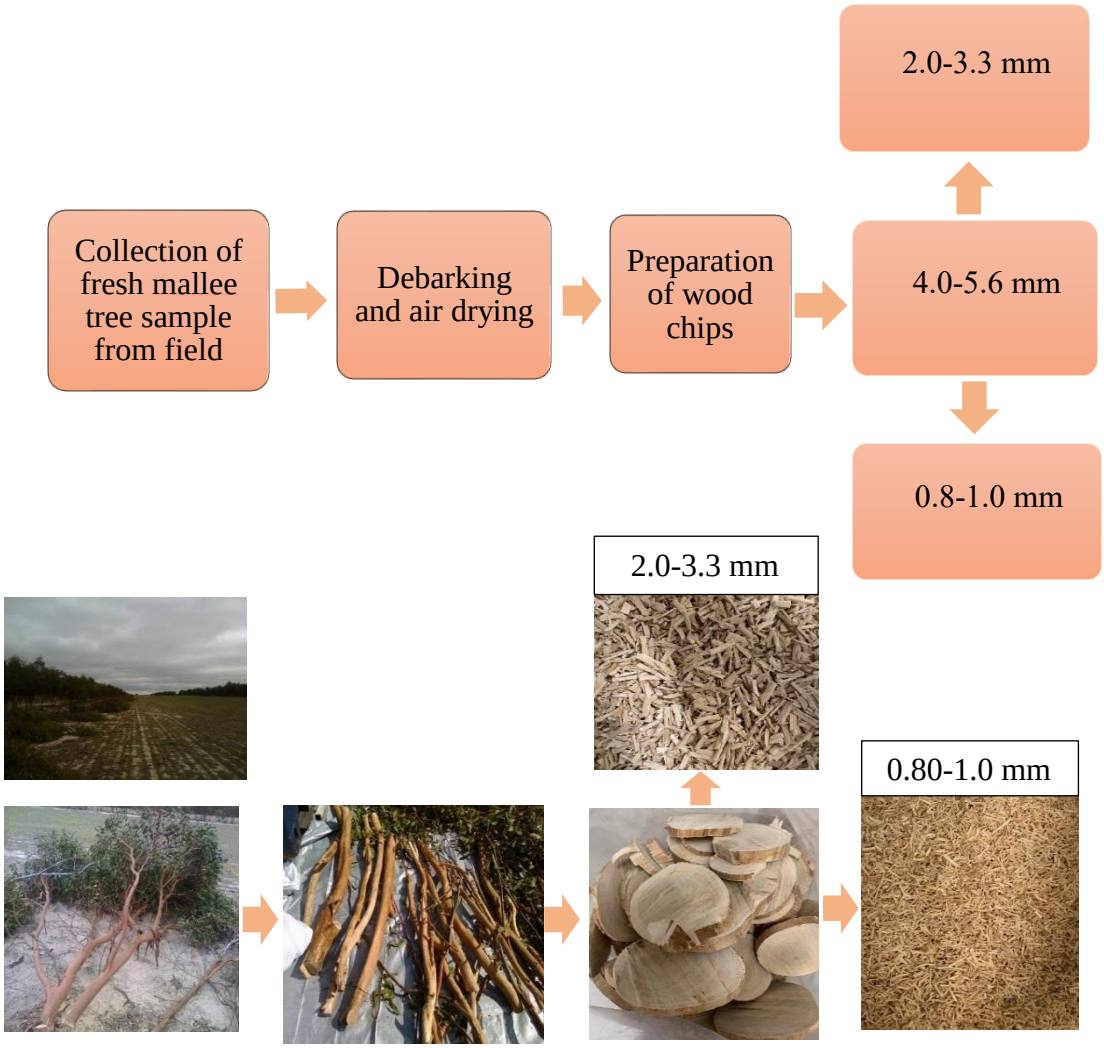

Figure 2-1 Steps in the preparation of mallee wood samples from mallee tree

after further crushing the 4.0-5.60 mm fraction and sieving it. The 4.0-5.60 mm fraction was used to prepare the other two size fractions in order to avoid the property

differences due to particle sizes. The wood sample was dried overnight at 105 °C in an oven prior to use in an experiment.

2.2 Feed Analysis

The mallee wood contains organic compounds comprising of four main elements: carbon (C), oxygen (O), hydrogen (H) and nitrogen (N) along with moisture (M) and minor amounts of inorganic constituents known as ash (ASH). The proximate analysis gives the yields of fixed carbon (FC), volatile matter (VM), moisture (M) and ash (ASH) in the sample. The following ASTM standards can be used for the determination of individual components in the proximate analysis of wood [2]:

- Moisture (M): ASTM E-871
- Volatile matter (VM): ASTM E-872
- Ash (ASH): ASTM D-1102
- Fixed carbon (FC): By difference

The ultimate analysis, which refers to the weight percentages of C, O, H, N and S, can be determined by the elemental analyser. The following ASTM standard are also available, which can be used for the determination of ultimate analysis of biomass fuels with reasonable accuracy [2]:

- Carbon, hydrogen: ASTM E-777
- Nitrogen: ASTM E-778
- Sulfur: ASTM E-775
- Oxygen: By difference

The mallee wood samples used in this study were from the same batch as those in reference [3]. The proximate and ultimate analysis of mallee wood are given in Table 2-1.

Table 2-1 Proximate and ultimate analyses of mallee wood [3]

Mallee wood	Proximate Analysis (wt.%)		
	ASH[a]	FC[b]	VM[b]
	0.9	18.4	81.6

Ultimate Analysis (%, daf)				
C[b]	H[b]	N[b]	S[b]	O[b,c]
48.2	6.1	0.2	0.0	45.5

[a] Dry basis.
[b] Dry and ash-free basis.
[c] By difference.

2.3 Experimental Procedure

The gasification experiments were carried out in a quartz fluidised-bed gasifier. Fluidised-bed gasifiers are particularly good for biomass gasification [4]. In a typical fluidised-bed gasifier, fuel and the gasifying medium undergo intense mixing in a bed of hot granular solids such as sand and the fuel particles are heated rapidly to the bed temperature. The temperature inside the fluidised-bed gasifier is uniform and provides uniform heat transfer characteristics in comparison to fixed-bed gasifier [4].

Fluidised-bed gasifiers are also flexible in terms of feedstocks unlike fixed-bed gasifiers, which require specific fuel [4]. This feature makes fluidised-bed gasifiers an attractive choice for the gasification of agricultural residues and wood, which are available at the different times of the year. The fluidised-bed gasifier also offers easier removal of ash in comparison to fixed-bed/entrained flow gasifiers as it operates at much lower temperatures [4]. The details of the fluidised-bed gasifier used in this study can be found elsewhere [1]. The reactor can be divided into two main sections:

1. The top section, which is used for the feeding of mallee wood inside the feeding tube through an electric vibrator.
2. The bottom section, which is the main reaction zone where mallee wood is pyrolysed and the biochar produced in situ is gasified subsequently.

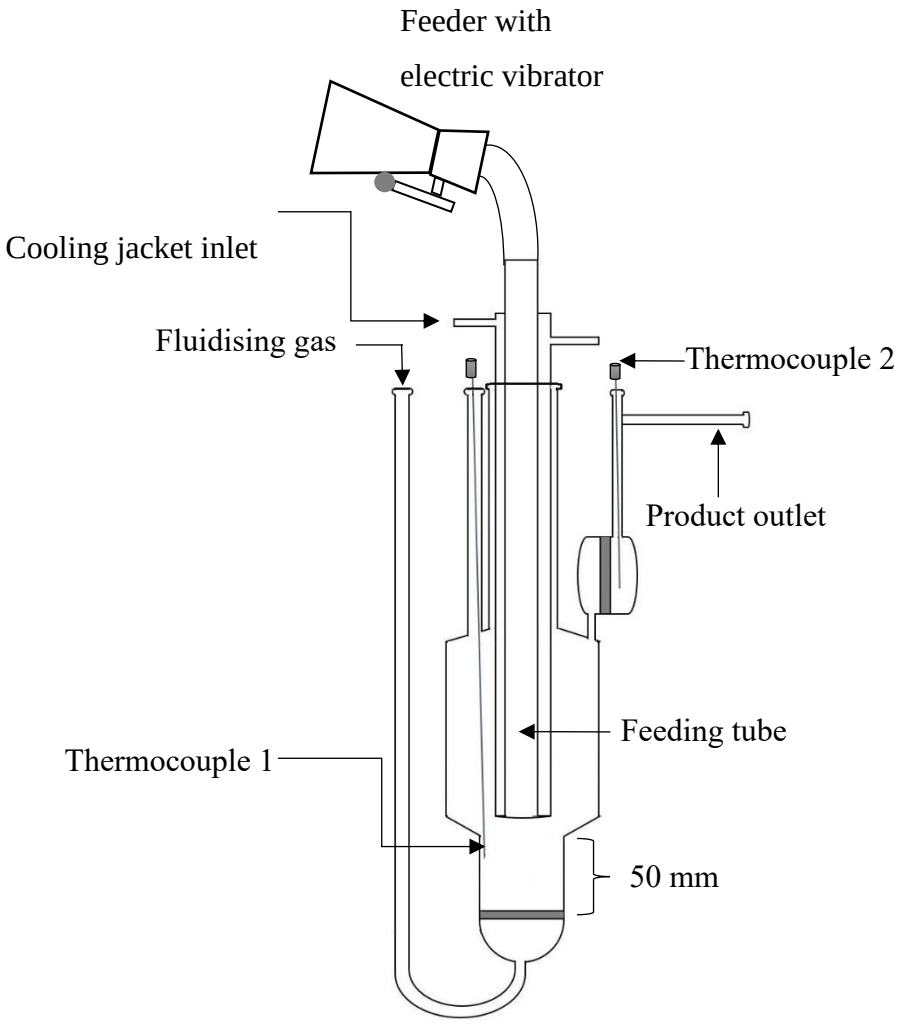

Figure 2-2 Schematic diagram of the fluidised-bed reactor for biomass gasification. Modified and reprinted with permission from Reference [1]. Copyright (2009) American Chemical Society.

The reactor has two frits: one at the bottom to distribute gas to fluidise the sand in the reaction zone and the other just before the outlet of the reactor to retain fine particles of the char entrained by the carrier gas. The reactor was heated to the target

temperature by an external electric furnace before feeding. The temperature of the bed was monitored using a type-K thermocouple. The biomass feeding tube of internal diameter of 14 mm was cooled by the compressed air flowing in a jacket outside the feeding tube to avoid any reaction inside the feeding tube.

A bed of zircon sand (100-300 µm) with unfluidised depth of 50 mm was fluidised by ultra-high purity argon (UHP, i.e. 99.999%). Based on fluidisation behaviour, solids are classified into four groups namely as A, B, C and D known as Geldart particle's classification [4]. The selected zircon bed material belongs to group B. The group B particles lie in the range of 100 to 500 µm ($\rho_p = 2500$ kg/m^3). There is a minor chance of channeling in group B particles. The majority of the fluidised bed boilers utilise group B particles as they fluidise well, and bubbles appear as soon as the superficial velocity surpasses the velocity of minimum fluidisation.

The velocity of minimum fluidisation was calculated by the correlation of Wen and Yu [5] and the sequence of calculations is as follows:

First, Reynold was calculated at the velocity of minimum fluidisation by the correlation:

$$(N_{Re})_{mf} = \sqrt{(33.7)^2 + 0.408N_{Ga}} - 33.7 \qquad (\text{Eq. } 2-1)$$

where N_{Ga} stands for the Galileo number and is a function of density and viscosity of the fluidising gas as well as the density and average diameter of the bed particle. The Galileo number can be determined as:

$$N_{Ga} = \frac{d_p^3 \rho_f (\rho_s - \rho_f) g}{\mu_f^2} \qquad (\text{Eq. } 2-2)$$

where ρ_f and μ_f represent the density and viscosity of the fluidising gas.

ρ_s and d_p represent the density and average diameter of the bed particles.

Finally, the velocity of minimum fluidisation was determined by the Eq. (3) as follows:

$$U_{mf} = \frac{(N_{Re})_{mf}\, \mu_f}{\rho_f d_p} \qquad (\text{Eq. } 2-3)$$

The gas mixture was metered through a mass flow controller to give a superficial velocity of $U \approx 10\ U_{mf}$, where U_{mf} is the minimum fluidisation velocity. The $U/U_{mf} = 10$ was used to avoid the resistance between the bubble phase and the particulate phase. The velocity of the gas phase also affects the thickness of the boundary layer around the char particle and, consequently, limits the rate of gasification. The $U/U_{mf} = 10$ was high enough to make the rate of gasification independent of the gas velocity. This ensured the isothermal bed and vigorous mixing of the particulate phase and the bubble phase. This is also in agreement with the literature [6,7]. Further, this was verified experimentally by conducting experiments at $U/U_{mf} = 10$ and at $U/U_{mf} = 14$, during the char-H_2O reaction in 15% H_2O-Ar at 800 °C and the rates of char gasification were found to be in a close agreement under both flow conditions. This shows that when the ratio i.e. $U/U_{mf} = 10$, the rate of char gasification becomes independent of the gas phase velocity under the conditions studied.

During an experiment, around 2.0 g (accurately weighed) of the mallee wood sample was fed into the fluidised bed at an average feeding rate of 0.20 g/min with an electric vibrator. The UHP argon was used as a carrier gas for feeding the wood particle inside the reactor. After the feeding was finished, the reactor was held further for 5 min under UHP argon to ensure that all the volatiles were released [8-10]. After 5 min of holding, the UHP argon was switched to 0.4% oxygen balanced with argon (0.4% O_2-Ar) during the gasification in O_2. For steam gasification, the feeding of the steam was commenced by means of an HPLC pump. The HPLC pump fed accurately metered demineralised water into the reaction zone, which was converted into 15% H_2O or 2% H_2O of the argon flow. The outlet of the reactor was connected to a quadrupole mass spectrometer (QMS Prisma^{TM} 200). The product gases were cooled to remove any water vapour/excess steam present in the product gas mixture before being introduced into the QMS 200. The product sampling line was continuously purged using UHP argon before a run to avoid any contamination from the atmospheric air.

The key reaction products including CO, CO_2, CH_4, and H_2 were monitored by the QMS 200 until the signal of CO, CO_2, CH_4 and H_2 on the mass spectrometer returned to initial baselines. The QMS 200 was calibrated using a certified calibration standard (ISO Guide 34 accredited) gas mixtures. The mass fragment of CO_2 at m/z = 28

overlaps with CO signal. Therefore, the CO signal was deconvoluted by subtracting the contribution of CO_2 at m/z = 28 before determining the specific rate of reaction.

After the char was gasified completely, the reactor was lifted up from the furnace and cooled down with argon flowing through the reactor. The volume of the sampling line was kept as small as possible. Care was taken to make sure that there was no adventitious entrance of atmospheric air into the sampling line during a run. The detailed schematic of the process rig. is shown in Figure 2-3.

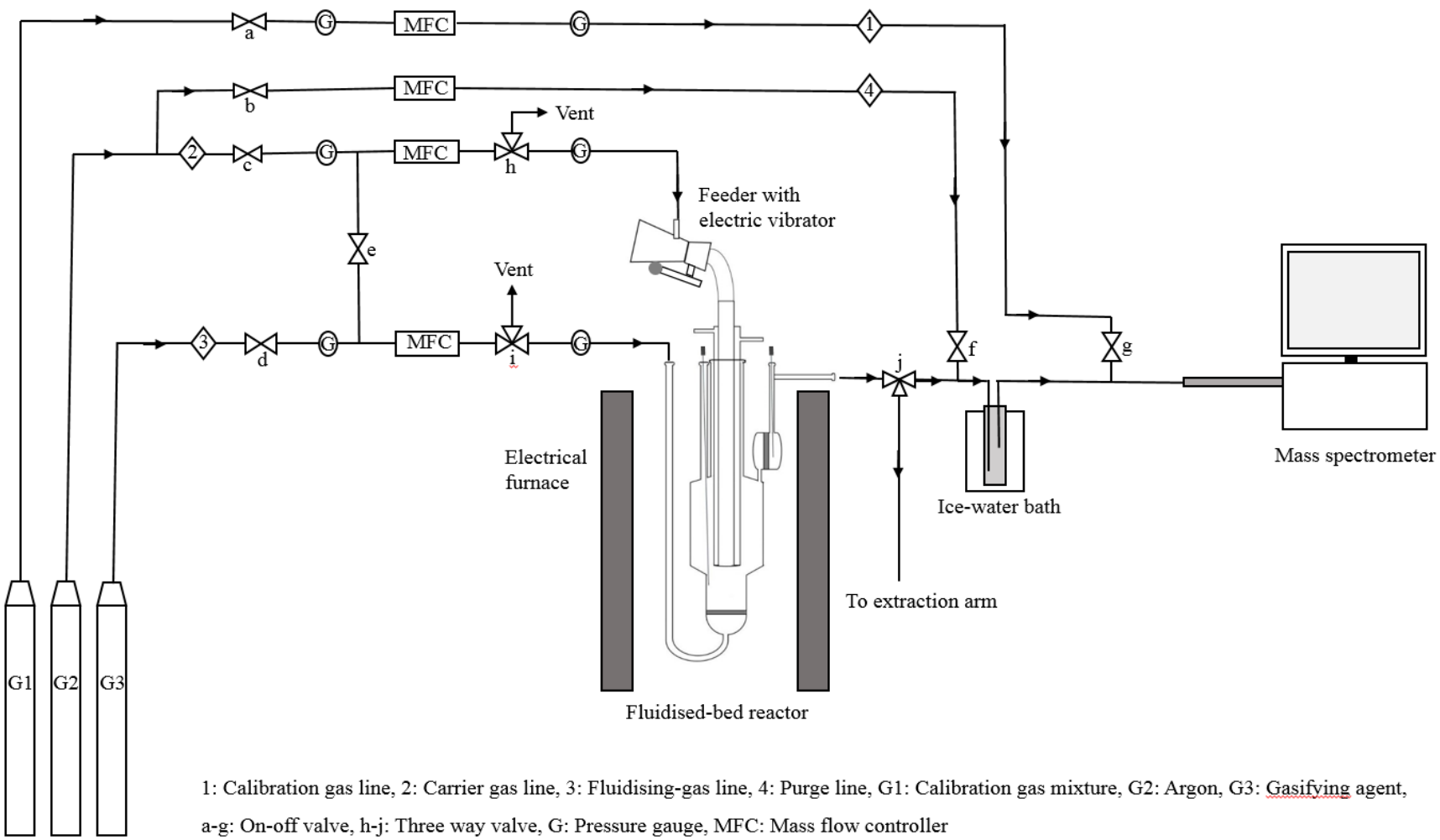

1: Calibration gas line, 2: Carrier gas line, 3: Fluidising-gas line, 4: Purge line, G1: Calibration gas mixture, G2: Argon, G3: Gasifying agent,
a-g: On-off valve, h-j: Three way valve, G: Pressure gauge, MFC: Mass flow controller

Figure 2-3 Schematic of the experimental set up

2.4 Rate of biochar consumption and formation rates of CO, CO_2, and H_2

The specific rate of reaction was calculated as the total number of moles of CO, CO_2, and CH_4 passing through the analyser per second per unit moles of carbon remaining inside the reactor. This is also equivalent to the differential mole release of carbon in the form of carbon species (moles of CO, CO_2 and CH_4) per unit moles of carbon remaining inside the reactor and can be expressed as:

$$r_C = -\frac{1}{W_C}\frac{dW_C}{dt} = \left(y_{CO} + y_{CO_2} + y_{CH_4}\right)\left(\frac{QP}{W_C R T_{amb}}\right) \qquad (\text{Eq. } 2-4)$$

where r_x is in s^{-1}, y = mole fraction, Q = volumetric flow rate of the fluidising gas (L/min), T_{amb} = ambient temperature (K), P = atmospheric pressure (bar) and R = 0.0831 gas constant (bar L $mol^{-1}K^{-1}$) and W_C = moles of biochar carbon remaining at any instant and are calculated as:

$$W_C = W_{Total\ char\ carbon} - W_{\ char\ carbon\ released} \qquad (\text{Eq. } 2-5)$$

$W_{Total\ char\ carbon}$ was determined based on the total yield of all carbon species (moles of CO, CO_2 and CH_4) produced during the gasification until there was no char left inside the reactor. For this purpose, preliminary experiments were conducted to verify the complete conversion of char. $W_{\ char\ carbon\ released}$ corresponds to the yield of the carbon species, which have been released up to any given conversion level. For instance, $W_{Total\ char\ carbon}$ was 0.0156 moles of carbon determined when the char was completely converted to carbon species during the gasification in 15% H_2O-Ar at 850 °C. For any given conversion e.g. 10% conversion of char carbon, $W_{\ char\ carbon\ released}$ was determined by summing up yields of CO, CO_2 and CH_4 until the conversion reached to 10% (0.00156 moles). The difference of $W_{Total\ char\ carbon}$ and $W_{\ char\ carbon\ released}$ gave the number of moles of the char carbon i.e. 0.01404 moles remaining inside the reactor.

These calculation results were also verified with the experimental results using the carbon balance in the solid (char) and in the gas-phase. As mentioned above, for the gasification in 15% H_2O at 850 °C for particle size 2.0-3.3 mm, the total number of moles of carbon in the gas-phase (CO, CO_2, and CH_4) were 0.0156 moles whereas, the number of carbon moles in the char were 0.0150. The total number of carbon moles in

the char were determined from the char yield after the pyrolysis of mallee wood. The elemental analyser was used to determine the wt.% of carbon in the char.

At a given biochar conversion, the formation rates of CO (r_{CO}), CO_2 (r_{CO_2}), and H_2 (r_{H_2}) were calculated by the following equations respectively:

$$r_{CO} = \frac{1}{W_{CO}}\frac{dW_{CO}}{dt} = (y_{CO})\left(\frac{QP}{W_{CO}RT_{amb}}\right) \quad (\text{Eq. } 2-6)$$

$$r_{CO2} = \frac{1}{W_{CO_2}}\frac{dW_{CO_2}}{dt} = (y_{CO2})\left(\frac{QP}{W_{CO_2}RT_{amb}}\right) \quad (\text{Eq. } 2-7)$$

$$r_{H2} = \frac{1}{W_{H_2}}\frac{dW_{H_2}}{dt} = (y_{H_2})\left(\frac{QP}{W_{H_2}RT_{amb}}\right) \quad (\text{Eq. } 2-8)$$

where W = moles of a chemical species potentially remaining at any instant and are calculated as:

$$W_{CO} = W_{Total\ CO\ formed} - W_{CO\ released} \quad (\text{Eq. } 2-9)$$

$$W_{CO_2} = W_{Total\ CO_2\ formed} - W_{CO_2\ released} \quad (\text{Eq. } 2-10)$$

$$W_{H_2} = W_{Total\ H_2\ formed} - W_{H_2\ released} \quad (\text{Eq. } 2-11)$$

When the partial pressure (p) of the gasification medium (H_2O) is constant, the biochar consumption rate and formation rates of CO, CO_2, and H_2, at any biochar conversion 'x', can be expressed [11] by the following equations respectively:

$$r_C = -\frac{1}{W_C}\frac{dW_C}{dt} = f(x)g(p)A\exp\left(-\frac{E_{app}}{RT}\right)$$
$$= A_{char\ consumption}\ exp\left(-\frac{E_{char\ consumption}}{RT}\right) \quad (\text{Eq. } 2-12)$$

$$r_{CO} = \frac{1}{W_{CO}}\frac{dW_{CO}}{dt} = f(x)g(p)A\exp\left(-\frac{E_{app}}{RT}\right)$$
$$= A_{CO\ formation}\ exp\left(-\frac{E_{CO\ formation}}{RT}\right) \quad (\text{Eq. } 2-13)$$

$$r_{CO_2} = \frac{1}{W_{CO_2}} \frac{dW_{CO_2}}{dt} = f(x)g(p)A \exp\left(-\frac{E_{app}}{RT}\right)$$

$$= A_{CO_2\, formation}\, exp\left(-\frac{E_{CO_2\, formation}}{RT}\right) \quad (\text{Eq. } 2-14)$$

$$r_{H_2} = \frac{1}{W_{H_2}} \frac{dW_{H_2}}{dt} = f(x)g(p)A \exp\left(-\frac{E_{app}}{RT}\right)$$

$$= A_{H_2\, formation}\, exp\left(-\frac{E_{H_2\, formation}}{RT}\right) \quad (\text{Eq. } 2-15)$$

$f(x)$ in Eq. 2-12 to Eq. 2-15 is a function representing the changes in biochar properties and would be a constant at any given char conversion level x. $A_{char\ consumption}$, $A_{CO\ formation}$, $A_{CO_2\, formation}$ and $A_{H_2\, formation}$ represent the apparent pre-exponential factors of biochar consumption and formation of CO, CO_2 and H_2 respectively and are the functions of partial pressure $g(p)$ of H_2O and $f(x)$. These terms also include many conversion-dependant factors that influence biochar gasification rate during biochar conversion e.g. the composition of biochar and number of active sites. E_{app} is the apparent activation energy. $E_{char\ consumption}$, $E_{CO\ formation}$, $E_{CO_2\, formation}$ and $E_{H_2\, formation}$ represent the apparent activation energies of biochar consumption, CO formation, CO_2 formation, and H_2 formation respectively in kJ mol^{-1}.

The apparent activation energy (E_{app}) and the apparent pre-exponential factors (A_{app}) of biochar consumption and formation of CO, CO_2 and H_2 were acquired by constructing the Arrhenius plots between *ln* (r_C), *ln* (r_{CO}), *ln* (r_{CO_2}) or *ln* (r_{H_2}) vs. 1/*T* at the given biochar conversions. The slopes and y-intercepts of the Arrhenius plots gave the apparent activation energies (E_{app}) and the apparent pre-exponential factors (lnA_{app}) respectively at different conversion levels. For instance, for the gasification in 15% H_2O in the kinetic-controlled regime (700-850 °C), the Arrhenius plots of char consumption, CO, CO_2 and H_2 formation were drawn using the rate data of char consumption, CO formation, CO_2 formation and H_2 formation respectively vs. 1/*T* from 973.15 to 1123.15 in the Kelvin scale.

2.5 Char characterisation

The biochar samples were characterised using Raman spectroscopy and X-ray photoelectron spectroscopies (XPS). A well-grounded 0.5 wt.% [1,3,12] char-KBr (KBr

Table 2-2 Raman bands/peaks and their descriptions. Adapted with permission from Reference [13]. Copyright (2006), Elsevier.

Band Name	Band position cm^{-1}	Description	Bond Type
G_L	1700	Carbonyl group C=O	sp^2
G	1590	Graphite E22g; aromatic ring quadrant breathing; alkene C=C	sp^2
G_R	1540	Aromatics with 3-5 rings; amorphous carbon structures	sp^2
V_L	1465	Methylene or methyl; semi-circle breathing of aromatic rings; amorphous carbon structures	sp^2 sp^3
V_R	1380	Methyl group; semi-circle breathing of aromatic rings; amorphous carbon structures	sp^2 sp^3
D	1300	D band on highly ordered carbonaceous materials; C-C between aromatic rings and aromatics with not less than 6 rings	sp^2
S_L	1230	Aryl-alkyl ether; para-aromatics	sp^2 sp^3
S	1185	Caromatic-Calkyl; aromatic (aliphatic) ethers; C-C on hydroaromatic rings; hexagonal diamond carbon sp3; C-H on aromatic rings	sp^2 sp^3
S_R	1060	C-H on aromatic rings; benzene (ortho-di-substituted) ring	sp^2
R	960-800	C-C on alkanes and cyclic alkanes; C-H on aromatic rings	sp^2 sp^3

of IR grade) mixture was used to acquire the Raman spectra using a Perkin-Elmer Spectrum GX FTIR/Raman spectrometer. For each sample, the Raman spectra were acquired with a resolution of 4 cm^{-1}. A baseline correction was applied to each Raman spectrum. These corrected Raman spectra were further deconvoluted into 10 Gaussian bands in the range of 800 cm^{-1} to 1800 cm^{-1} by following the procedure outlined before [13]. The band names with their corresponding peaks and description are mentioned in Table 2-2.

The total Raman area and the ratio of the area of D band and the sum of areas of Gr + V_l + V_r bands were used as indicators to trace the structural changes in the biochar. The area of D band (1300 cm^{-1}), I_D, reflects the relative concentration of aromatic rings with at least 6 or more fused benzene rings while the sum of the band areas $I_{(Gr + Vl+ Vr)}$ is an indicator of the relative concentration of aromatic rings with 3-5 fused benzene rings present in the biochar sample. The G_r, V_l and V_r bands correspond to the bands centred around 1540 cm^{-1}, 1465 cm^{-1} and 1380 cm^{-1} respectively. Thus, $I_D/(I_{(Gr + Vl+ Vr)}$ reflects the evolution of aromatic ring condensation during gasification.

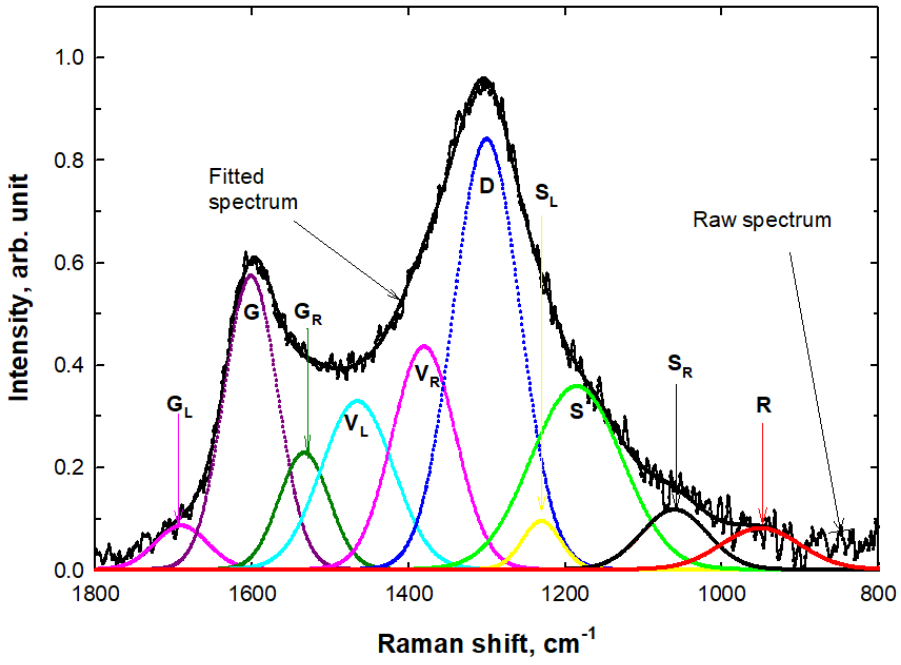

Figure 2-4 Spectral deconvolution of a Raman spectrum of a typical char sample. Adapted with permission from Reference [13]. Copyright (2006), Elsevier.

XPS was used to investigate the elemental composition of the biochar surface. For this purpose, the char samples were stored in sealed glass vials in the argon atmosphere at low temperatures to avoid oxidation by air. A Kratos Ultra DLD XPS instrument with Al monochromated X-rays source (photon energy 1486 eV) was used. Operating power of 225 Watt was used for the X-ray gun. The survey spectra were acquired in the range of 1200 to 0 eV with a pass energy of 160 eV. These XPS spectra were processed using the Shirley background on the CasaXPS software. The atomic percent of an element in the CasaXPS was calculated by the peak area of the element above the background divided by its relative sensitivity factor (R.S.F).

2.6 References

[1] Asadullah M, Zhang S, Min Z, Yimsiri P, Li C.-Z. Importance of biomass particle size in structural evolution and reactivity of char in steam gasification. Ind Eng Chem Res 2009;48:9858–63. doi:10.1021/ie901214z.

[2] Basu P. Biomass Gasification and Pyrolysis. Elsevier; 2010. https://doi.org/10.1016/C2009-0-20099-7.

[3] Asadullah M, Zhang S, Min Z, Yimsiri P, Li C.-Z. Effects of biomass char structure on its gasification reactivity. Bioresour Technol 2010;101:7935–43. doi:10.1016/j.biortech.2010.05.048.

[4] Basu P. Combustion and Gasification in Fluidized Beds. 2006. doi:10.1201/9781420005158.

[5] Wen CY, Yu YH. A generalized method for predicting the minimum fluidization velocity. AIChE J 1966;12:610–2. doi:10.1002/aic.690120343.

[6] Dennis JS, Lambert RJ, Milne AJ, Scott SA, Hayhurst AN. The kinetics of combustion of chars derived from sewage sludge. Fuel 2005;84:117–26. doi:10.1016/j.fuel.2004.08.020.

[7] Scott SA, Davidson JF, Dennis JS, Fennell PS, Hayhurst AN. The rate of gasification by CO_2 of chars from waste. Proc Combust Inst 2005;30:2151–9. doi:10.1016/j.proci.2004.08.061.

[8] Li C.-Z. Importance of volatile–char interactions during the pyrolysis and gasification of low-rank fuels – A review. Fuel 2013;112:609–23. https://doi.org/10.1016/j.fuel.2013.01.031.

[9] Song Y, Xiang J, Hu S, Quyn DM, Zhao Y, Hu X, et al. Importance of the aromatic structures in volatiles to the in-situ destruction of nascent tar during the volatile-char interactions. Fuel Process Technol 2015;132:31–8. https://doi.org/10.1016/j.fuproc.2014.12.035.

[10] Song Y, Wang Y, Hu X, Xiang J, Hu S, Mourant D, et al. Effects of volatile-

char interactions on in-situ destruction of nascent tar during the pyrolysis and gasification of biomass. Part II. Roles of steam. Fuel 2015;143:555–62. https://doi.org/10.1016/j.fuel.2014.11.096.

[11] Wu H, Li X, Hayashi JI, Chiba T, Li C.-Z. Effects of volatile-char interactions on the reactivity of chars from NaCl-loaded Loy Yang brown coal. Fuel 2005;84:1221–8. doi:10.1016/j.fuel.2004.06.037.

[12] Wang S, Wu L, Hu X, Zhang L, Li T, Li C.-Z. Effects of the particle size and gasification atmosphere on the changes in the char structure during the gasification of mallee biomass. Energy and Fuels 2018;32:7678–84. doi:10.1021/acs.energyfuels.8b01309.

[13] Li X, Hayashi J, Li C.-Z. FT-Raman spectroscopic study of the evolution of char structure during the pyrolysis of a Victorian brown coal. Fuel 2006;85:1700–7. doi:10.1016/j.fuel.2006.03.008.

3.0 Chapter

Kinetic compensation effects in the chemical reaction-controlled regime and mass transfer-controlled regime during the gasification of biochar in O_2

3.1 Abstract

This study aims to investigate the kinetic compensation effects during the char-O_2 reaction in a fluidised-bed reactor for two particle sizes of 0.80-1.0 mm and 2.0-3.3 mm. The rate of char-O_2 reaction was determined by analysing the gasification product gas composition in a quadrupole mass spectrometer. The char-O_2 reaction exhibited different kinetic compensation effects between apparent activation energy and apparent pre-exponential factor in the kinetics-controlled, diffusion-controlled and mixed regimes for both particle sizes. The same reaction mechanism is followed during the char-O_2 reaction in the kinetic regime at same or at different pyrolysis temperatures as revealed by the kinetic compensation effects. In the mixed regime, higher diffusion limitations increased the 'm' and 'c' values in the kinetic compensation effect i.e. $lnA_{app} = mE_{app} + c$ for any given particle size. Due to higher rates of reaction at higher char conversions, the char-O_2 reaction switched from kinetics-controlled to mixed regimes, resulting in higher slopes 'm' and y-intercepts 'c' in the kinetic compensation effects. The absence of isokinetic temperature at higher conversions indicates that char properties changed significantly at higher conversions compared with those at lower conversions.

Keywords: Gasification; Kinetic compensation effect; Biomass; Mallee wood biochar.

3.2 Introduction

Biomass gasification is an effective way to utilise biomass as a renewable energy source. Understanding the fundamental gasification mechanism is very important for the development of advanced gasification technologies. The gasification of char is normally the rate-limiting step in the whole gasification process and affects the efficiency of the process [1–3]. The char-O_2 reaction is a fundamental reaction in the gasification process and is a major source of energy to drive the endothermic gasification reactions. Many kinetic studies have been conducted on the char-O_2 reaction. However, past studies frequently utilise a single set of kinetic parameters based on the initial properties of char to examine the reaction mechanism. These studies do not incorporate the effects of change in char properties on kinetics, which become significant with the progress of char conversion [4–13].

There is a kinetic compensation effect (KCE) reported during the heterogeneous char-gas reactions and various explanations have been proposed to explain the reaction mechanisms [14–16]. For the KCE, apparent activation energy (E_{app}) and apparent pre-exponential factor (lnA_{app}) in the Arrhenius equation vary in proportion to each other for a series of related reactions at different conversion levels [17–19]. This can be represented by a linear equation of the form:

$$lnA_{app} = mE_{app} + c \qquad (\text{Eq. } 3-1)$$

where *m* is the slope on the plot between lnA_{app} and E_{app} and *c* is the y-intercept. The relation is referred to as the KCE. According to this, the reaction rate is varied by less than the change in the $exp\left(-\frac{E}{RT}\right)$ term as there is a compensating variation in lnA_{app}. Our previous work [20] reported the KCE during the oxidation of brown coal char and a plausible explanation was given on the compensation effect. According to this, char has sites of a wide range of energy levels that are not uniformly distributed in char. New sites are generated and consumed continuously with char conversion levels, giving rise to the KCE. Our previous study [21] also reported the KCE during the low-temperature oxidation of different carbon materials. However, these studies were limited to the kinetics-controlled regime and did not provide information in the diffusion-controlled regime where the mass transport of O_2 to the char surface and/or

to the active sites inside the char particles becomes significant and starts to affect the observed reaction rate.

Most commercial gasification processes, at least partially, operate in the diffusion-controlled regime to achieve higher reactions rates. Therefore, it is imperative to understand the char-O_2 reaction in the diffusion-controlled regime in order to have a better understanding on the char-O_2 kinetics. Moreover, in the diffusion-controlled regime, it is still unclear how the kinetic parameters vary with char conversion levels and particle size. Therefore, to understand the difference between diffusion-controlled and kinetics-controlled regimes in terms of KCE is an important topic, which has not received sufficient attention in the past studies.

The focus of this study is on the KCE for the char-O_2 reaction and will investigate how the KCE differs in the kinetics- and diffusion-controlled regimes. The study also focuses on the changes in KCE with char conversion level for two biomass particle sizes of 0.80-1.0 mm and 2.0-3.3 mm. This study will provide mechanistic insight into the char-O_2 reaction in the kinetics-controlled, diffusion-controlled and mixed (kinetic plus diffusion) regimes.

3.3 Experimental

The gasification experiments were carried out in a quartz fluidised-bed reactor. The details of the sample preparation and the experimental procedure have been described in Chapter 2. Briefly, around 2.0 g (accurately weighed) of the mallee wood sample was fed into the fluidised bed at a feeding rate of 0.20 g/min with an electric vibrator during an experiment. After the feeding was finished, the reactor was held further for 5 min under UHP argon to ensure that all the volatiles were removed. After 5 min of holding, the UHP argon was switched to 0.4% oxygen balanced with argon. The outlet of the reactor was connected to a quadrupole mass spectrometer (QMS Prisma^{TM} 200) to monitor the gas composition during the char-O_2 reaction. The product gases were cooled to remove any water vapour present in the product gas mixture before being introduced into the QMS 200. After the char was gasified completely, the reactor was lifted up from the furnace and cooled down with argon flowing through the reactor.

For a fixed partial pressure (p) of the gasifying agent (O_2), at a given conversion level x, the reaction rate can be expressed by the following equation as:

$$r_c = \frac{1}{W}\frac{dW}{dt} = f(x)g(p)A\exp\left(-\frac{E_{app}}{RT}\right) = A_{app}\,exp\left(-\frac{E_{app}}{RT}\right) \qquad (\text{Eq. } 3-2)$$

$f(x)$ in Eq. 3-2 represents the changes in char properties and would be a constant at any given char conversion level x. A_{app} is the apparent pre-exponential factor and is a function of the partial pressure of O_2 and $f(x)$. It also includes the sum of conversion-dependent factors, e.g. char composition, number of active sites that influence the rate of char gasification during char conversion. E_{app} is the apparent activation energy in kJ/mol.

3.4 Results and Discussion

3.4.1 Char reactivity

The specific rate of reaction (r_x) of the char-O_2 reaction was determined using Eq. 3-2 and char conversion (X) was calculated by taking the ratios of moles of char carbon reacted/released ($N_{\ char\ carbon\ released}$) in the form of CO, CO_2, and CH_4 to the total number of moles of char carbon ($N_{\ Total\ char\ carbon}$) . This can be expressed as:

$$X = \frac{N_{char\ carbon\ released}}{N_{Total\ char\ carbon}} \qquad (\text{Eq. } 3-3)$$

Our results indicate (Figure 3-1 a-d) that the rate of reaction increased with increasing temperature from 400 to 900 °C consistently for both particle sizes due to enhanced gasification reactions. Moreover, at any temperature in the range from 400 to 900 °C, the rate of reaction increased with increasing char conversion for all samples. There are several factors, which affect the reactivity of chars particularly those from low-rank fuels [3]. These factors include char structure, concentration of alkali and alkaline earth metallic (AAEM) species, distribution/dispersion of AAEM species, and the physico-chemical forms of AAEM species [3]. However, the data in Figure 3-1 suggest that the increasing char reactivity with conversion seems to be affected predominantly by the catalytic effects of alkali and alkaline earth metallic (AAEM) species

[13,23,24]. To understand this from the perspective of kinetic parameters, the kinetic analysis is carried out and will be discussed later.

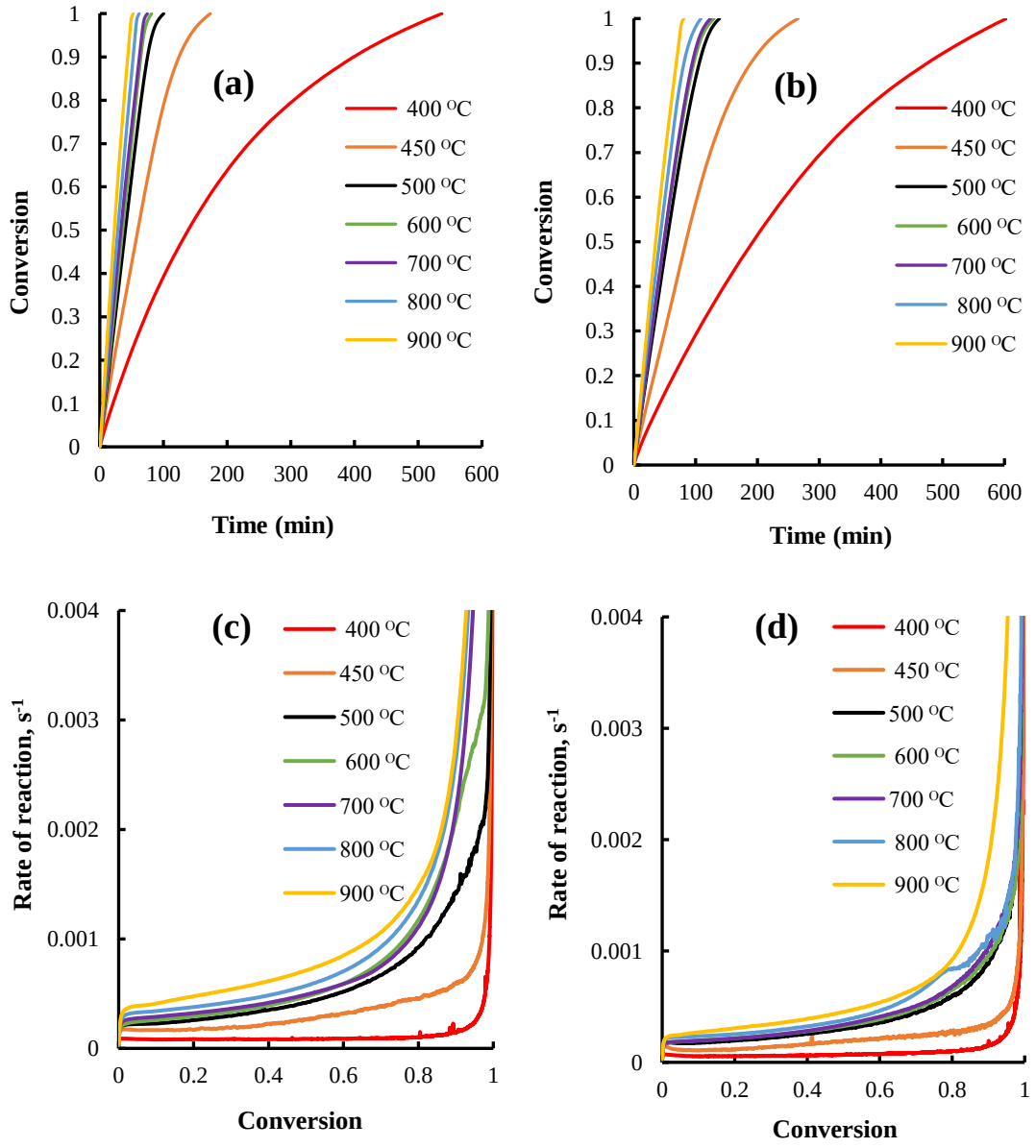

Figure 3-1 Char conversion as a function of time at different temperatures for particle sizes, (a) 0.80-1.0 mm, (b) 2.0-3.3 mm, and rate of reaction as a function of char conversion at different temperatures for particle sizes, (c) 0.80-1.0 mm and (d) 2.0-3.3 mm.

3.4.2 Differentiation between kinetics-controlled and diffusion-controlled regimes

Figure 3-2 shows the dependence of the char gasification rate on temperature during the char-O_2 reaction. The straight Arrhenius lines indicate that Eq. (3-2) is a good approximation of the char-O_2 reaction rate. The Arrhenius plots for the char-O_2 reaction demonstrate that in the lower temperature range from 400 to 500 °C, the slopes of the Arrhenius plots were much higher than those in the higher temperature range from 700 to 900 °C. This behaviour was found to be consistent for both particle sizes i.e., 0.8-1.0 mm and 2.0-3.3 mm (Figure 3-2). This shows that the apparent reaction rate in the lower temperature range is much more sensitive to temperature than that in the higher temperature range. It is also obvious that, in the higher temperature range, the rate of the char-O_2 reaction increased (despite sharp decrease in slopes relative to kinetic-controlled regime) at all conversions for both particle sizes (Figure 3-2 a-b). Based on the variation in the rate of the char-O_2 reaction with temperature, the Arrhenius plots can be divided into three regimes i.e. low-temperature

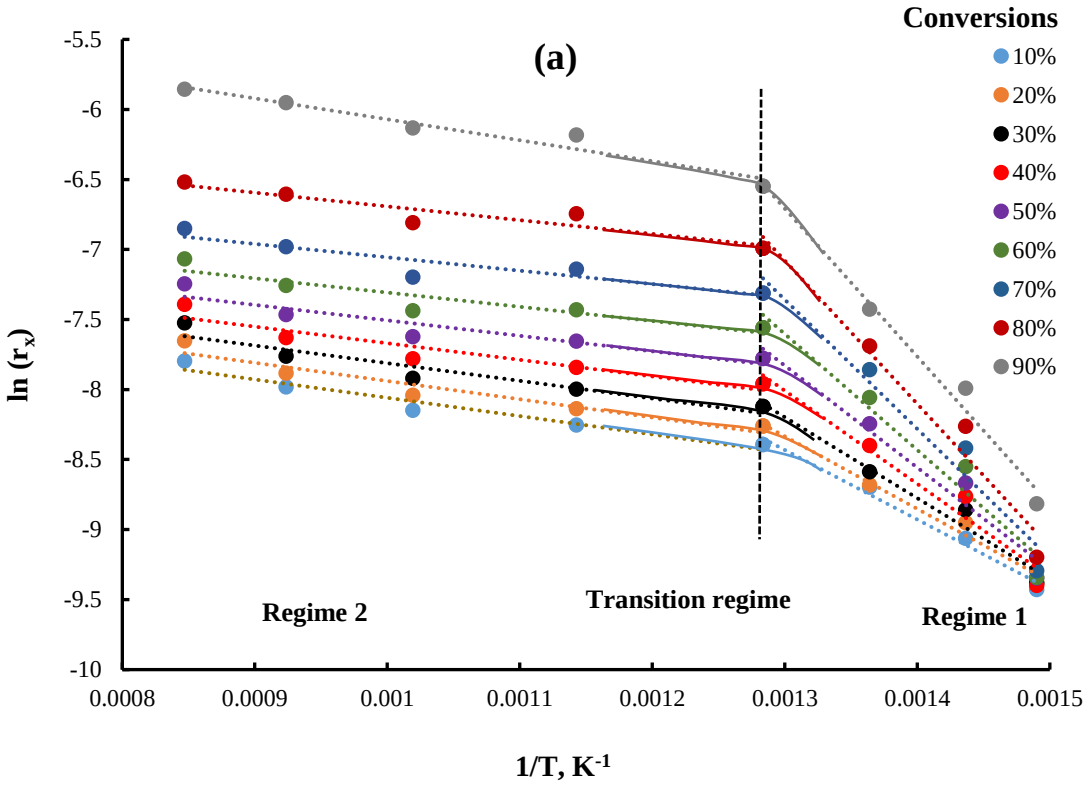

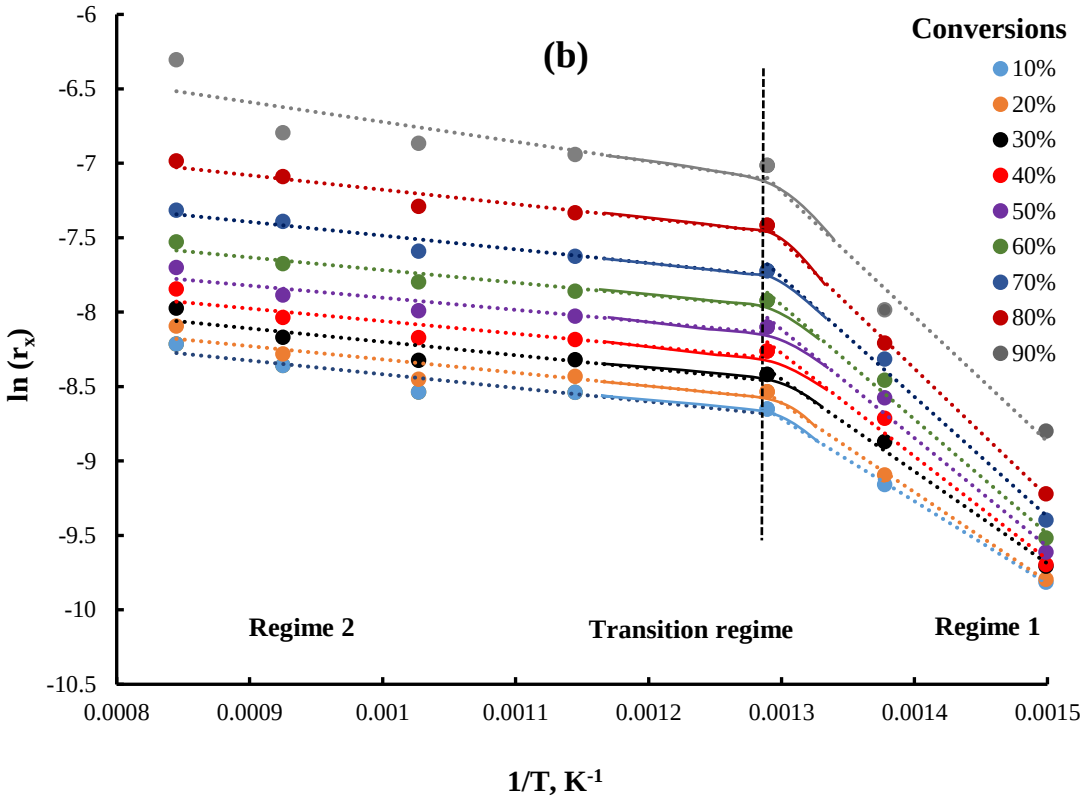

Figure 3-2 Arrhenius plots of the char-O_2 reaction at different char conversions for particle size ranges (a) 0.8- 1.0 mm and (b) 2.0-3.3 mm.

regime from 400 to 500 °C (Regime 1), high-temperature regime from 700 to 900 °C (Regime 2) and transition regime (between low temperature and high-temperature regimes). To gain insight from the perspective of kinetics, the kinetic analysis was carried out in a subsequent section.

3.4.3 Kinetic Analysis

3.4.3.1 Effect of pyrolysis temperature on kinetic parameters

In this study, char samples were prepared by the pyrolysis of mallee wood. The study investigated the effects of pyrolysis temperature on the char structure and on the kinetic parameters during the char-O_2 reaction. The char samples were prepared at the

same pyrolysis temperature i.e. 500 °C or at different pyrolysis temperatures i.e. 400, 450 and 500 °C and were subsequently gasified at 400, 450 and 500 °C.

To carry out pyrolysis at different temperatures, char samples were prepared under UHP argon at 400, 450 and 500 °C followed by in situ gasification in the presence of 0.4% O_2 balanced with argon at 400, 450 and 500 °C respectively. Our results (Figure 3-3) reveal that apparent activation energy and apparent pre-exponential factor both increased with conversion under both conditions. For any char conversion level, there was an insignificant effect of pyrolysis temperature on apparent activation energies and apparent pre-exponential factors. It is obvious that the char produced under both pyrolysis conditions have, essentially, the same structural features as revealed by the kinetic parameters [25]. In other words, the above temperature range is too narrow to result in a considerable difference in the char structure and, consequently, in the kinetic parameters of the char-O_2 reaction.

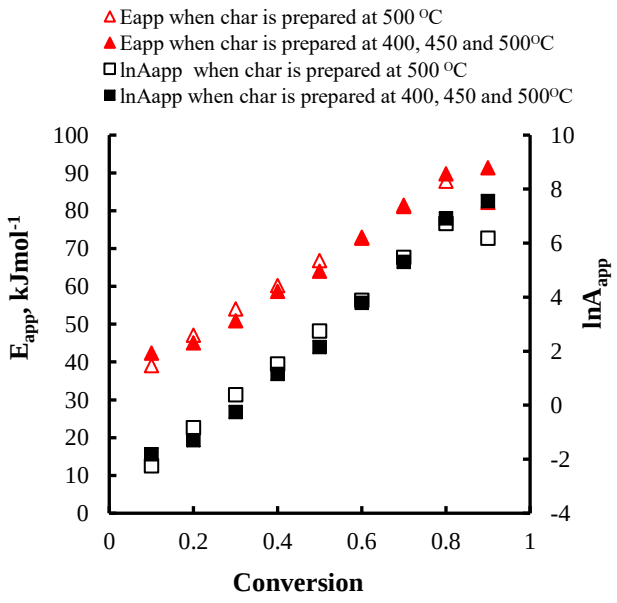

Figure 3-3 Effect of pyrolysis temperature on apparent activation energy and apparent pre-exponential factor for 0.8-1.0 mm particle size.

3.4.3.2 Effect of conversion on kinetic parameters

The effect of conversion on kinetic parameters was analysed in regime 1 and regime 2 for both particle sizes (Figure 3-4). Our results show that, for any given particle size, the apparent activation energy and apparent pre-exponential factor increased with conversion consistently in regime 1 (from 400 to 500 °C). This shows that, in regime 1, the rate of the char-O_2 reaction is controlled by the char-O_2 heterogeneous reactions or by the chemical reactivity of char. This implies that temperature has a very significant influence on the rate of the char-O_2 reaction in regime 1. This regime can be called as the kinetics-controlled regime. Moreover, in the kinetics-controlled regime at lower char conversions (up to 0.5 conversion; Figure 3-4 a), apparent activation energy values were very close for both particle sizes. For instance, at conversion 0.5, E_{app} was 64 kJ/mol for 0.8-1.0 mm particle size, and 61 kJ/mol for 2-3.35 mm particle size. However, at higher char conversion levels, bigger particles (2.0-3.35 mm) showed lower apparent activation energy than smaller particles (0.80-1.0 mm). For instance, at conversion 0.8, E_{app} was 90 kJ/mol for 0.8-1.0 mm particle size, and 71 kJ/mol for 2-3.35 mm particle size. This difference in activation energies could be attributed to intraparticle diffusion limitations in bigger particles [22,26–28], which become significant towards higher char conversion levels when the reaction rates were high (Figure 3-1).

However, in regime 2 (from 700 to 900 °C), a decrease in the apparent activation energy was observed while apparent pre-exponential factor increased slightly with increasing char conversion. Further, activation energy values were slightly lower for bigger particles than smaller ones showing higher intraparticle diffusion in regime 2. Moreover, the activation energy values in this regime are found to be in the range of 12-24 kJ/mol at various char conversion levels for both particle sizes. These apparent activation energy values are reduced to nearly half or less than half of the activation energy values in the kinetic-controlled regime i.e. $E_{diffusion} \leq \frac{1}{2} E_T$ where E_T is the activation energy in the kinetic-controlled regime. This is primarily the indication that the char-O_2 reaction becomes less temperature sensitive due to the presence of mass transfer limitations. This suggests that in regime 2, the char-O_2 reaction is controlled

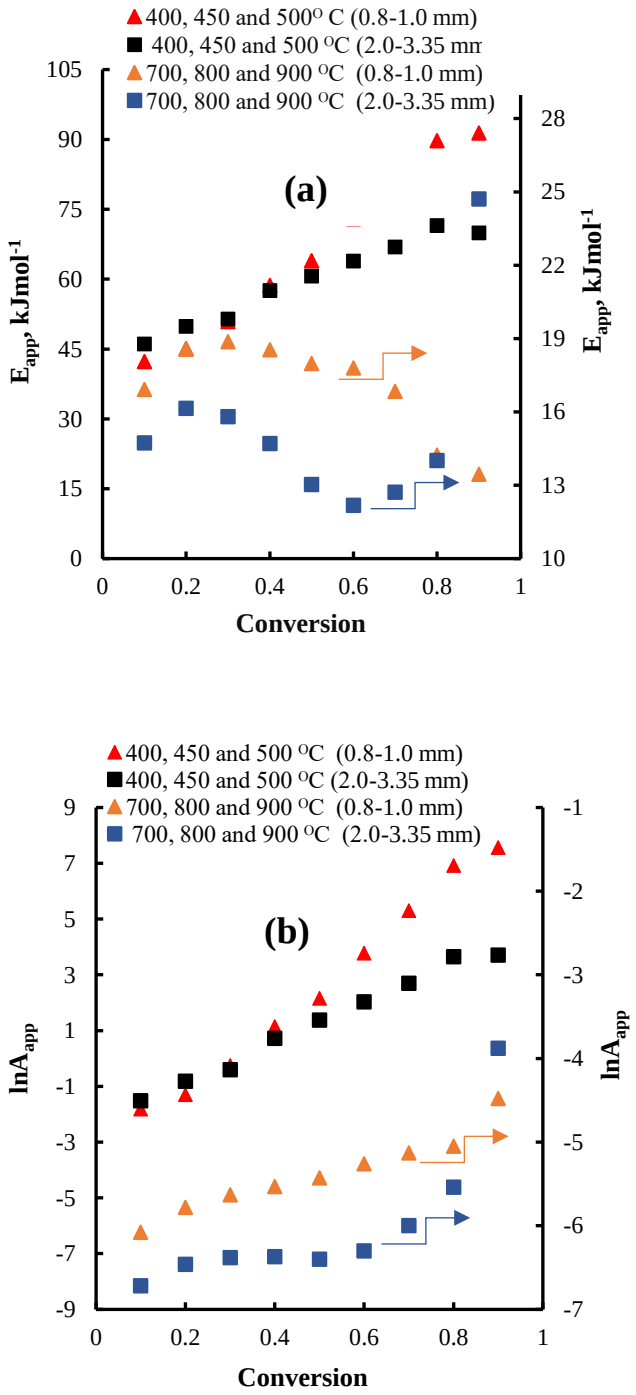

Figure 3-4 The (a) apparent activation energy (E_{app}) as a function of char conversion over different temperature ranges for 0.80-1.0 mm and 2.0-3.3 mm particles sizes and (b) The apparent pre-exponential factor (lnA_{app}) as a function of char conversion over different temperature ranges for 0.8-1.0 mm and 2.0-3.3 mm particle sizes. Symbols ▲,■,● etc. show the temperatures used to determine the kinetic parameters e.g. ▲ 400, 450 and 500 °C (0.80-1.0 mm) shows the E_{app} and lnA_{app} determined at temperatures 400, 450 and 500 °C for 0.80-1.0 mm particle size in Figure 3-4 a and b respectively. The data of E_{app} and lnA_{app} at 700, 800 and 900 °C for both particle sizes has been shown on the secondary vertical axis.

by internal and/or external diffusion and is strongly limited by the mass transport of the O_2 through the pore structure in the char matrix and/or to the char surface. This regime can be named as the diffusion-controlled regime. The data were further analysed in terms of the KCEs in a section later.

3.4.4 Kinetic compensation effects (KCEs)

3.4.4.1 Effects of char making conditions on the kinetic compensation effects

The data of E_{app} and lnA_{app} were plotted to get further insight into the char-O_2 reaction under different pyrolysis temperatures. Our results indicate that E_{app} varied in linear proportion with lnA_{app} showing the so-called KCEs (Figure 3-5). It can be seen clearly that KCEs are almost the same under both char-making conditions. It implies that all the char samples prepared under different pyrolysis temperatures in the range indicated follow the same reaction mechanism during the char-O_2 reaction.

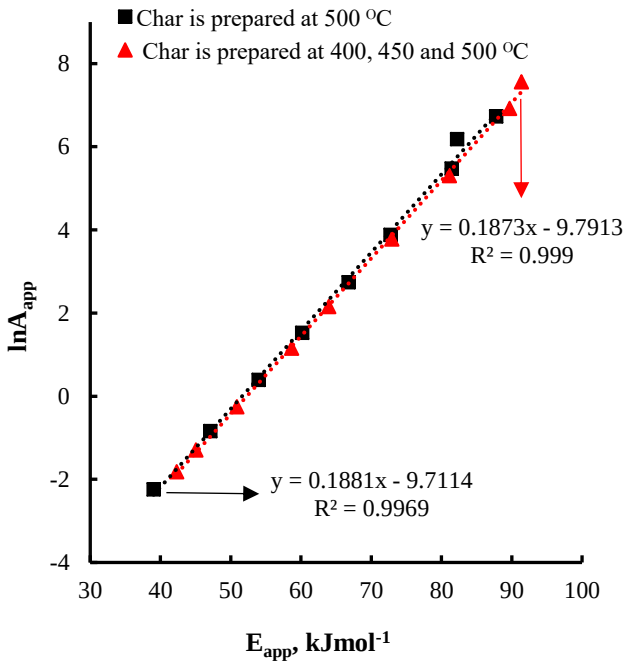

Figure 3-5 The insignificant effects of pyrolysis temperature on the apparent kinetic compensation effect at 400, 450 and 500 °C for 0.80-1.0 mm particle size.

3.4.4.2 Kinetic compensation effects in different regimes

The data of lnA_{app}vs. E_{app} were further plotted to get mechanistic insight into the char-O_2 reaction in terms of KCEs in different temperature regimes. For this purpose, the temperature ranges in the kinetic, mixed and diffusion-controlled regimes were used to calculate slopes 'm' and y-intercepts 'c' in the KCEs. Further, the effect of increasing temperature on slopes 'm' and y-intercepts 'c' was investigated in the KCEs of the mixed regime (Table 3-1). For the given particle sizes, the data in plots of lnA_{app}versus E_{app} demonstrate the following distinct trends (Figure 3-6):

a. In the kinetics-controlled regime, lnA_{app} and E_{app} increased simultaneously with char conversion level (Figure 3-4) in a strong linear functionality, exhibiting the so-called KCE that can be represented by Equation (3-1). The values of *m* and *c* in the kinetic-controlled regime are the functions of the char chemical structure and the reaction pathways followed during the char-O_2 reaction. The data in Figure 3-6 illustrate that the chemical nature and activation energy level of carbon atoms keep changing during char gasification. At any given conversion level, the KCE defines the activation energy level of the reactive sites present in the char structure during the char-O_2 reaction. It is considered that, at lower char conversion levels, reactive sites on small aromatic rings are preferentially consumed, resulting in a lower apparent activation energy and apparent pre-exponential factor [20]. As the char conversion increases, reactive sites on larger aromatic ring clusters become the more dominant sites of reaction, which result in a higher apparent activation energy and apparent pre-exponential factor. There was no considerable difference observed in the KCEs in the temperature range of 400 to 500 °C for 0.80-1.0 mm particle size (Figure 3-6). For instance, at temperatures of 400, 425 and 450 °C, the kinetic compensation relation is in close agreement with kinetic compensation relation at 400, 450 and 500 °C.

b. The KCE for particle size 2.0-3.3 mm at temperatures 400, 450 and 500 °C is considerably different from that of 0.80-1.0 mm particle size. This is obviously due to mass transfer limitations which start appearing in bigger particles at higher char conversions. Due to these mass transfer limitations, *m* and *c* values

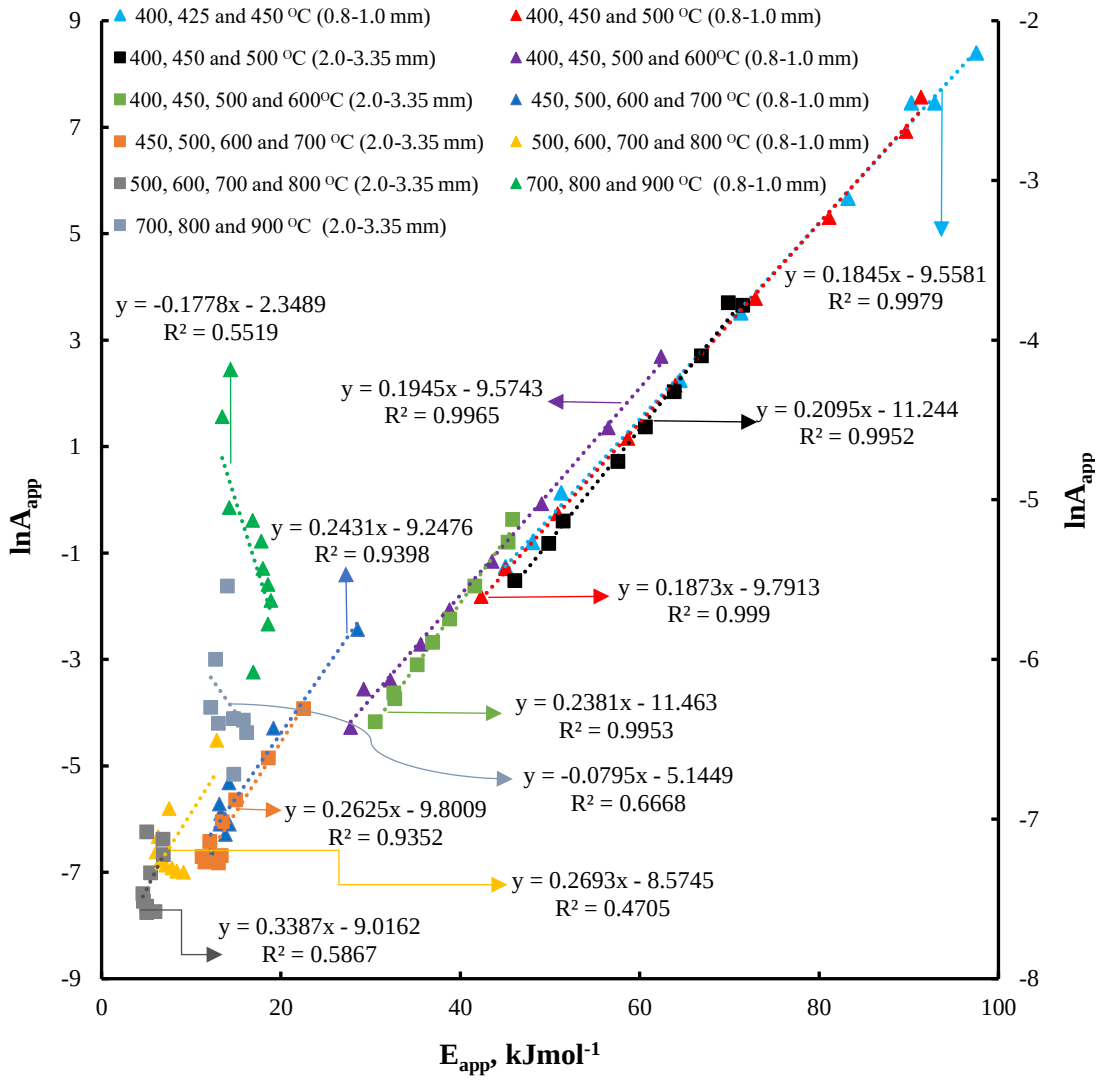

Figure 3-6 Kinetic compensation effects in the kinetic, mixed and diffusion-controlled regimes for 0.8-1.0 mm and 2.0-3.3 mm particle sizes. The data of lnA_{app} in the kinetics and mixed regimes have been shown on the primary vertical axis and the data of lnA_{app} in the diffusion-controlled regime have been shown on the secondary vertical axis. Symbols ▲ and ■ show the temperature range of char gasification used to determine the kinetic parameters.

in the KCE of 2.0-3.3 mm particles become higher than that of 0.80-1.0 mm particles (Table 3-1). This follows that *m* and *c* values are subject to change as a result of mass transfer limitations as being observed in the case of the bigger particles.

Table 3-1 Slopes '*m*' and y-intercepts '*c*' from the kinetic compensation effects in the kinetic, mixed and diffusion-controlled regimes.

Regime	**Temperature Range (Char gasification) °C**	**Slopes '*m*'**		**y-intercepts '*c*'**	
		Particle size, mm		Particle size, mm	
		0.80-1.0	**2.0-3.3**	**0.80-1.0**	**2.0-3.3**
Kinetic	400, 425, 450	0.1845		-9.5581	
	400, 450, 500	0.1873	0.2095	-9.7913	-11.244
Mixed	400, 450, 500, 600	0.1945	0.2381	-9.5743	-11.463
	450, 500, 600, 700	0.2431	0.2625	-9.2476	-9.8009
	500, 600, 700, 800	0.2693	0.3387	-8.5745	-9.0162
Diffusion	700, 800, 900	-0.1778	-0.0795	-2.3489	-5.1449

c. The KCEs observed in the mixed regime are pushed more towards the left of Figure 3-6 as the temperature range is increased in the mixed regime. Under such conditions, the char-O_2 reaction is jointly controlled by the mass transport of O_2 from the external char surface to active sites in the char and by the chemical reactivity of char. As a result, the *m* and *c* values in KCEs start increasing. For instance, at temperature range 450, 500, 600 and 700 °C, *m* and *c* values increase to $m = 0.2431$ and $c = -9.2476$ from $m = 0.1873$ and $c = -9.7913$ at temperature range 400, 450 and 500 °C for 0.8-1.0 mm particle size. Similar observations can be made on the KCEs of both particle sizes in the mixed regime where *m* and *c* values increase more for bigger particles than for smaller ones in any temperature range selected (Table 3-1). This is clearly due to higher internal-diffusion limitations in bigger particles that result in lower apparent activation energy and higher *m* values. This

indicates that *m* and *c* values in the mixed regime are higher than in the kinetics-controlled regime. The degrees of increase in *m* and *c* values within the mixed regime depends on the temperature range. Higher temperatures lead to more increase in *m* and *c* values and higher diffusion limitations in the mixed regime during the char-O_2 reaction.

d. There was a decrease in E_{app} with char conversions in the diffusion-controlled regime, although apparent pre-exponential factor increased with conversion. This shows the weak KCE. Moreover, due to decreasing activation energy with conversion, a negative slope '*m*' is observed on the kinetic compensation relation for both particle sizes. This shows that, in the diffusion-controlled regime, the KCE turns into a weak and/or negative KCE.

3.4.5 Isokinetic Temperature

Isokinetic temperature is the temperature at which the rates of the char-O_2 reaction become the same at various char conversion levels or a temperature at which the rates of the char-O_2 reaction at various char conversions undergo an inversion. The data in Figure 3-7 (a) demonstrate the possible existence of an isokinetic temperature at lower char conversion levels as Arrhenius plots seem to converge at one point. But at higher char conversions, it is difficult to determine the true isokinetic temperature. It is clear from Figure 3-7 (a) that Arrhenius plots at higher char conversions do not show an isokinetic temperature [20]. This implies that the compensation effect and isokinetic effect does not necessarily coexist [29]. It is evident from Figure 3-1 (c-d) that the reaction rate increases almost abruptly at higher char conversions in comparison with lower conversion levels. This is also revealed by the kinetic parameters that, at higher char conversion levels, apparent pre-exponential factor jumps higher suddenly to compensate the increase in apparent activation energy (Figure 3-4 a-b).

This effect can further be observed by the KCE at higher char conversions. The slope '*m*' in the KCE increases to m = 0.2106 for x = 0.70-0.90 from m = 0.1826 for x = 0.10-0.60. This infers that, at higher char conversion levels, the reaction switches from the kinetics-controlled regime to the mixed regime. Due to the presence of mass

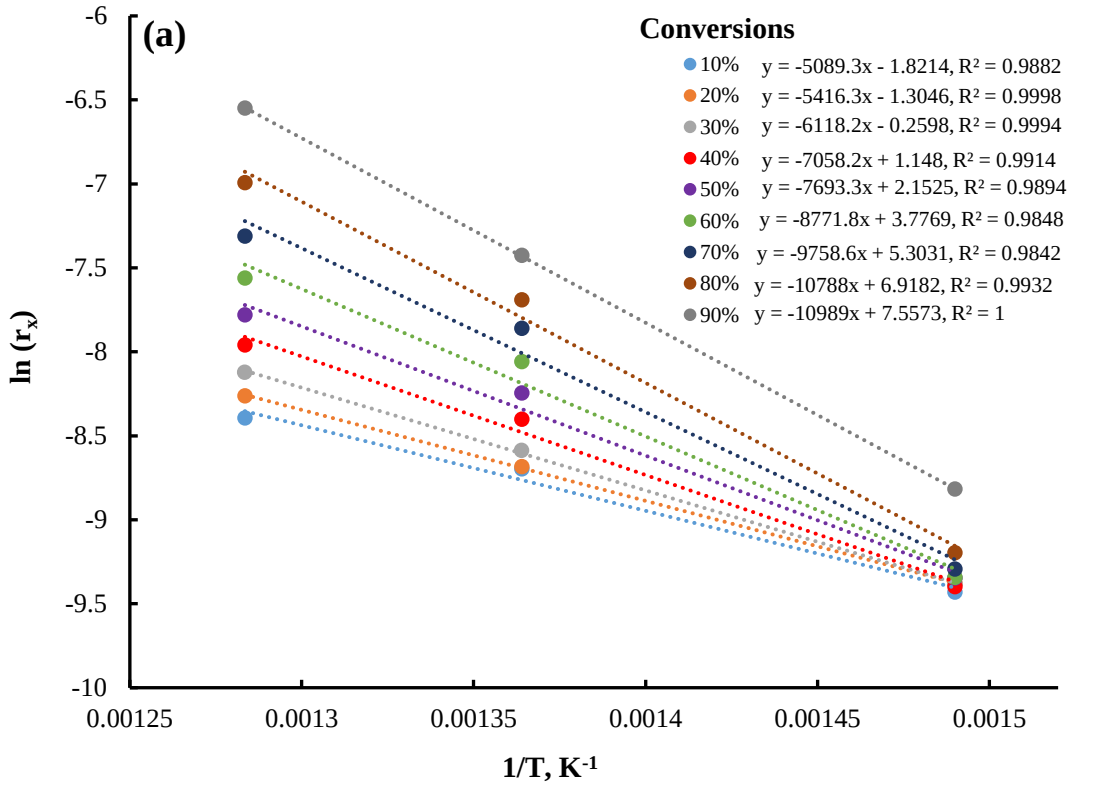

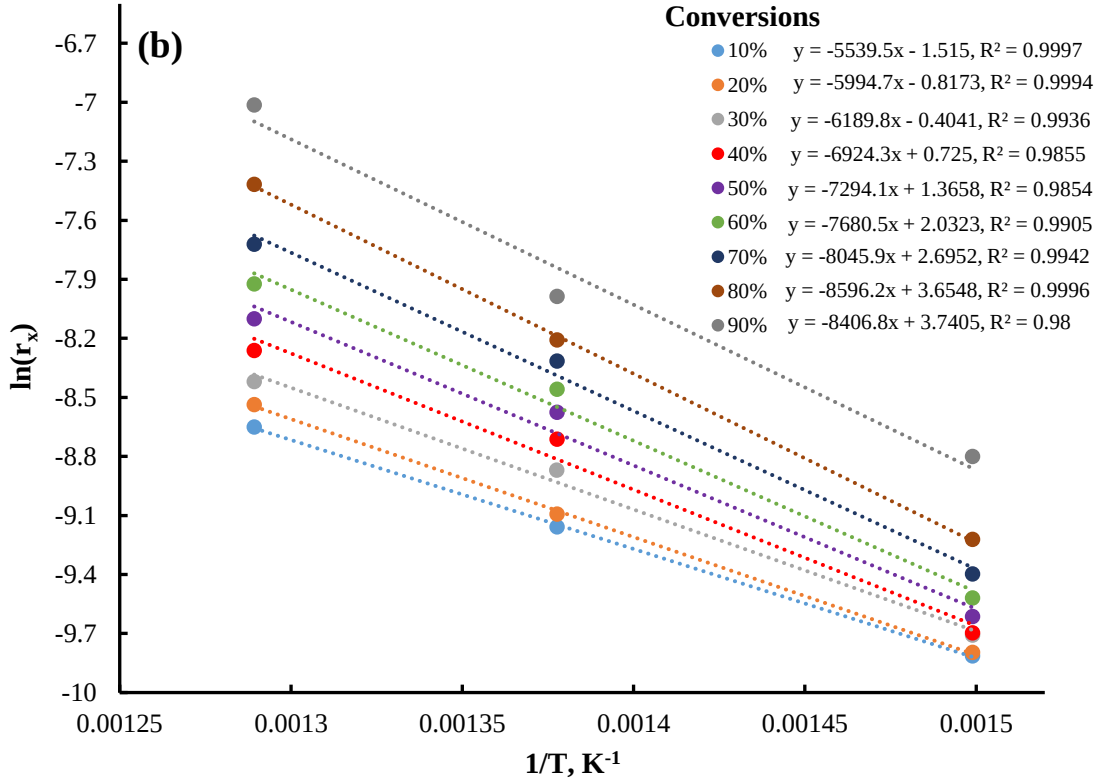

Figure 3-7 Arrhenius plots in the kinetic-controlled regime (400, 450 and 500 °C) at different char conversions for particle size ranges (a) 0.8-1.0 mm and (b) 2.0-3.3 mm.

transfer effects at higher char conversion levels, the isokinetic effect is also absent. Furthermore, the apparent pre-exponential factor includes the change in char properties as a result of the conversion. The absence of isokinetic temperature at higher char conversion also indicates that the change in char properties at higher conversions becomes significant as compared to those at lower conversions. Similarly, there seems to be a lesser tendency to converge in Arrhenius plots for bigger particles than the smaller ones (Figure 3-7 b). The bigger particles exhibit a strong KCE (Figure 3-6). However, the less tendency of bigger particles to show the isokinetic temperature in comparison with smaller particles is again due to intraparticle diffusion limitations and change in char properties that become significant at higher char conversions [20] (Figure 3-4).

3.5 Conclusions

The char-O_2 reaction demonstrates the kinetic compensation effect between apparent activation energy and apparent pre-exponential factors in the kinetics-controlled regime and in the mixed regime for both particle sizes i.e. 0.80-1.0 mm and 2.0-3.3 mm. However, in the diffusion-controlled regime, a weak and/or negative kinetic compensation effect is observed. The pyrolysis temperature has no effect on the kinetic compensation effects during the char-O_2 reaction in the kinetic regime, which indicates that the same reaction mechanism is followed at the same or at different pyrolysis temperatures over a narrow temperature range investigated. The char-O_2 reaction switches from the kinetics-controlled regime to the mixed regime at higher char conversions. Due to the appearance of these mass transfer limitations, the slopes '*m*' and y-intercepts '*c*' in the kinetic compensation effects are increased at higher conversion. The diffusion limitations in the mixed regime also increase the *m* and *c* values in the kinetic compensation effects for given particle size. The absence of tendency in Arrhenius plots to converge at higher char conversions shows that char properties change drastically at higher conversions.

3.6 References

[1] C.-Z. Li, Special issue - Gasification: A route to clean energy, Process Saf. Environ. Prot. 84 (2006) 407–408. doi:10.1205/psep.ed.0606.

[2] C.-Z. Li, Some recent advances in the understanding of the pyrolysis and gasification behaviour of Victorian brown coal, Fuel. 86 (2007) 1664–1683. doi:10.1016/j.fuel.2007.01.008.

[3] C.-Z. Li, Importance of volatile–char interactions during the pyrolysis and gasification of low-rank fuels – A review, Fuel. 112 (2013) 609–623. doi:10.1016/j.fuel.2013.01.031.

[4] H.L. Tay, C.-Z. Li, Changes in char reactivity and structure during the gasification of a Victorian brown coal: Comparison between gasification in O_2 and CO_2, Fuel Process. Technol. 91 (2010) 800–804. doi:10.1016/j.fuproc.2009.10.016.

[5] X. Guo, H.L. Tay, S. Zhang, C.-Z. Li, Changes in char structure during the gasification of a Victorian brown coal in steam and oxygen at 800 °C, Energy and Fuels. 22 (2008) 4034–4038. doi:10.1021/ef800528c.

[6] S. Zhang, J.I. Hayashi, C.-Z. Li, Volatilisation and catalytic effects of alkali and alkaline earth metallic species during the pyrolysis and gasification of Victorian brown coal. Part IX. Effects of volatile-char interactions on char-H_2O and char-O_2 reactivities, Fuel. 90 (2011) 1655–1661. doi:10.1016/j.fuel.2010.11.008.

[7] G. Ballal, K. Zygourakis, Gasification of coal chars with carbon dioxide and oxygen, Chem. Eng. Commun. 49 (1986) 181–195. doi:10.1080/00986448608911802.

[8] N.M. Laurendeau, Heterogeneous kinetics of coal char gasification and combusion, Prog. Energy Combust. Sci. 4 (1978) 221–270. doi:10.1016/0360-1285(78)90008-4.

[9] L. Nowicki, A. Antecka, T. Bedyk, P. Stolarek, S. Ledakowicz, The kinetics of gasification of char derived from sewage sludge, J. Therm. Anal. Calorim. 104

(2011) 693–700. doi:10.1007/s10973-010-1032-1.

[10] H.L. Tay, S. Kajitani, S. Zhang, C.-Z. Li, Effects of gasifying agent on the evolution of char structure during the gasification of Victorian brown coal, Fuel. 103 (2013) 22–28. doi:10.1016/j.fuel.2011.02.044.

[11] E. Bar-Ziv, I.I. Kantorovich, Mutual effects of porosity and reactivity in char oxidation, Prog. Energy Combust. Sci. 27 (2001) 667–697. doi:10.1016/S0360-1285(01)00006-5.

[12] T. Li, L. Zhang, L. Dong, S. Wang, Y. Song, L. Wu, C.-Z. Li, Effects of char chemical structure and AAEM retention in char during the gasification at 900 °C on the changes in low-temperature char-O_2 reactivity for Collie sub-bituminous coal, Fuel. 195 (2017) 253–259. doi:10.1016/j.fuel.2017.01.076.

[13] X. Li, J. ichiro Hayashi, C.-Z. Li, Volatilisation and catalytic effects of alkali and alkaline earth metallic species during the pyrolysis and gasification of Victorian brown coal. Part VII. Raman spectroscopic study on the changes in char structure during the catalytic gasification in air, Fuel. 85 (2006) 1509–1517. doi:10.1016/j.fuel.2006.01.011.

[14] T.W. Kwon, J.R. Kim, S.D. Kim, W.H. Park, Catalytic steam gasification of lignite char, Fuel. 68 (1989) 416–421. doi:10.1016/0016-2361(89)90261-5.

[15] S. Li and Y.Cheng, Catalytic gasification of gas-coal char in CO_2, Fuel. 74 (1995) 456–458.

[16] A.P. Dhupe, A.N. Gokarn, L.K. Doraiswamy, Investigations into the compensation effect at catalytic gasification of active charcoal by carbon dioxide, Fuel. 70 (1991) 839–844. doi:10.1016/0016-2361(91)90192-D.

[17] G.C. Bond, M.A. Keane, H. Kral, J.A. Lercher, Compensation phenomena in heterogeneous catalysis: general principles and a possible explanation, Catal. Rev. 42 (2000) 323–383. doi:10.1081/CR-100100264.

[18] N. Koga, A review of the mutual dependence of Arrhenius parameters evaluated by the thermoanalytical study of solid-state reactions: The kinetic compensation

effect, Thermochim. Acta. 244 (1994) 1–20. doi:10.1016/0040-6031(94)80202-5.

[19] T. Bligaard, K. Honkala, A. Logadottir, J.K. Nørskov, S. Dahl, C.J.H. Jacobsen, On the Compensation Effect in Heterogeneous Catalysis, J. Phys. Chem. B. 107 (2003) 9325–9331. doi:10.1021/jp034447g.

[20] H. Wu, X. Li, J.I. Hayashi, T. Chiba, C.-Z. Li, Effects of volatile-char interactions on the reactivity of chars from NaCl-loaded Loy Yang brown coal, Fuel. 84 (2005) 1221–1228. doi:10.1016/j.fuel.2004.06.037.

[21] K. Yip, E. Ng, C.-Z. Li, J.I. Hayashi, H. Wu, A mechanistic study on kinetic compensation effect during low-temperature oxidation of coal chars, Proc. Combust. Inst. 33 (2011) 1755–1762. doi:10.1016/j.proci.2010.07.073.

[22] M. Asadullah, S. Zhang, Z. Min, P. Yimsiri, C.-Z. Li, Importance of biomass particle size in structural evolution and reactivity of char in steam gasification, Ind. Eng. Chem. Res. 48 (2009) 9858–9863. doi:10.1021/ie901214z.

[23] D.M. Quyn, H. Wu, J. Hayashi, C.-Z. Li, Volatilisation and catalytic effects of alkali and alkaline earth metallic species during the pyrolysis and gasification of Victorian brown coal. Part IV. Catalytic effects of NaCl and ion-exchangeable Na in coal on char reactivity☆, Fuel. 82 (2003) 587–593. doi:10.1016/S0016-2361(02)00323-X.

[24] D.M. Quyn, H. Wu, C.-Z. Li, Volatilisation and catalytic effects of alkali and alkaline earth metallic species during the pyrolysis and gasification of Victorian brown coal. Part I. Volatilisation of Na and Cl from a set of NaCl-loaded samples, Fuel. 81 (2002) 143–149. doi:10.1016/S0016-2361(01)00127-2.

[25] C.-Z. Li, Advances in the science of Victorian Brown Coal, 2004. doi:10.1016/B978-0-08-044269-3.X5000-6.

[26] M. Asadullah, S. Zhang, C.-Z. Li, Evaluation of structural features of chars from pyrolysis of biomass of different particle sizes, Fuel Process. Technol. 91 (2010) 877–881. doi:10.1016/j.fuproc.2009.08.008.

[27] J.J. Hernández, G. Aranda-Almansa, A. Bula, Gasification of biomass wastes in an entrained flow gasifier: Effect of the particle size and the residence time, Fuel Process. Technol. 91 (2010) 681–692. doi:10.1016/j.fuproc.2010.01.018.

[28] S. Zhang, Z. Min, H.L. Tay, Y. Wang, L. Dong, C.-Z. Li, Changes in char structure during the gasification of mallee wood: Effects of particle size and steam supply, Energy and Fuels. 26 (2012) 193–198. doi:10.1021/ef2011589.

[29] L. Liu, Q.X. Guo, Isokinetic relationship, isoequilibrium relationship, and enthalpy-entropy compensation, Chem. Rev. 101 (2001) 673–695. doi:10.1021/cr990416z.

4.0 Chapter

Mechanistic insights into the kinetic compensation effects during the gasification of biochar in H_2O

4.1 Abstract

This study aims to gain insight into the mechanism and kinetics during the gasification of biochar in steam, which was formed in situ in a fluidised-bed reactor using mallee wood in two particle size ranges of 0.80-1.0 mm and 2.0-3.3 mm. The overall biochar gasification rate and the formation rates of key product components were calculated by continuously monitoring the product gas stream with a quadrupole mass spectrometer. The kinetic compensation effects reveal that CO and CO_2 are both formed from the heterogeneous reactions between the biochar surface and H_2O. CO_2 is formed either by the surface (biochar)-catalysed water-gas-shift reaction or directly from the carbon active sites involving the same intermediate for the formation of CO, as revealed by the apparent activation energies and apparent pre-exponential factors for CO and CO_2 formation. The changes in the particle size of biomass substrate do not affect the extent of the kinetic compensation effects of biochar consumption and formation of CO, CO_2, and H_2 in the kinetics-controlled and mixed regimes. The similar extent of the kinetic compensation effects of H_2 formation and biochar consumption for both particle sizes indicates that the formation of H_2 also mainly involves the carbon active sites on the biochar surface instead of the gas-phase water-gas-shift reaction.

Keywords: Kinetic compensation effect; biochar gasification; carbon active sites; mallee wood.

4.2 Introduction

Gasification is an important route for the clean utilisation of biomass [1-3]. The kinetics and mechanism of biochar gasification are important to understand the gasification process [1–3]. The biochar-H_2O reaction is the most important reaction during gasification, playing a vital role in the production of synthesis gas. Numerous kinetic studies have examined the mechanism of the char-H_2O reaction [4–13]. There is still a debate whether CO and CO_2 are the primary products of the char-H_2O gasification or CO_2 is formed mainly from the subsequent gas-phase water-gas-shift reaction [14-19]. Further work is required to understand the mechanisms of CO and CO_2 formations during the char-H_2O gasification.

The kinetic compensation effects (KCEs) are a key feature for understanding the char-gas reaction mechanisms [20–22]. The KCE relates the apparent activation energy (E_{app}) and apparent pre-exponential factor (lnA_{app}) during the char gasification at various conversion levels [23–25]. This can be represented by the following equation:

$$lnA_{app} = mE_{app} + c \qquad (\text{Eq. } 4-1)$$

Eq. 4-1 is named as the KCE. Our previous study [26] on the oxidation of brown coal char has reported the KCE and given a probable explanation for it. This study explained that there were sites of various energy levels dispersed inside the char non-homogeneously. The KCE was observed because of the continuous formation and consumption of active sites during char conversion. The KCE was also observed during the oxidation of various carbon materials [27]. Our recent work [28] has investigated the KCEs during the gasification of biochar in O_2 in a fluidised-bed reactor. This study has revealed that the extent of KCE is different in the kinetics-controlled, mixed and diffusion-controlled regimes during the biochar-O_2 reaction. However, all these studies have been limited to the O_2 atmosphere only. Therefore, it is significant to understand the biochar-H_2O gasification from the perspective of the KCE to have more understanding of the char-H_2O reaction. Moreover, it is still unclear how the KCEs of the char gasification and formation of key product components i.e. CO, CO_2 and H_2 change during the char-H_2O reaction. During steam gasification of char, CO, CO_2 and H_2 can be formed by the following overall reactions:

$C(s) + H_2O(g) \longrightarrow CO(g) + H_2(g)$ (R 4-1)

$C(s) + 2H_2O(g) \longrightarrow CO_2(g) + 2H_2(g)$ (R 4-2)

$CO(g) + H_2O(g) \longrightarrow CO_2(g) + H_2(g)$ (R 4-3)

It is commonly believed that CO is formed from the char surface during the char-H_2O reaction [29, 30]. However, there is a debate in the literature on CO_2 formation. Some past studies [14,16,19] on the char-H_2O reaction considered the overall carbon reactivity to examine the char-H_2O reaction and considered that the water-gas-shift reaction was mainly responsible for the formation of CO_2. On the contrary, other studies [15,17,18] believed that CO and CO_2 were the primary products of the char-H_2O surface reaction. Fundamental knowledge is required in terms of the kinetics of CO, CO_2 and H_2 formation. Moreover, it is fundamentally important to study the kinetics of CO, CO_2 and H_2 formation at higher temperatures. At higher temperatures, gasification reaction rates are affected or even controlled by the diffusion of the H_2O to the interior pores inside the char in addition to the intrinsic kinetics of the char surface. The water-gas-shift reaction rate also increases and acquires equilibrium rapidly at higher temperatures in comparison to that at lower temperatures. Therefore, the steam gasification of char requires an investigation in terms of KCEs over a broad range of temperature, which has not gained significant attention previously.

This study focuses on investigating the mechanism of biochar-H_2O reaction from the perspective of the KCEs. The study investigates the kinetics and the KCEs of biochar consumption and formation of CO, CO_2, and H_2 in the kinetics-controlled and mixed regimes and provides an insight into the reaction pathways during the gasification of biochar in steam.

4.3 Experimental

The gasification experiments were performed using a quartz fluidised-bed reactor. The experimental procedures have been outlined in Chapter 2. Around 2.0 g of the mallee wood sample was used in each experiment with the feeding rate of 0.20 g/min. The reactor was held in UHP argon for 5 minutes after feeding. This ensures the complete

removal of volatiles. After 5 min of holding, the feeding of the steam was commenced by means of an HPLC pump. The HPLC pump fed accurately metered demineralised water into the reaction zone, which was converted into 15% steam of the argon flow. The key reaction products including CO, CO_2, CH_4 and H_2 were monitored by a quadrupole mass spectrometer (QMS Prisma^{TM} 200) until the signal of CO, CO_2, CH_4 and H_2 on mass spectrometer returned to initial baselines. The product gas mixture was cooled to remove excess steam before being introduced into the QMS 200.

At a given biochar conversion, the rate of char consumption (r_c) and the formation rates of CO (r_{CO}), CO_2 (r_{CO_2}), and H_2 (r_{H_2}) were calculated using the Eq. below:

$$r_i = \frac{1}{W_i}\frac{dW_i}{dt} = f(x)g(p)A\exp\left(-\frac{E_{app}}{RT}\right) = A_i\, exp\left(-\frac{E_i}{RT}\right) \qquad (\text{Eq. } 4-2)$$

Where i in Eq. 4-2 stands for the char gasification, CO, CO_2 or H_2 formation. The details of Eq. 4-2 are described in Chapter 2. The apparent activation energy (E_{app}) and the apparent pre-exponential factors (A_{app}) of biochar consumption and formation of CO, CO_2 and H_2 were acquired by constructing the Arrhenius plots between *ln* (r_C) *ln* (r_{CO}), *ln* (r_{CO2}) or *ln* (r_{H2}) vs. 1/*T* at the given biochar conversions where *T* is in the Kelvin scale.

4.4 Results and Discussion

4.4.1 Biochar Reactivity

Figure 4-1 (a-d) represent the rate of biochar consumption (r_c) and the rate of hydrogen formation (r_{H_2}) during the in situ gasification of biochar in H_2O using mallee wood in two particle size ranges of 0.80-1.0 mm and 2.0-3.3 mm. The gasification of mallee biochar in H_2O is insignificant below 700 °C [5,6] and the maximum temperature, which can be achieved in the furnace available is 950 °C. Because of these considerations, a temperature range of 700 to 950 °C has been selected in this study. The data in Figure 4-1 (a-d) indicate that the rates of biochar consumption and hydrogen formation both increased as the temperature is increased from 700 to 950 °C

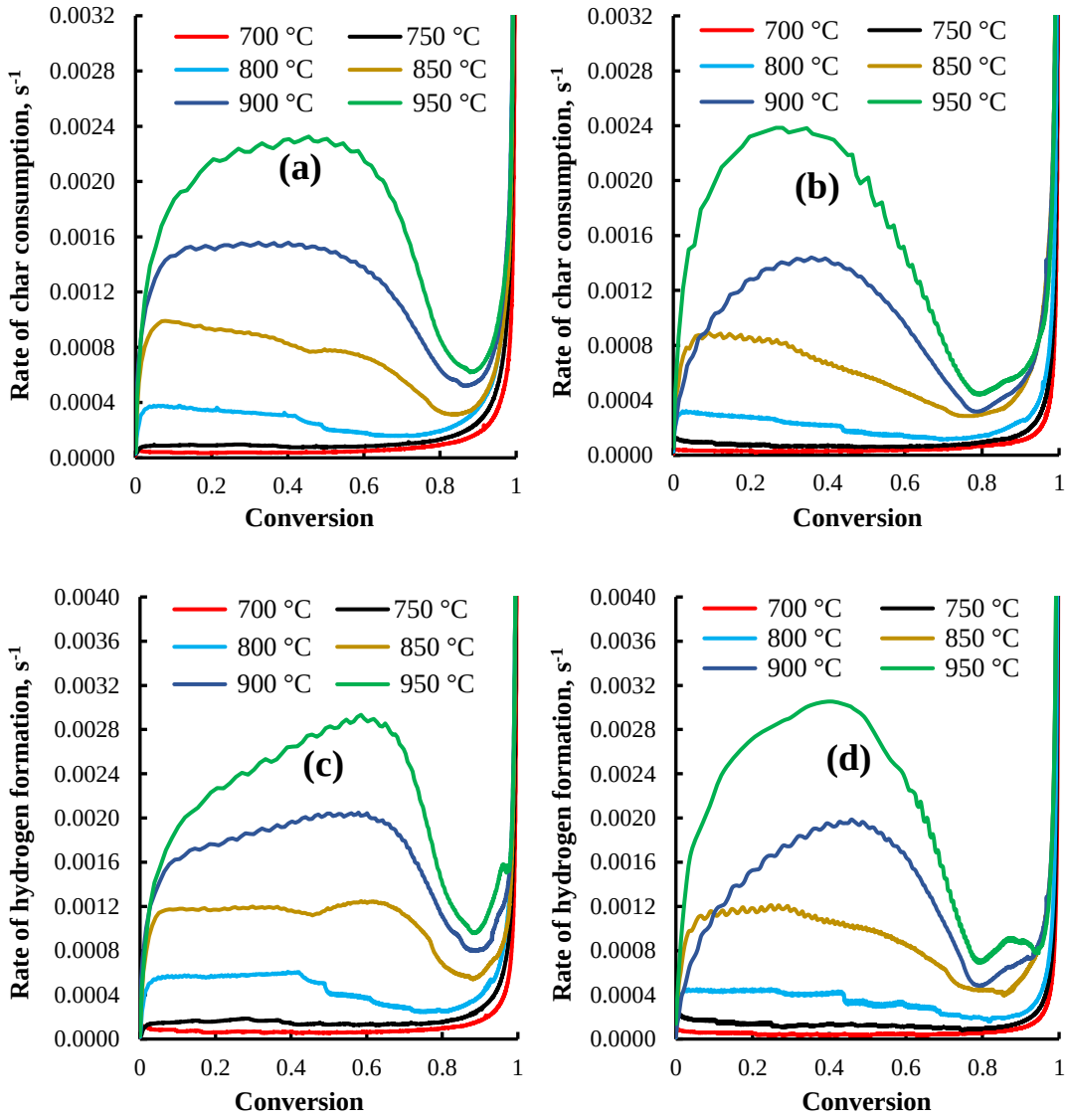

Figure 4-1 Rate of char gasification vs. char conversion from 700 to 950 °C for particle sizes of (a) 0.80-1.0 mm and (b) 2.0-3.3 mm; and rate of hydrogen formation vs. char conversion from 700 to 950 °C for particle sizes of (c) 0.80-1.0 mm and (d) 2.0-3.3 mm.

for both particle sizes. However, the smaller size particles i.e. 0.80-1.0 mm exhibited slightly higher rates of biochar consumption and H_2 formation in the given temperature range. Moreover, both rates varied with conversion in a similar way in the given temperature range for both particle sizes.

4.4.2 Differentiation between kinetics-controlled and mixed regimes

It is evident from Figure 4-2 that Arrhenius plots had significantly high slopes in the temperature range from 700 to 850 °C and started decreasing as the temperature range is increased from 850 to 950 °C. Based on this variation, the Arrhenius plots are

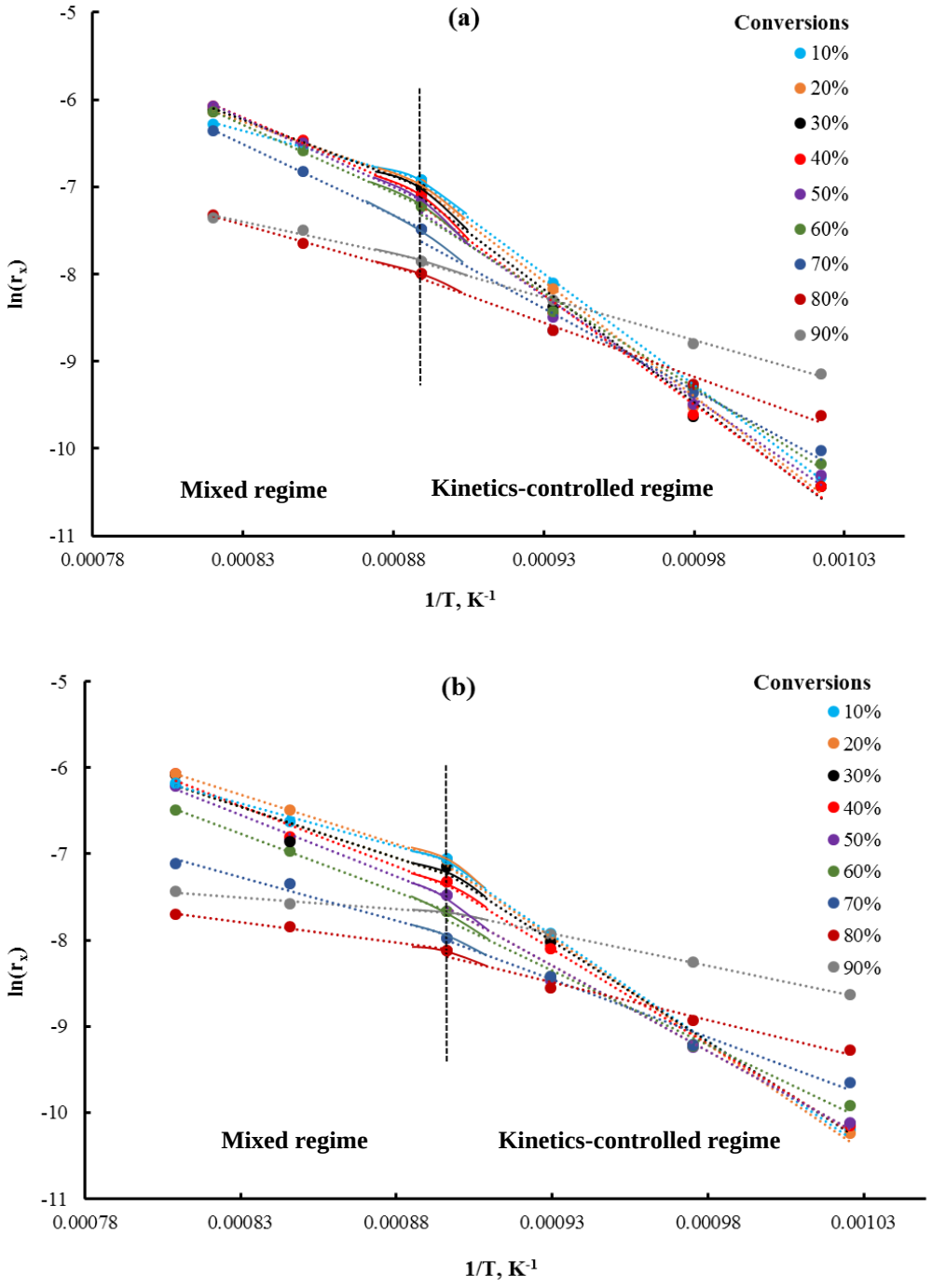

Figure 4-2 Arrhenius plots of the biochar-H_2O reaction at different char conversions for the particle size ranges of (a) 0.8- 1.0 mm and (b) 2.0-3.3 mm.

categorised into two sections i.e. 700 to 850 °C (kinetics-controlled regime) and 850 to 950 °C (mixed regime).

4.4.3 Effects of conversion on the kinetic parameters

The data in Figure 4-3 (a-d) display the kinetic parameters of biochar consumption and formation of the key products i.e. CO, CO_2 and H_2 during the biochar-H_2O reaction in the kinetics-controlled and mixed regimes for 0.80-1.0 mm and 2.0-3.3 mm particle sizes. Figure 4-3 illustrates that, for both particle sizes, the apparent activation energy and apparent pre-exponential factor of biochar consumption and formation of CO, CO_2, and H_2 varied with biochar conversion level both in the kinetics-controlled and mixed regimes.

In the kinetics-controlled regime, the apparent activation energy and apparent pre-exponential factors of biochar consumption and formation of CO, CO_2, and H_2 appeared to decrease with conversion for both particle sizes. Further, for both particle

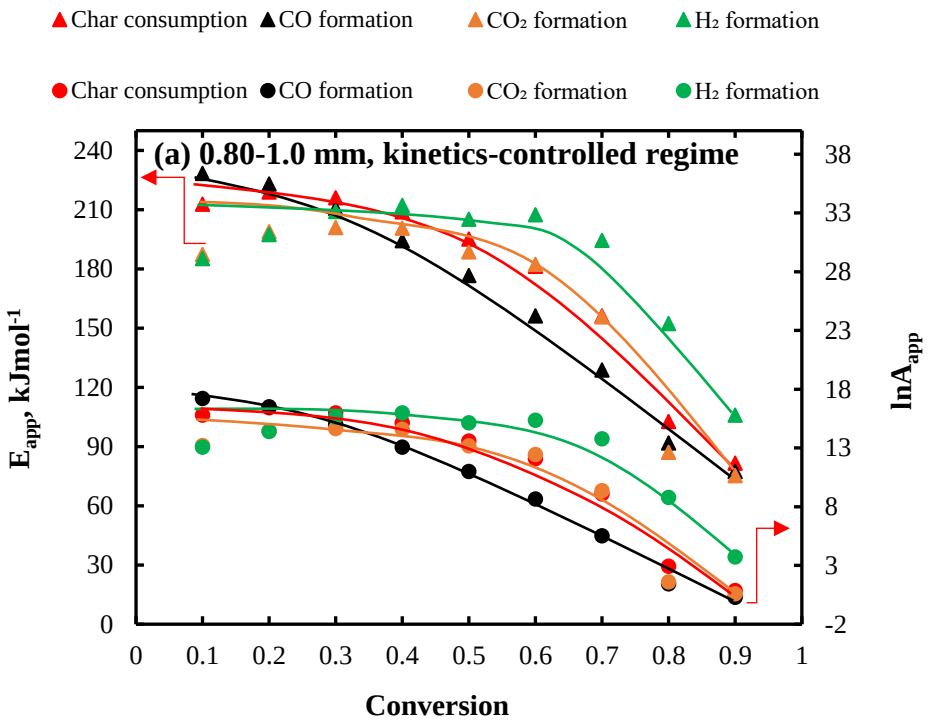

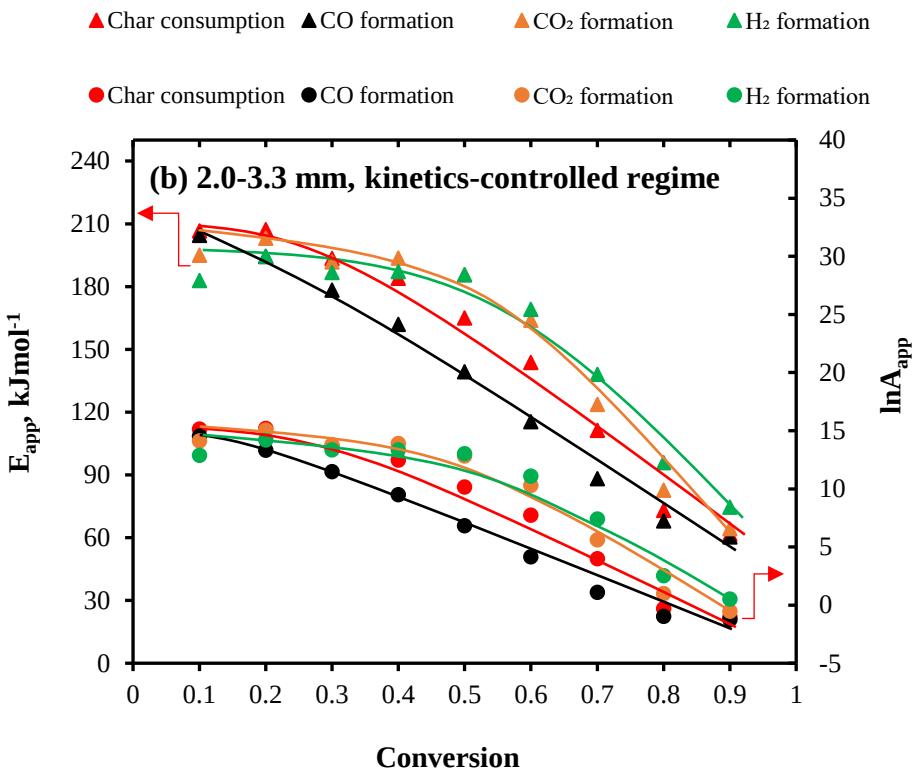
Char consumption
CO formation
CO₂ formation
H₂ formation
Char consumption
CO formation
CO₂ formation
H₂ formation
(b) 2.0-3.3 mm, kinetics-controlled regime
E_app, kJmol-1
lnA_app
Conversion
0
30
60
90
120
150
180
210
240
-5
0
5
10
15
20
25
30
35
40
0
0.1
0.2
0.3
0.4
0.5
0.6
0.7
0.8
0.9
1

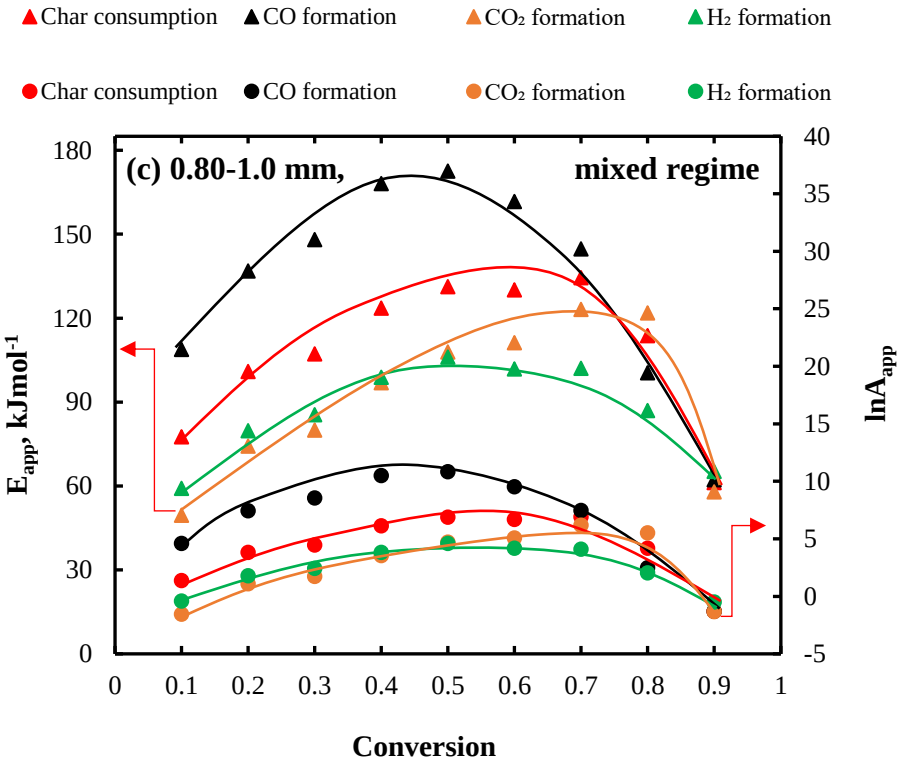
Char consumption
CO formation
CO₂ formation
H₂ formation
Char consumption
CO formation
CO₂ formation
H₂ formation
(c) 0.80-1.0 mm,
mixed regime
E_app, kJmol-1
lnA_app
Conversion
0
30
60
90
120
150
180
-5
0
5
10
15
20
25
30
35
40
0
0.1
0.2
0.3
0.4
0.5
0.6
0.7
0.8
0.9
1

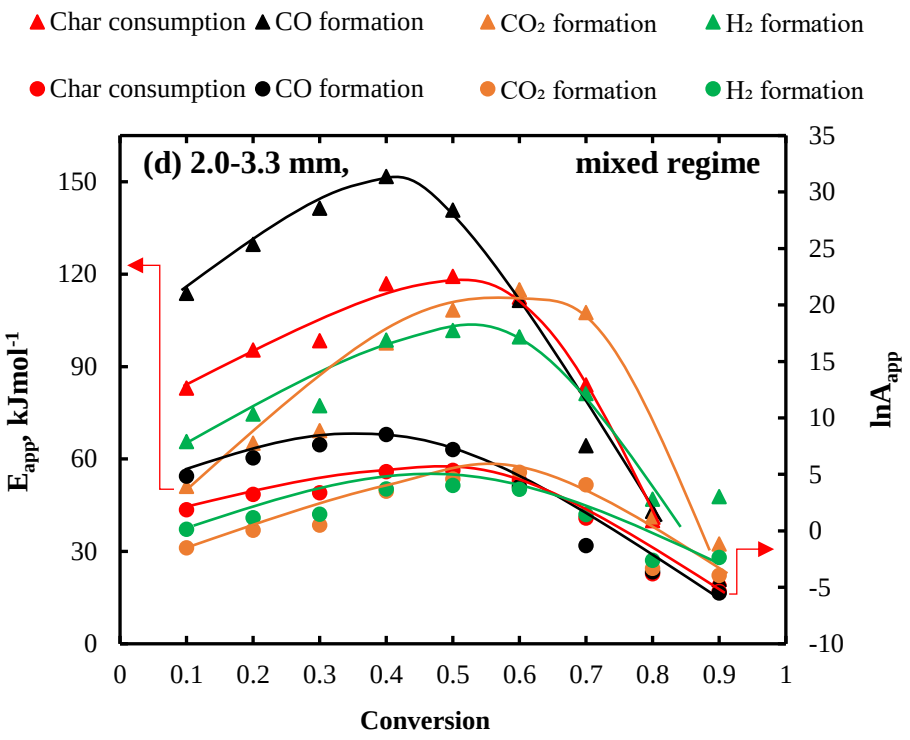

Figure 4-3 The apparent activation energy (E_{app}) and the apparent pre-exponential factor (lnA_{app}) of biochar consumption and formation of CO, CO_2 and H_2 as a function of biochar conversion in the kinetics-controlled regime for particle sizes of (a) 0.80-1.0 mm and (b) 2.0-3.3 mm. The apparent activation energy and apparent pre-exponential factor of biochar consumption and formation of CO, CO_2 and H_2 as a function of biochar conversion in the mixed regime for particle sizes of (c) 0.80-1.0 mm and (d) 2.0-3.3 mm particles sizes, ▲ and ● are used to indicate E_{app} and lnA_{app} respectively in Figure 4-3 (a-d). The data of lnA_{app} are shown on the secondary vertical axis in Figure 4-3 (a-d).

sizes, there is an insignificant difference in the apparent activation energy and the apparent pre-exponential factors for biochar consumption and formation of CO, CO_2, and H_2 implying a true kinetics-controlled regime in the temperature range from 700 to 850 °C.

The decrease in the apparent activation energy and apparent pre-exponential factor of biochar gasification and formation of CO, CO_2, and H_2 with conversion indicates that active sites on the biochar surface, which essentially form CO, CO_2, and H_2, change with biochar conversion. Further, if CO_2 were formed mainly because of gas-phase

water-gas-shift reaction, the formation of CO_2 would follow kinetics represented by a single set of activation energy and pre-exponential factor and should not change with biochar conversion level. However, the apparent activation energy and apparent pre-exponential factor of CO and CO_2 formation have changed with biochar conversion, indicating that large proportions of CO and CO_2 are formed because of a heterogeneous biochar-H_2O reaction. In addition to this, the activation energy levels of CO and CO_2 formation are found to be quite close to each other (compared at the same conversion levels). This suggests that CO_2 can be formed either by the surface-catalysed water-gas-shift reaction or it can be formed directly from the biochar surface through the same intermediate as that for CO formation. For example, this can be represented as:

$$C(O) \longrightarrow CO(g) \qquad \text{(R 4-4)}$$

$$C(O) + C(O) \longrightarrow CO_2(g) + C \qquad \text{(R 4-5)}$$

$$C(CO) + H_2O(g) \longrightarrow CO_2(g) + H_2(g) + C \qquad \text{(R 4-6)}$$

In the mixed regime, the kinetic parameters of biochar consumption and formation of CO, CO_2, and H_2 followed a quite different trend from that in the kinetics-controlled regime for the given particle sizes. The apparent activation energy and pre-exponential factor of biochar consumption and formation of CO, CO_2 and H_2 increased with conversion up to x = 0.5 or 0.6 and then decreased at higher conversions. The same trends were observed for both particle sizes. However, nearly at all conversion levels, the larger particles demonstrated slightly lower apparent activation energy and lower apparent pre-exponential factor of biochar consumption and formation of CO, CO_2, and H_2 due to higher diffusion limitations.

Moreover, the apparent activation energy and the apparent pre-exponential factors of CO and CO_2 formation also changed with biochar conversion level in the mixed regime. On the contrary, the gas phase water-gas-shift reaction would have given a single activation energy and single pre-exponential factor independent of biochar conversion level. These results in the mixed regime also indicate that both CO and CO_2 are mainly formed because of the heterogeneous reaction between the biochar surface and H_2O.

4.4.4 Kinetic compensation effects (KCEs)

4.4.4.1 Effect of biochar making conditions on the observed KCEs

The effect of pyrolysis temperature on the kinetic parameters was investigated during the steam gasification of biochar in the kinetics-controlled regime. For this purpose, samples of biochar were made at single pyrolysis temperature i.e. 850 °C or at different pyrolysis temperatures (700, 750, 800 and 850 °C). The biochar samples prepared at single or at different pyrolysis temperatures were further gasified in situ at 700, 750, 800 and 850 °C with 15% H_2O-Ar.

Our results indicate that the apparent activation energy and the apparent pre-exponential factor both decreased with biochar conversion when pyrolysis temperature was the same or when pyrolysis temperatures were different (Appendix-I, Figure S1). Further, E_{app}decreased in linear proportion with lnA_{app} demonstrating the KCEs at both biochar preparation conditions (Figure 4-4). It is found that pyrolysis at single temperature i.e. 850 °C with subsequent in situ gasification resulted in slightly lower apparent activation energy and lower apparent pre-exponential factor than pyrolysis at different temperatures followed by in situ gasification. This change is more likely because of the ageing effects in the biochar, which appear when the pyrolysis and the biochar gasification temperatures were different. For instance, at a biochar-making temperature of 850 °C and biochar gasification temperature of 700 °C, the temperature of the biochar (850 °C) was to be decreased to 700 °C, which resulted in a higher holding time (ageing effect) in comparison to when the pyrolysis and biochar gasification temperatures were same [30]. However, the similar KCEs for both biochar preparing conditions suggest that the single or different pyrolysis temperatures do not affect the reaction pathways during the biochar gasification in 15% H_2O-Ar [28].

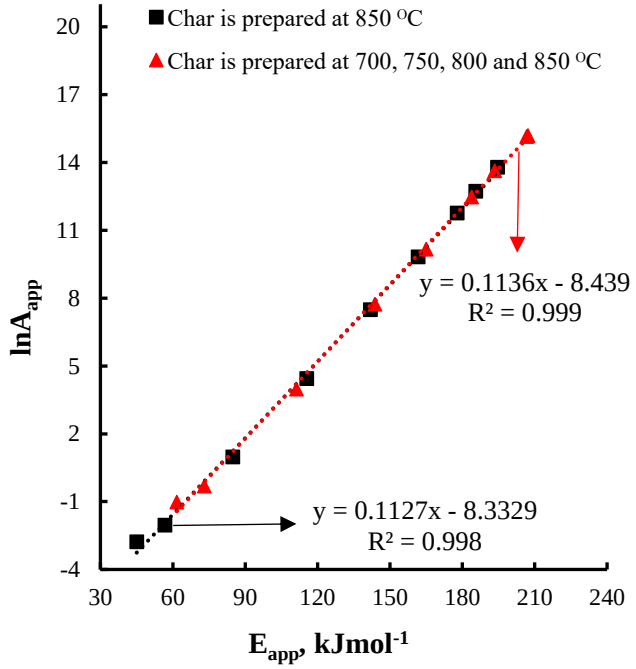

Figure 4-4 The insignificant effect of pyrolysis temperature on the kinetic compensation effects during the biochar-H_2O gasification at 700, 750, 800 and 850 °C for 2.0-3.3 mm particle size

4.4.4.2 Kinetic compensation effects (KCEs) in the kinetics-controlled and mixed regimes

The kinetic parameters of biochar consumption and formation of CO, CO_2, and H_2 were utilised to calculate the KCEs in the kinetics-controlled and mixed regimes. For this purpose, the temperature ranges of kinetics-controlled and mixed regimes were utilised to determine '*m*' and '*c*' in the KCEs. Figure 4-5 (a-b), revealed the following features of the KCEs during the biochar-H_2O gasification:

a. In the kinetics-controlled regime, lnA_{app} and E_{app} of biochar consumption and formation of CO, CO_2 and H_2 demonstrated an obvious KCE as represented by Equation (4-1). Figure 4-3 (a-b) shows that the apparent activation energy and pre-exponential factors are different at different biochar conversion levels. This indicates that the chemical nature of the reactive sites/intermediate formed on the biochar surface (pore) changes with the progress of biochar conversion during the biochar-H_2O reaction. It is also clear

(Figure 4-3 a-b) that at lower biochar conversion, it requires higher activation energy to activate the biochar substrate resulting in a higher pre-exponential factor. With the progress of biochar conversion, the concentration of the oxygen-containing active sites e.g. C(O) increases in the biochar matrix. This has been demonstrated by the increase in the observed Raman intensity with increasing conversion for low-rank fuels [9,11]. Moreover, the concentrations of alkali and alkaline earth metallic (AAEM) species in the residual biochar also increase as the biochar conversion is progressed [28,31–33]. Therefore, toward increasing biochar conversion levels, oxygen-containing active sites e.g. C(O) and AAEM species become increasingly available in the biochar matrix. This results in lowering the activation energy towards higher biochar conversion.

b. The similar activation energy levels and similar '*m*' and '*c*' suggest that the extent of the KCEs of biochar consumption and formation of CO, CO_2, and H_2

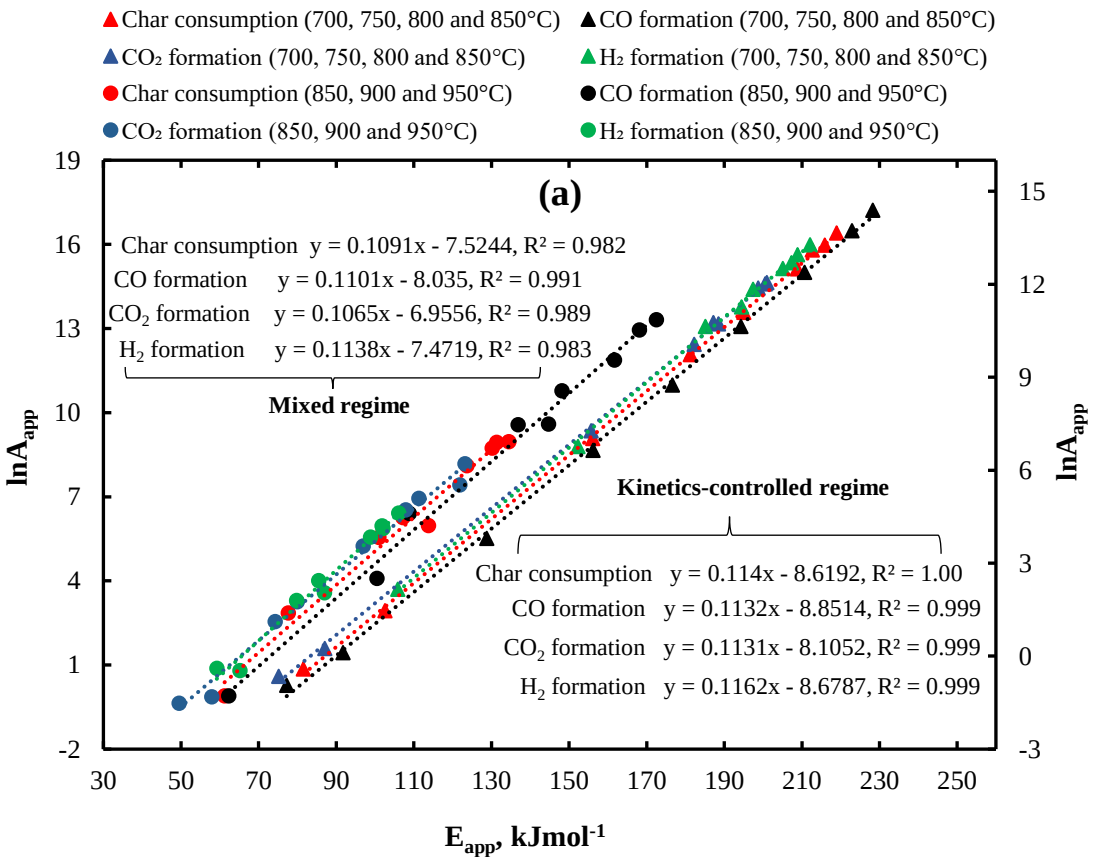

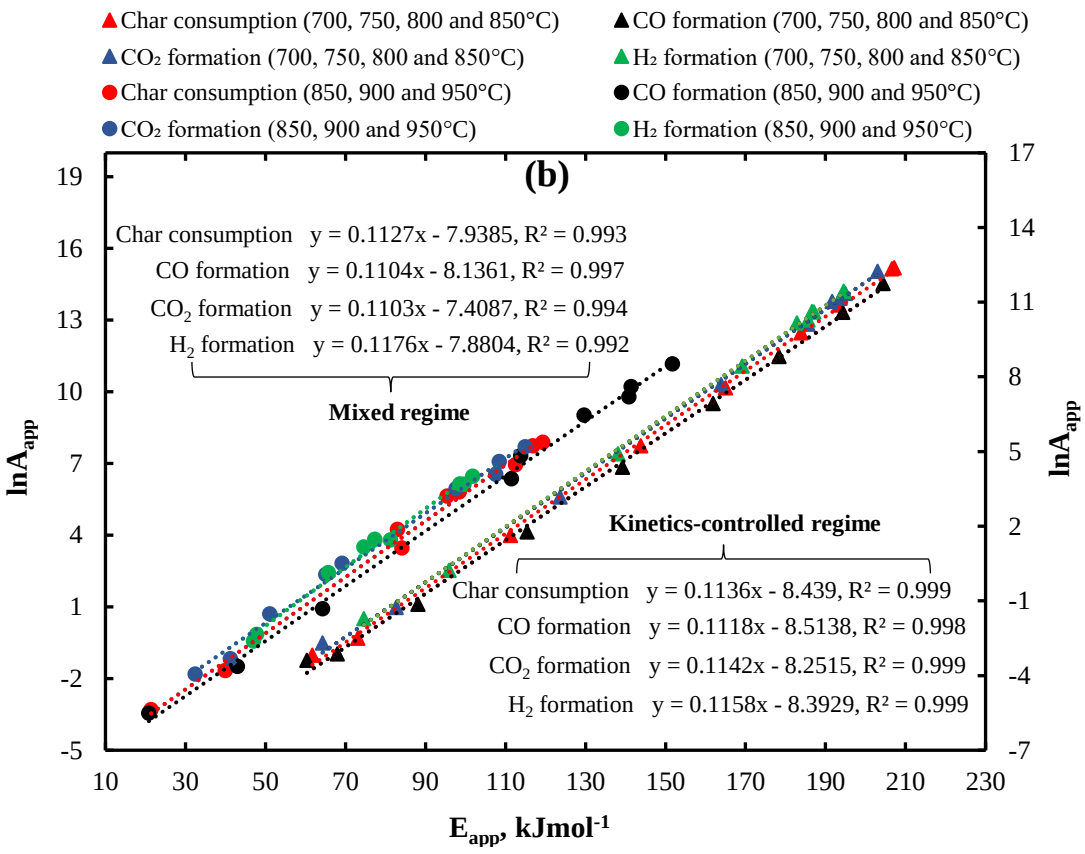

Figure 4-5 The kinetic compensation effects of biochar gasification, CO, CO_2, and H_2 formation in the kinetics-controlled and mixed regimes for (a) 0.80-1.0 mm and (b) 2.0-3.3 mm particle sizes. The data of $\ln A_{app}$ in the mixed regime have been shown on secondary vertical axis respectively.

is similar for both particle sizes in the kinetics-controlled regimes. This suggests that the formation of CO, CO_2, and H_2 involves the carbon active sites on the biochar surface during the gasification in 15% H_2O-Ar.

c. In the mixed regime, lnA_{app} and E_{app} of char consumption and formation of CO, CO_2, and H_2 also exhibited a significant KCE. Further, the activation energy levels significantly reduced in the mixed regime in comparison with the kinetics-controlled regime. This reflects that the biochar-H_2O reaction has been affected by the presence of the mass transfer effects. The values of slope 'm' in this regime remained similar to those in the kinetics-controlled regime but the intercepts 'c' values increased slightly. This implies that, in the mixed regime, the extent of the KCEs has not changed significantly. Another reason

of slight variations in the extent of the KCEs could be the temperature range in the mixed regime, which is not too broad to observe significant differences in the extent of the KCEs.

d. The similar activation energy levels and similar extent of KCEs (similar '*m*' and '*c*' values) of CO and CO_2 formation reveal that CO and CO_2 both are formed from the biochar surface through a common intermediate. Therefore, it can be inferred that oxygen-containing active species i.e. C(O) leading to the formation of CO and CO_2 are essentially the same. During the biochar-H_2O reaction, certain active sites in the biochar matrix dissociate the H_2O molecule, and oxygen from H_2O molecule is exchanged to the biochar surface [34,35].

$$2C + H_2O(g) \longrightarrow C(O) + C(H_2) \quad \text{(R 4-7)}$$

or

$$2C + H_2O(g) \longrightarrow C(OH) + C(H) \quad \text{(R 4-8)}$$

$$C(OH) + C(H) \longrightarrow C(O) + C(H_2) \quad \text{(R 4-9)}$$

The oxygen-containing active sites i.e. C(O) remove carbon from the biochar surface in the form of CO(g) and CO_2(g) as mentioned in the earlier section as:

$$C(O) \longrightarrow CO(g) \quad \text{(R 4-4)}$$

$$C(O) + C(O) \longrightarrow CO_2(g) + C \quad \text{(R 4-5)}$$

It is believed that the reactions which lead to the formation of oxygen containing surface species [C(O)] i.e. R 4-6, R 4-7, and R 4-8 are fast in comparison to R 4-4. Therefore, R 4-4 is the rate-limiting step during the biochar-H_2O reaction.

e. The formation of H_2 also observed the KCE. The extent of the KCEs i.e. '*m*' and '*c*' values of biochar consumption and H_2 formation are quite similar, indicating that the formation of H_2 mainly involves the carbon active sites on

the biochar surface. The H_2 formed on the carbon active sites is released leaving behind free active sites, which can be represented, e.g. as:

$$C(H_2) \rightleftharpoons H_2(g) + C \qquad \text{(R 4-10)}$$

4.5 Conclusions

The observation of the kinetic compensation effects of CO and CO_2 formation confirms that CO and CO_2 are formed from the biochar surface during the biochar-H_2O reaction. The apparent activation energy and apparent pre-exponential factor of CO and CO_2 formation suggest that CO_2 can be formed either by the surface-catalysed water-gas-shift reaction or directly from the biochar surface through the same intermediates as those for CO formation. Both particle sizes i.e. 0.80-1.0 mm and 2.0-3.3 mm exhibit the similar extent of the kinetic compensation effects of biochar consumption and formation of CO, CO_2, and H_2 in the kinetics-controlled and mixed regimes. The extent of the kinetic compensation effects of H_2 formation and biochar gasification reveals that the H_2 formation involves the carbon active sites on the biochar surface.

4.6 References

[1] Li C.-Z. Special issue - Gasification: A route to clean energy. Process Saf Environ Prot 2006;84:407–8. doi:10.1205/psep.ed.0606.

[2] Li C.-Z. Some recent advances in the understanding of the pyrolysis and gasification behaviour of Victorian brown coal. Fuel 2007;86:1664–83. doi:10.1016/j.fuel.2007.01.008.

[3] Li C.-Z. Importance of volatile-char interactions during the pyrolysis and gasification of low-rank fuels - A review. Fuel 2013;112:609–23. doi:10.1016/j.fuel.2013.01.031.

[4] Tay HL, Kajitani S, Zhang S, Li C.-Z. Inhibiting and other effects of hydrogen during gasification: Further insights from FT-Raman spectroscopy. Fuel 2014;116:1–6. doi:10.1016/j.fuel.2013.07.066.

[5] Asadullah M, Zhang S, Min Z, Yimsiri P, Li C.-Z. Importance of biomass particle size in structural evolution and reactivity of char in steam gasification. Ind Eng Chem Res 2009;48:9858–63. doi:10.1021/ie901214z.

[6] Zhang S, Min Z, Tay HL, Wang Y, Dong L, Li C.-Z. Changes in char structure during the gasification of mallee wood: Effects of particle size and steam supply. Energy and Fuels 2012;26:193–8. doi:10.1021/ef2011589.

[7] Guo X, Tay HL, Zhang S, Li C.-Z. Changes in char structure during the gasification of a Victorian brown coal in steam and oxygen at 800 °C. Energy and Fuels 2008;22:4034–8. doi:10.1021/ef800528c.

[8] Zhang S, Hayashi JI, Li C.-Z. Volatilisation and catalytic effects of alkali and alkaline earth metallic species during the pyrolysis and gasification of Victorian brown coal. Part IX. Effects of volatile-char interactions on char-H_2O and char-O_2 reactivities. Fuel 2011;90:1655–61. doi:10.1016/j.fuel.2010.11.008.

[9] Tay HL, Kajitani S, Zhang S, Li C.-Z. Effects of gasifying agent on the evolution of char structure during the gasification of Victorian brown coal. Fuel 2013;103:22–8. doi:10.1016/j.fuel.2011.02.044.

[10] Tay H-L, Kajitani S, Wang S, Li C.-Z. A preliminary Raman spectroscopic perspective for the roles of catalysts during char gasification. Fuel 2014;121:165–72. doi:10.1016/j.fuel.2013.12.030.

[11] Li T, Zhang L, Dong L, Li C.-Z. Effects of gasification atmosphere and temperature on char structural evolution during the gasification of Collie sub-bituminous coal. Fuel 2014;117:1190–5. doi:10.1016/j.fuel.2013.08.040.

[12] Keown DM, Hayashi J-I, Li C.-Z. Drastic changes in biomass char structure and reactivity upon contact with steam. Fuel 2008;87:1127–32. doi:10.1016/j.fuel.2007.05.057.

[13] Bayarsaikhan B, Hayashi J, Shimada T, Sathe C, Li C, Tsutsumi a, et al. Kinetics of steam gasification of nascent char from rapid pyrolysis of a Victorian brown coal. Fuel 2005;84:1612–21. doi:10.1016/j.fuel.2005.02.008.

[14] Fushimi C, Araki K, Yamaguchi Y, Tsutsumi A. Effect of heating rate on steam gasification of biomass. 2. Thermogravimetric-mass spectrometric (TG-MS) analysis of gas evolution. Ind Eng Chem Res 2003;42:3929–36. doi:10.1021/ie0300575.

[15] Li J, Van Heiningen ARP. Kinetics of gasification of black liquor char by steam. Ind Eng Chem Res 1991;30:1594–601. doi:10.1021/ie00055a027.

[16] Pereira P, Somorjai GA, Heinemann H. Catalytic steam gasification of coals. Energy and Fuels 1992;6:407–10. doi:10.1021/ef00034a009.

[17] Wang J, Jiang M, Yao Y, Zhang Y, Cao J. Steam gasification of coal char catalyzed by K_2CO_3 for enhanced production of hydrogen without formation of methane. Fuel 2009;88:1572–9. doi:10.1016/j.fuel.2008.12.017.

[18] Wigmans T, Elfring R, Moulijn JA. On the mechanism of the potassium carbonate catalysed gasification of activated carbon: the influence of the catalyst concentration on the reactivity and selectivity at low steam pressures. Carbon 1983;21:1–12. doi:10.1016/0008-6223(83)90150-1.

[19] Yip K, Tian F, Hayashi JI, Wu H. Effect of alkali and alkaline earth metallic

species on biochar reactivity and syngas compositions during steam gasification. Energy and Fuels 2010;24:173–81. doi:10.1021/ef900534n.

[20] Kwon TW, Kim JR, Kim SD, Park WH. Catalytic steam gasification of lignite char. Fuel 1989;68:416–21. doi:10.1016/0016-2361(89)90261-5.

[21] Shufen Li and Yuanlin Cheng. Catalytic gasification of gas-coal char in CO_2. Fuel 1995;74:456–8.

[22] Dhupe AP, Gokarn AN, Doraiswamy LK. Investigations into the compensation effect at catalytic gasification of active charcoal by carbon dioxide. Fuel 1991;70:839–44. doi:10.1016/0016-2361(91)90192-D.

[23] Bond GC, Keane MA, Kral H, Lercher JA. Compensation phenomena in heterogeneous Catalysis: General Principles and a Possible Explanation. Catal Rev 2000;42:323–83. doi:10.1081/CR-100100264.

[24] Koga N. A review of the mutual dependence of Arrhenius parameters evaluated by the thermoanalytical study of solid-state reactions: The kinetic compensation effect. Thermochim Acta 1994;244:1–20. doi:10.1016/0040-6031(94)80202-5.

[25] Bligaard T, Honkala K, Logadottir A, Norskov JK, Dahl S, Jacobsen CJH. On the compensation effect in heterogeneous catalysis. J Phys Chem B 2003;107:9325–31. doi:10.1021/jp034447g.

[26] Wu H, Li X, Hayashi JI, Chiba T, Li C.-Z. Effects of volatile-char interactions on the reactivity of chars from NaCl-loaded Loy Yang brown coal. Fuel 2005;84:1221–8. doi:10.1016/j.fuel.2004.06.037.

[27] Yip K, Ng E, Li C.-Z., Hayashi JI, Wu H. A mechanistic study on kinetic compensation effect during low-temperature oxidation of coal chars. Proc Combust Inst 2011;33:1755–62. doi:10.1016/j.proci.2010.07.073.

[28] Akhtar M.A., Zhang S, Shao X, Dang H, Liu Y, Li T, Zhang Lei, Li C.-Z. Kinetic compensation effects in the chemical reaction-controlled regime and mass transfer-controlled regime during the gasification of biochar in O_2. Fuel Process Technol 2018;181:25–32. doi:10.1016/j.fuproc.2018.09.009.

[29] Christopher, Higman V. der B.M. Gasification. Second. Elsevier Inc.; 2008. doi:10.1016/B978-0-7506-8528-3.X0001-6.

[30] Li C.-Z. Advances in the science of Victorian Brown Coal. 2004. doi:10.1016/B978-0-08-044269-3.X5000-6.

[31] Quyn DM, Wu H, Li C.-Z. Volatilisation and catalytic effects of alkali and alkaline earth metallic species during the pyrolysis and gasification of Victorian brown coal. Part I. Volatilisation of Na and Cl from a set of NaCl-loaded samples. Fuel 2002;81:143–9. doi:10.1016/S0016-2361(01)00127-2.

[32] Li X, Hayashi J ichiro, Li C.-Z. Volatilisation and catalytic effects of alkali and alkaline earth metallic species during the pyrolysis and gasification of Victorian brown coal. Part VII. Raman spectroscopic study on the changes in char structure during the catalytic gasification in air. Fuel 2006;85:1509–17. doi:10.1016/j.fuel.2006.01.011.

[33] Quyn DM, Wu H, Hayashi J, Li C.-Z. Volatilisation and catalytic effects of alkali and alkaline earth metallic species during the pyrolysis and gasification of Victorian brown coal. Part IV. Catalytic effects of NaCl and ion-exchangeable Na in coal on char reactivity☆. Fuel 2003;82:587–93. doi:10.1016/S0016-2361(02)00323-X.

[34] Walker PL, Rusinko F, Austin LG. Gas reactions of carbon. Adv Catal 1959;Volume 11:133–221. doi.org/10.1016/S0360-0564(08)60418-6.

[35] Hermann G, Huttinger KJ. Mechanism of water vapour gasification of carbon-A new model. Carbon 1986;24:705–13. doi:10.1016/0008-6223(86)90178-8.

5.0 Chapter

Mechanistic insights into the kinetic compensation effects during the gasification of biochar: Effects of the partial pressure of H_2O

5.1 Abstract

This study has focused on the kinetic compensation effects (KCE) during the gasification of biochar in 15% H_2O-Ar and 2% H_2O-Ar. The biochar samples were characterised by FT-Raman and X-ray photoelectron spectroscopies. Our results showed that the extent of the KCE of char gasification and formation of CO, CO_2, and H_2 was higher during the gasification in 15% H_2O-Ar than that in 2% H_2O-Ar. The relative ratio of $I_D/(I_{(Gr + Vl+ Vr)}$ was higher in 15% H_2O-Ar than that in 2% H_2O-Ar, which reflects that the relative concentration of large aromatic rings is higher during the gasification in 15% H_2O-Ar than that in 2% H_2O-Ar. The partial pressure of H_2O affected the relative concentration of O-containing surface species [C(O)] on the biochar external surface and inside the pores of the char matrix. The concentration of these O-containing species [C(O)] on the char surface led to different relative rates of CO and CO_2 release, resulting in lower CO/CO_2 ratios (at lower char conversions) during the gasification in 15% H_2O-Ar than those in 2% H_2O-Ar. The lower relative ratio of $I_D/(I_{(Gr + Vl+ Vr)}$ and lower extent of the kinetic compensation effects revealed that the relative concentration of active sites (with similar properties), which were created on the activation of aromatic rings, was lower for the gasification in 2% H_2O-Ar than that in 15% H_2O-Ar.

Keywords: Carbon release kinetics; Gasification; H_2O partial pressure; Kinetic compensation effects; Mallee wood.

5.2 Introduction

The kinetic compensation effects (KCEs) refer to the phenomena whereby the effects of the changes in apparent activation energy E_{app} on reaction rate are at least partially offset by those of the changes in apparent pre-exponential factor A_{app}. The KCEs have been observed in many gas-solid reactions and are the key feature of the biochar-gas reactions, which can provide a better understanding of the biochar gasification mechanisms [1–5]. Our previous work has demonstrated the significance of the KCEs for the char-O_2 and char-H_2O reactions [1,2]. During gasification, the active sites on the char surface are created and consumed continuously, giving rise to the KCEs. The KCE can be represented as [6–8]:

$$lnA_{app} = mE_{app} + c \qquad \text{(Eq. 5-1)}$$

where 'c' is the y-intercept on the plot between lnA_{app} vs. E_{app} and 'm' is the slope. A_{app} and E_{app} stand for the apparent pre-exponential factor and the apparent activation energy respectively.

Our past study reported and explained the KCE for the gasification of brown coal char [9]. The study was carried out at low temperatures i.e. 330 °C to 430 °C. A recent study [2] in our group on the biochar-O_2 reaction has investigated and reported the KCE over a wide range of temperatures covering the kinetics- and diffusion-controlled regimes. The extent of the KCE varies significantly as the temperature regime changes from the kinetics-controlled to the mixed regime or to the diffusion-controlled regime. Our more recent work [1] has reported the KCE and its plausible explanation during the gasification of biochar in 15% H_2O-Ar. The concentration of O-containing carbon surface species [C(O)] as well as the concentration of alkali and alkaline earth metallic species (AAEM) in the char increase with biochar conversion during steam gasification. These AAEM species are bonded with Raman-active oxygen species and, consequently, enhance the catalytic activities with increasing conversion [10]. It is believed that the increasing catalytic effects mainly contribute to decreasing the apparent activation energy as the char gasification is progressed in H_2O.

There is a contradiction in literature [11–16] on CO_2 formation during steam gasification. Our recent study [1] has reported that CO_2 formation is from the char surface either directly or by the surface-catalysed water-gas-shift (WGS) reaction instead of homogeneous (gas phase) WGS reaction. This can be shown as:

$$C(O) \longrightarrow CO(g) \quad \text{(R 5-1)}$$

$$C(O) + C(O) \longrightarrow CO_2(g) + C \quad \text{(R 5-2)}$$

$$C(O) + C(CO) \longrightarrow CO_2 + 2C \quad \text{(R 5-3)}$$

$$C(CO) + H_2O(g) \longrightarrow CO_2(g) + H_2(g) + C \quad \text{(R 5-4)}$$

It is believed [1] that the same O-containing carbon surface species i.e. [C(O)] is involved in the formation of CO and CO_2. However, the study was carried out during the gasification in 15% H_2O-Ar only. The partial pressure of H_2O could change the concentration of steam surrounding the char particle. The change in the concentration of H_2O can influence the relative rates of formation and consumption of active sites and even possibly the distribution of active sites, which can also affect the relative rates of CO and CO_2 formation as well as the extent of the KCE. To the best of authors' knowledge, there are no data available in the literature about how the concentration of H_2O would change the extent of the KCE of char gasification and the extent of the KCE of the formation of CO, CO_2, and H_2 during the biochar gasification.

Therefore, this study has investigated the mechanism of biochar-H_2O reaction in 15% H_2O and 2% H_2O (balanced with argon) with the aid of the KCE. The study compares the KCE of char gasification and formation of CO, CO_2, and H_2 in the kinetics-controlled regime and gives a mechanistic insight into the biochar gasification in 15% H_2O-Ar and 2% H_2O-Ar.

5.3 Experimental

5.3.1 Experimental procedure

The wood samples were prepared from the freshly harvested Australian mallee tree. The procedures were outlined in a previous study [17]. The moisture in the wood samples was removed by drying in an oven overnight at 105 °C.

The mallee wood comprising of around 2.0 g sample was pyrolysed in ultra-high purity (UHP) argon in a fluidised-bed reactor. The superficial gas velocity was set at $U \approx 10$ U_{mf} where U_{mf} denotes the minimum fluidisation velocity. After 5 min of holding in argon, steam was fed by using an HPLC pump to commence gasification. Two partial pressures of the steam i.e. 15% H_2O-Ar and 2% H_2O-Ar, were employed. The steam gasification was carried out in the temperature range of 700-850 °C. The product gas mixture was monitored continuously by a quadrupole mass spectrometer (QMS Prisma^{TM} 200). The product gas monitoring was stopped when the signals of all the product components practically reached the initial baselines, which indicated the complete conversion of char. The CO and CO_2 signals overlapped. The CO_2 signal was subtracted from CO signal at m/z = 28. The detailed experimental procedure was outlined in a previous study [1]. The following Arrhenius equations [9] were used to calculate the rate of char gasification (r_c) and the rates of product formation for CO (r_c), CO_2 (r_{CO_2}) and H_2 (r_{H_2}) at any conversion.

$$r_i = \frac{1}{W_i}\frac{dW_i}{dt} = f(x)g(p)A\exp\left(-\frac{E_{app}}{RT}\right) = A_i\, exp\left(-\frac{E_i}{RT}\right) \qquad (\text{Eq. } 5-2)$$

Where i represents char gasification, CO, CO_2 or H_2 formation in Eq. 5-2. $f(x)$ is a function, which incorporates the changes in char properties with conversion in Eq. 5-2 and is a constant when conversion 'x' is fixed. A_i stands for the apparent pre-exponential factors and depends on the partial pressure $g(p)$ of H_2O and $f(x)$. E_i stands for the apparent activation energy. The details of Eq. 5-2 can be found in Chapter 2.

5.3.2 Char characterisation

The biochar samples were characterised using FT-Raman and X-ray photoelectron spectroscopies (XPS). A well-grounded 0.5 wt.% [17–19] char-potassium bromide (KBr of IR grade) mixture was used to acquire Raman spectra. A baseline correction was applied to each Raman spectrum and then deconvoluted into 10 Gaussian bands in the range of 800 cm^{-1} to 1800 cm^{-1} by following the procedure outlined before [20]. $BaSO_4$ was used as reference/standard material for FT-Raman spectroscopy. Raman spectrum of $BaSO_4$ was acquired before and after each biochar sample to observe any

changes in the laser intensity of Raman spectrometer during analysis. Additionally, the char samples were repeated for FT-Raman analysis and there were no significant differences observed in the results.

The total Raman area and the ratio of $I_D/(I_{(Gr + Vl+ Vr)}$ were used as indicators to investigate the biochar structural changes. The area of D band (1300 cm^{-1}), I_D, reflects the relative concentration of aromatic rings with at least 6 or more fused benzene rings while the sum of the band areas $I_{(Gr + Vl+ Vr)}$ is an indicator of the relative concentration of aromatic rings with 3-5 fused benzene rings present in the biochar sample. Therefore, the ratio of $I_D/(I_{(Gr + Vl+ Vr)}$ reflects the evolution of aromatic ring condensation during gasification. XPS was used to investigate the elemental composition on the biochar external surface. The details of these methods are mentioned in Chapter 2.

5.4 Results and discussion

5.4.1 Char Reactivity

The data in Figure 5-1 (a-d) compare the rate of char gasification (r_c) and the formation rates of CO (r_{CO}), CO_2 (r_{CO_2}) and H_2 (r_{H_2}) during the gasification of char in 15% H_2O-Ar and 2% H_2O-Ar in the temperature range from 700 to 850 °C for 2.0-3.3 mm particle size. These rates i.e. r_c, r_{CO}, r_{CO_2} and r_{H_2} were calculated using Eq. 5-2. Our results indicate that the rate of char gasification (r_c) and formation rates of CO (r_{CO}), CO_2 (r_{CO_2}) and H_2 (r_{H_2}) reduced with decreasing steam partial pressure from 15% H_2O-Ar to 2% H_2O-Ar (Figure 5-1 a-d). In a lower temperature range, i.e. 700 °C and 750 °C, the decreases in the rates were relatively slow, however, at higher temperatures i.e. 800 °C and 850 °C, the rates decreased drastically with decreasing steam partial pressure. These rates (r_c, r_{CO}, r_{CO_2} and r_{H_2}) followed quite similar trends with biochar conversion during the gasification in 2% H_2O-Ar and 15% H_2O-Ar (despite the rates were reduced in 2% H_2O-Ar).

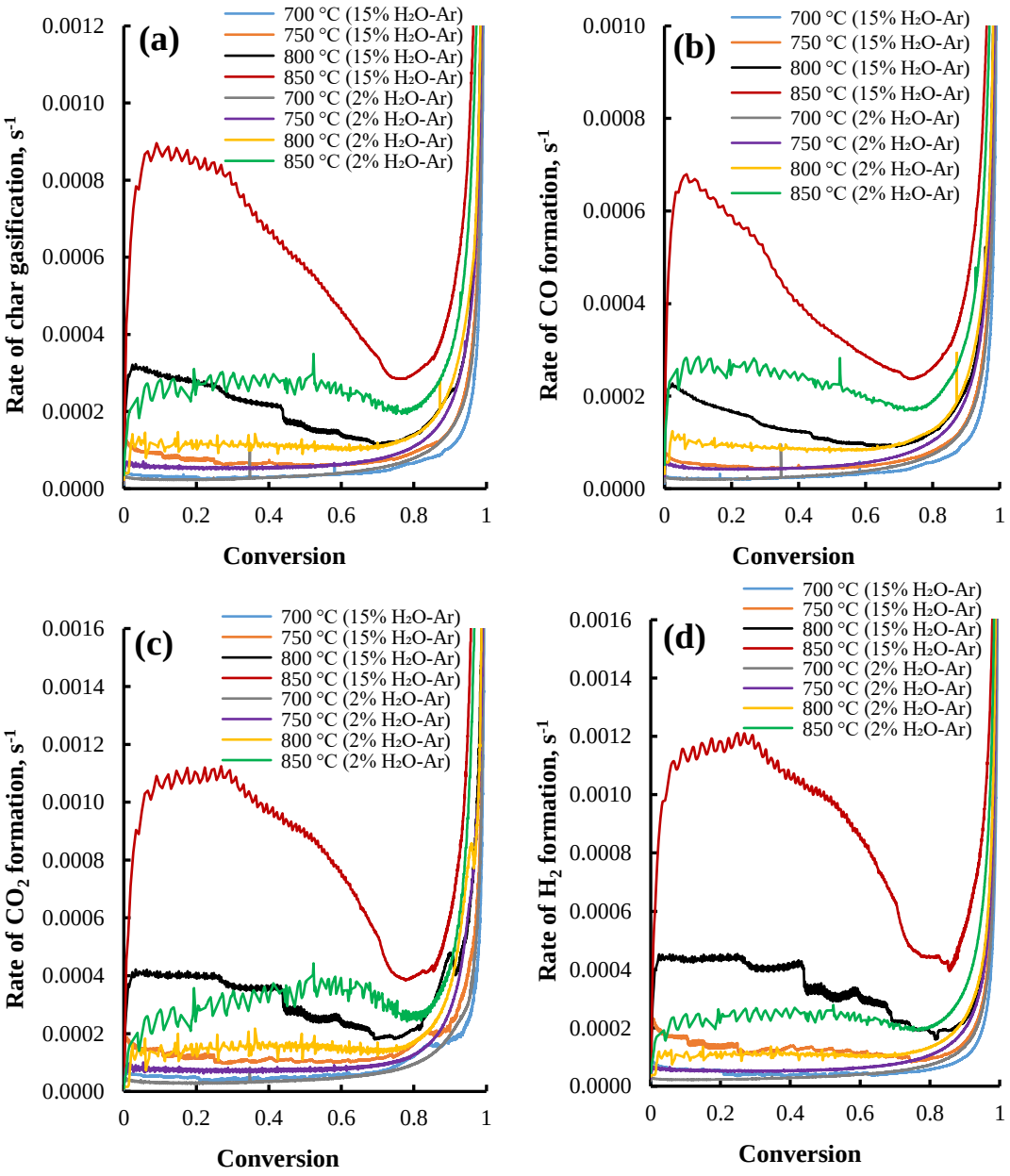

Figure 5-1 (a) Char gasification rate, (b) rate of CO formation, (c) rate of CO_2 formation and (d) rate of H_2 formation vs. biochar conversion during the gasification of 2.0-3.3 mm particle sizes in 15% H_2O-Ar and 2% H_2O-Ar. The data of 15% H_2O-Ar have been published in reference [1].

5.4.2 Effects of conversion and H_2O partial pressure on the kinetic parameters

Figure 5-2 (a-d) display the kinetic parameters for char gasification and formation of CO, CO_2, and H_2 during the biochar-H_2O reaction in 15% H_2O-Ar and 2% H_2O-Ar. It

has been demonstrated previously [13] that the kinetics-controlled regime lies in the temperature range of 700-850 °C during the gasification of biochar in 15% H_2O-Ar. The diffusion from the bulk gas phase to the external surface of the char particle depends on the gas phase velocity inside the reactor and the particle diameter. The data in Figure S2 (Appendix-I) show that rate of char gasification is independent of gas mixture velocity during the gasification in 15% H_2O-Ar. The velocity of gas mixture remained same during the gasification in 2% H_2O-Ar to that of 15% H_2O-Ar. Therefore, we inferred that external diffusion does not limit the rate of gasification.

However, a decrease in the partial pressure of H_2O from 15% H_2O-Ar to 2% H_2O-Ar would reduce the H_2O concentration at the char surface. This can result in concentration gradients in the interior pores of the char and, consequently, can lead to internal diffusion limitations. To calculate the internal diffusion limitations, we used Weisz-Prater (WP) criterion. From the calculation results, we observed that effectiveness factors (η) reduced during the gasification in 2% H_2O-Ar relative to 15% H_2O-Ar, which indicates the possible presence of enhanced internal diffusion limitations in 2% H_2O-Ar. However, these calculations were based on the assumption

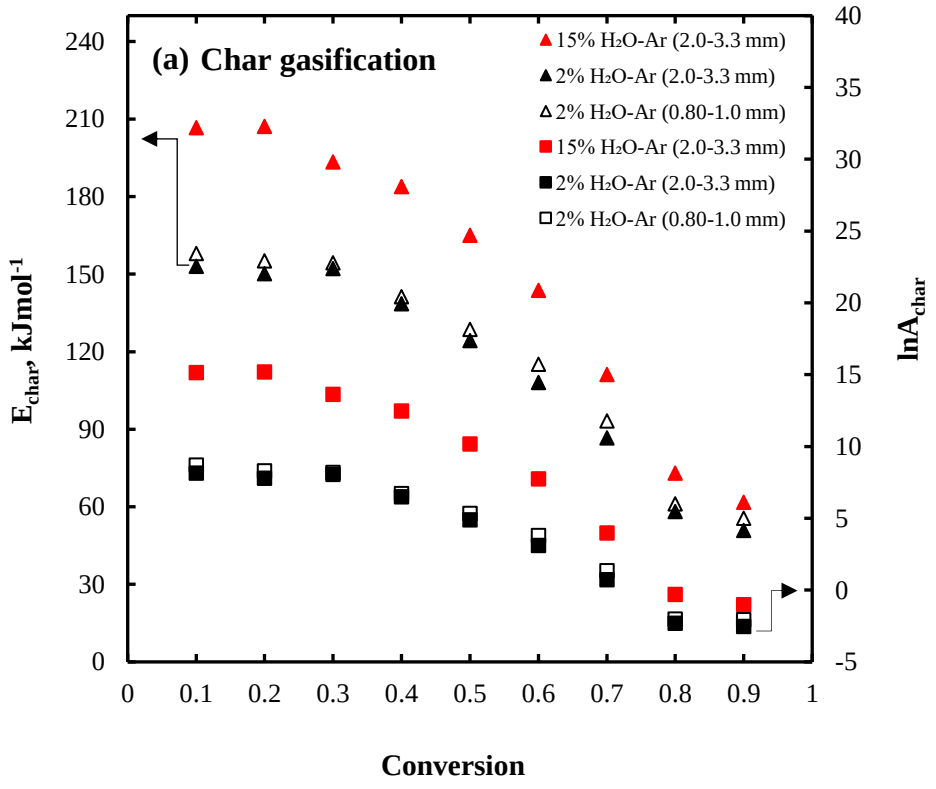

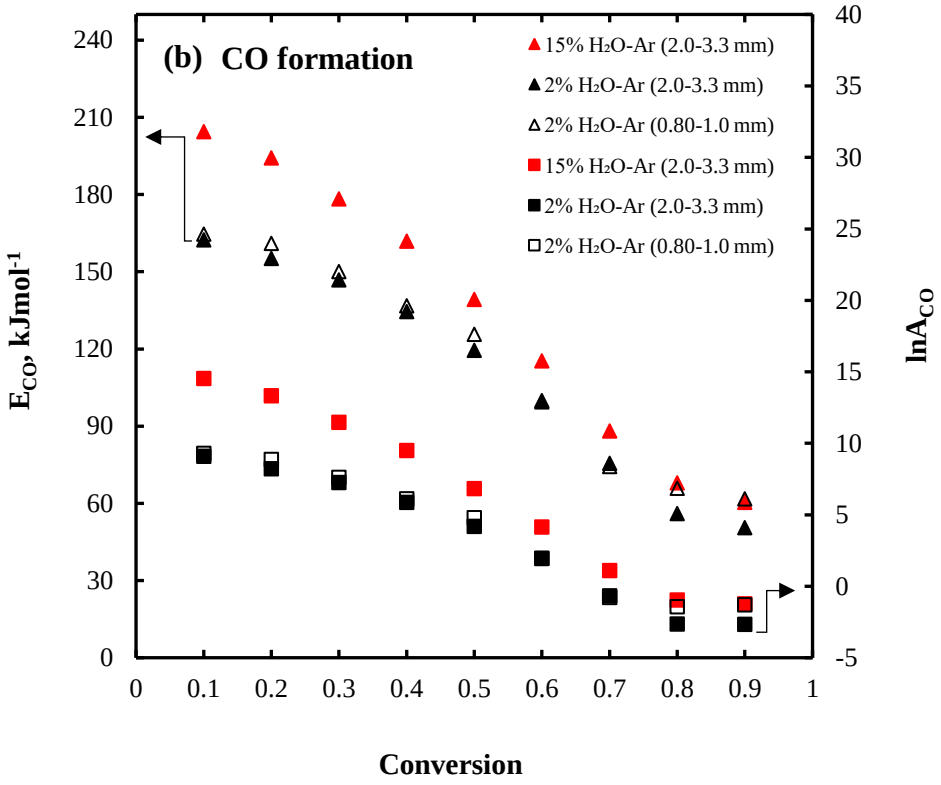
(b) CO formation
15% H2O-Ar (2.0-3.3 mm)
2% H2O-Ar (2.0-3.3 mm)
2% H2O-Ar (0.80-1.0 mm)
15% H2O-Ar (2.0-3.3 mm)
2% H2O-Ar (2.0-3.3 mm)
2% H2O-Ar (0.80-1.0 mm)
E_CO, kJmol-1
lnA_CO
Conversion

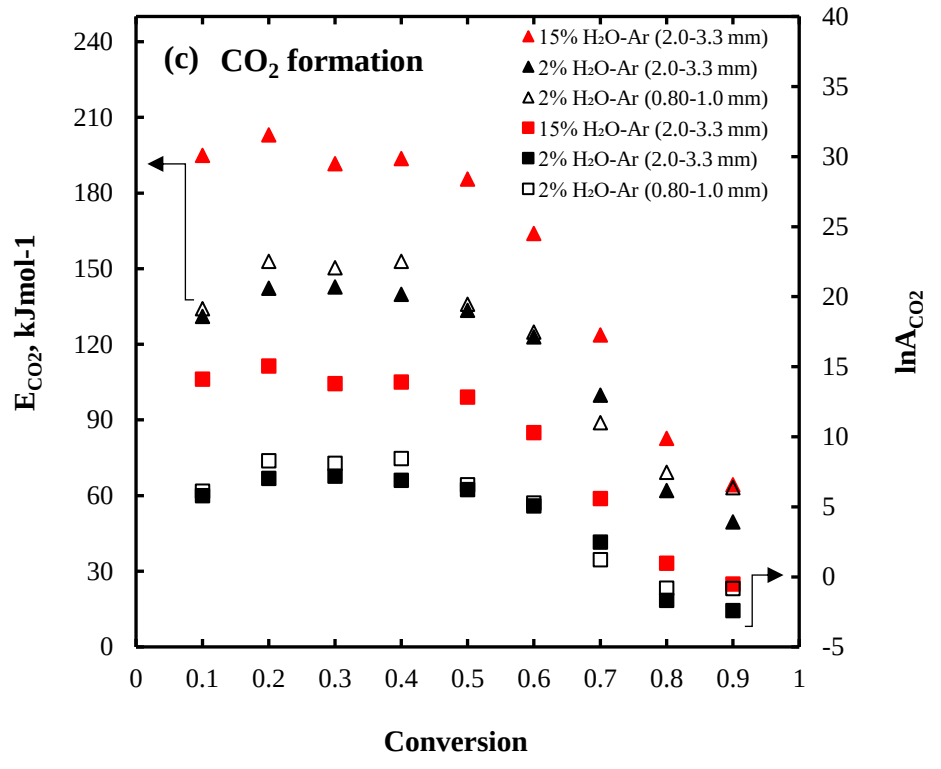
(c) CO2 formation
15% H2O-Ar (2.0-3.3 mm)
2% H2O-Ar (2.0-3.3 mm)
2% H2O-Ar (0.80-1.0 mm)
15% H2O-Ar (2.0-3.3 mm)
2% H2O-Ar (2.0-3.3 mm)
2% H2O-Ar (0.80-1.0 mm)
E_CO2, kJmol-1
lnA_CO2
Conversion

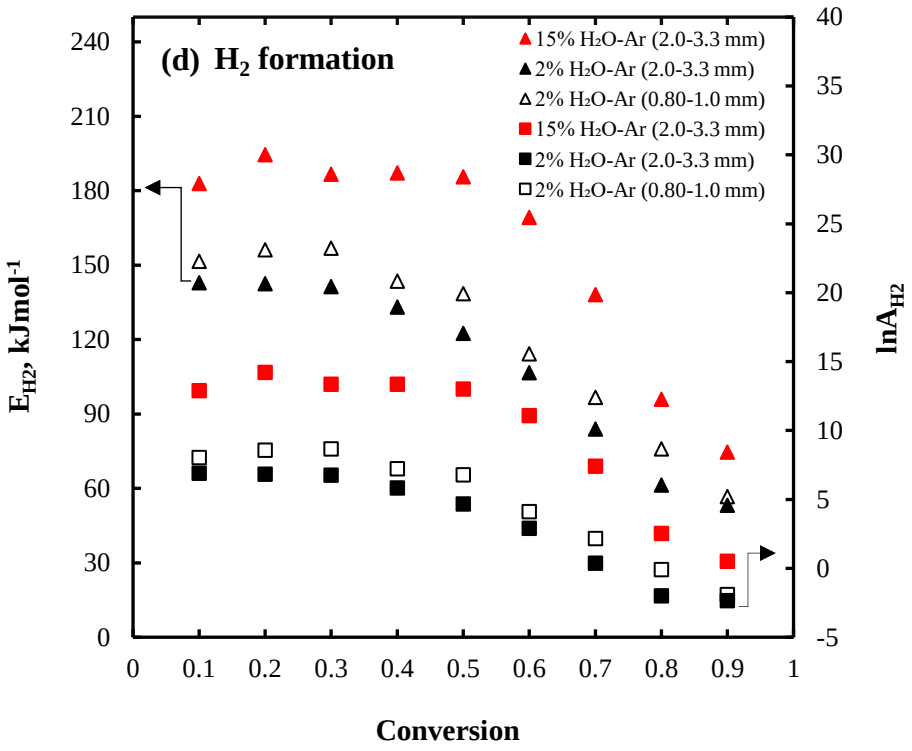

Figure 5-2 E_{app} and A_{app} of (a) char gasification, (b) CO formation (E_{CO}), (c) CO_2 formation (E_{CO_2}), and (d) H_2 formation (E_{H_2}) vs. biochar conversion at 700, 750, 800 and 850 °C in 15% H_2O-Ar and 2% H_2O-Ar. Symbols ▲ and Δ indicate E_{app} and the symbols ■ and □ indicate lnA_{app} in Figure 5-2 (a-d). The data of lnA_{app} in 15% H_2O-Ar and 2% H_2O-Ar are displayed on the secondary vertical axis in Figure 5-2 (a-d). The data of 15% H_2O-Ar have been published in reference [1].

that the ratio of surface reaction rates in 15% H_2O and 2% H_2O is equal to the ratio of the overall observed reaction rates in 15% H_2O and 2% H_2O.

Therefore, to verify whether diffusion limitations are present during the gasification in 2% H_2O, gasification experiments were carried out using particle sizes of 0.8-1.0 mm and 2.0-3.3 mm in 2% H_2O-Ar from 700 to 850 °C. The kinetic parameters i.e. E_{app} and A_{app} of char gasification and formation of CO, CO_2, and H_2 during the gasification of different particle sizes are found to be very similar. This shows that the rate of char gasification is independent of the particle size during the gasification in 2% H_2O-Ar, which also implies that the internal diffusion limitations are not significant during the gasification in 2% H_2O-Ar.

Further, the data in Figure 5-2 (a-d) indicate that E_{app} and A_{app} of char gasification and formation of CO and CO_2 decreased with the progress of char conversion under both conditions i.e. 15% H_2O-Ar and 2% H_2O-Ar. The decreases in the apparent activation energy can be caused by the char chemical structure. During the biochar steam gasification, there is an increase in the O-containing carbon surface species [C(O)] on the char surface with increasing conversion. This has been reported previously by an increase in the total Raman area with increasing conversion for low-rank fuels [18,21–24]. The concentration of AAEM species also increases with increasing char conversion [10,25–27], which enhances the catalytic effects and contributes to decreasing apparent activation energy with increasing conversion during steam gasification.

The comparison of the kinetic parameters in Figure 5-2 reveals that E_{app} and A_{app} of char gasification and formation of CO and CO_2 reduced significantly with decreasing steam partial pressure from 15% H_2O-Ar to 2% H_2O-Ar. The steam gasification involves the breakage of aromatic rings, which can be either released/gasified or recombined to become bigger rings during steam gasification [17,21,23,24,28–33]. The H_2O molecule during gasification dissociates on the char surface as [34,35]:

$$2C + H_2O(g) \longrightarrow C(O) + C(H_2) \quad \text{(R 5-5)}$$

or

$$2C + H_2O(g) \longrightarrow C(OH) + C(H) \quad \text{(R 5-6)}$$

It is believed that the H radical formed on the char carbon surface is able to migrate in the char matrix and can induce the aromatic ring condensation reactions [21,29,30,36,37] while they can also be desorbed as H_2 e.g.

$$C(OH) + C(H) \longrightarrow C(O) + C(H_2) \quad \text{(R 5-7)}$$

$$C(H) + C(H) \longrightarrow C(H_2) + C \quad \text{(R 5-8)}$$

$$C(H_2) \rightleftharpoons H_2(g) + C \quad \text{(R 5-9)}$$

Thus, the carbon active sites on the char surface are oxygenated to form oxygen-containing active species [C(O)]. Similarly, H radicals also occupy the carbon active sites e.g. [C(H)] and can recombine/condense the aromatic rings.

During steam gasification, the concentration of [C(O)] formed on the char surface can be correlated with the molar flux of CO and CO_2. The gasification in 2% H_2O-Ar decreased the molar fluxes of CO and CO_2 compared with the data for gasification in 15% H_2O-Ar, particularly at lower char conversion levels (Figure S3 a-f, Appendix-I).

The formation of CO and CO_2 during steam gasification involves the same O-containing carbon surface species [C(O)]. Therefore, the decrease in the fluxes of CO and CO_2 with decreasing H_2O partial pressure implies that the relative concentrations of [C(O)] formed on the char surface decrease with decreasing steam partial pressure. It is believed that the concentration of [C(O)] contributes to the biochar reactivity during steam gasification. To investigate how the concentration of [C(O)] affects the char structural features during the gasification in 15% H_2O-Ar and 2% H_2O-Ar, we characterised the biochar samples by FT-Raman and XPS and will be discussed in the following section.

Furthermore, E_{app} and A_{app} of CO and CO_2 formation were very close to each other under both gasification conditions i.e. 15% H_2O-Ar and 2% H_2O-Ar. This suggests that CO and CO_2 are formed from a common carbon-oxygen surface complex [C(O)] under both conditions i.e. 15% H_2O-Ar and 2% H_2O-Ar. The kinetic parameters i.e. activation energy values and the apparent pre-exponential factors of CO_2 and H_2 formation were also found to be quite close to each other (Figure 5-2). Additionally, there is also a similarity in the rate profiles of CO_2 and H_2 formation (Figure 5-1). This infers that CO_2 and H_2 can also be formed simultaneously on the char surface involving a common carbon-oxygen surface complex [C(O)]. This can be represented as:

$$C(O) + H_2O \longrightarrow CO_2(g) + H_2(g) \qquad \text{(R 5-10)}$$

Therefore, the release of char carbon in the form of CO(g) and CO_2(g) can be represented by the reactions i.e. R 5-1 to R 5-4 and R 5-10.

Moreover, the decrease in the kinetic parameters (E_{CO_2} and A_{CO_2}) of CO_2 with biochar conversion also indicates that CO_2 formation mainly involves active sites on the char surface instead of gas-phase water-gas-shift reaction irrespective of H_2O partial pressure. On the contrary, the formation of CO_2 by homogeneous gas-phase water-gas-shift reaction would have given discrete values of the kinetic parameters represented by a single set of E_{CO_2} and A_{CO_2}.

5.4.3 Biochar characterization by FT-Raman and XPS

The Figure 5-3 (a-c) displays the total Raman area in the range of 800-1800 cm^{-1} and the band intensities ratio of $I_D/(I_{(Gr + Vl+ Vr)}$ determined by Raman spectroscopy. The O/C ratio on the biochar external surface was determined by XPS.

The biochar samples were prepared in 15% H_2O-Ar and 2% H_2O-Ar at 800 °C and 850 °C at a biochar conversion of 10%. For this purpose, $W_{Total\ char\ carbon}$ and $W_{char\ carbon\ released}$ were calculated in 15% H_2O-Ar and 2% H_2O-Ar at 800 °C and 850 °C. $W_{Total\ char\ carbon}$ refers to the total yield of all gaseous carbon species (moles of CO, CO_2 and CH_4) produced during the gasification until there was no char left inside the reactor whereas $W_{char\ carbon\ released}$ corresponds to the yield of the gaseous carbon species (moles of CO, CO_2 and CH_4), which have been released up to any given conversion level.

For instance, for 10% conversion of char carbon, $W_{Total\ char\ carbon}$ was equal to 0.0156 moles of carbon and determined when the biochar was completely converted to gaseous carbon species during gasification in 15% H_2O-Ar at 850 °C. For 10% conversion of biochar carbon, $W_{char\ carbon\ released}$ was determined by summing up yields of all gaseous carbon species i.e. 0.00156 moles. The ratio of $W_{char\ carbon\ released}$ (0.00156 moles) to $W_{Total\ char\ carbon}$ (0.0156 moles) gives char conversion of 0.1 during gasification in 15% H_2O-Ar at 850 °C and the reactor was lifted out of the furnace at this time. Similarly, char samples were prepared for gasification in 15% H_2O-Ar at 800 °C and in 2% H_2O-Ar at 800 °C and 850 °C.

Our results indicate that the total Raman area and the O/C ratio on the biochar external surface were higher during the gasification in 15% H_2O-Ar than those in 2% H_2O-Ar.

The total Raman area is an indicator of Raman active species present in the bulk of the biochar samples, which have the Raman scattering ability such as the O-containing species (electron-rich structures) that give a resonance effect when connected to aromatic rings.

The increasing total Raman area with increasing steam partial pressure during gasification indicates the increase in the concentration of O-containing Raman active species present in the biochar bulk sample. Similarly, the oxygen content bound on the biochar external carbon surface, which is reflected by the O/C ratio, is higher in 15% H_2O-Ar than that in 2% H_2O-Ar. These results infer that the gasification of biochar in 15% H_2O-Ar yielded higher concentrations of O-containing functional groups both in the interior pores of the biochar and on the biochar external surface than that in 2% H_2O-Ar. The higher molar fluxes of CO and CO_2 from the char surface also suggest that there is an increase in O-containing carbon surface species during gasification with increasing steam partial pressure (Appendix-I, Figure S3 a-f). This reveals that

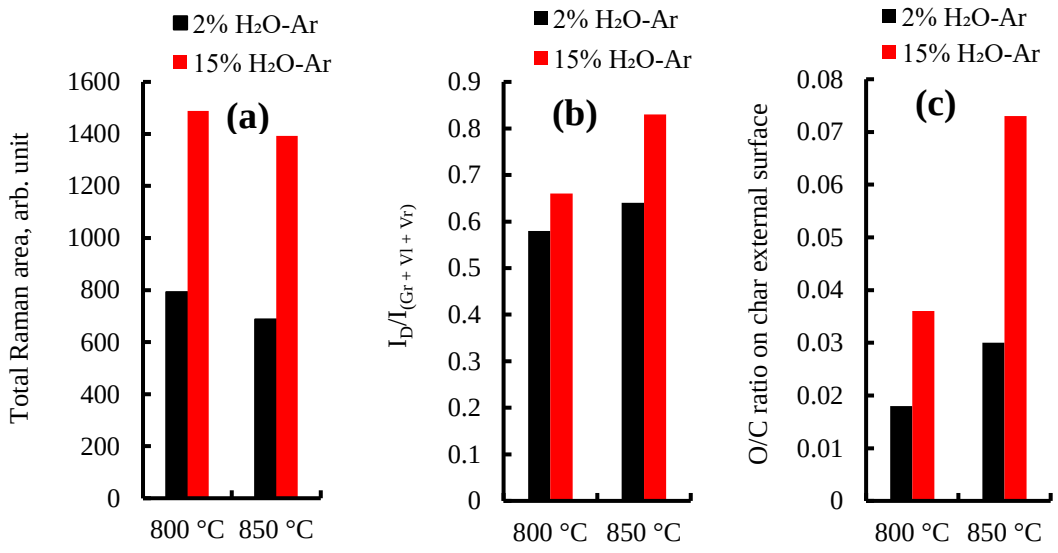

Figure 5-3 (a) Total Raman area, (b) D band and sum of the (G_r + V_l + V_r) bands areas ratio and (c) O/C ratio on the char external surface during the gasification of biochar in 15% H_2O-Ar and 2% H_2O-Ar at 800 °C and 850 °C. The biochar samples were prepared using particle size ranges of 2.0-3.3 mm mallee wood and the reactor was lifted out of the furnace at a pre-determined time corresponding to char conversion i.e. x = 0.1.

the increase in the O-containing functional groups present on the biochar surface leads to increased rates of CO, CO_2, and H_2 formation and increased biochar reactivity with increasing steam partial pressure (Figure 5-1 a-d).

Further, the ratio of $I_D/(I_{(Gr + Vl+ Vr)}$ is higher during the gasification of biochar in 15% H_2O-Ar than that in 2% H_2O-Ar, indicating that the char is richer in larger aromatic rings during the gasification of biochar in 15% H_2O-Ar than in 2% H_2O-Ar. This implies that gasification in 15% H_2O-Ar increases the relative rates of aromatic rings condensation compared with that in 2% H_2O-Ar. In other words, gasification in 15% H_2O-Ar makes the residual char more aromatised i.e. richer in larger aromatic rings at any given char conversion level requiring higher apparent activation energy to activate these aromatic rings than in 2% H_2O-Ar.

5.4.4 Effects of partial pressure of H_2O on CO/CO_2 ratio

Figure 5-4 (a-d) show the data of CO/CO_2 (mole basis) ratio from 700 to 850 °C in 15% H_2O-Ar and 2% H_2O-Ar. It is quite evident from the data that, at lower char conversion levels, CO/CO_2 ratio was higher during the gasification in 2% H_2O-Ar than in 15% H_2O-Ar while at higher char conversion levels, the trends were either reversed or became similar.

It is believed that the relative ratio of CO to CO_2 depends at least partly on the stability of carbon-oxygen surface complex [C(O)] and the relative concentration of [C(O)] formed on the char surface. At lower char conversions, the lower CO/CO_2 ratios in 15% H_2O-Ar than in 2% H_2O-Ar imply that CO_2 formation is a second-order reaction (R 5-2) with respect to the concentration of [C(O)] while CO formation is a first-order reaction (R 5-1), particularly at higher temperatures. For instance, the concentration of CO_2 is nearly doubled the CO concentration at 800 °C and 850 °C except at higher char conversion. An alternative explanation is that the carbon-oxygen complex [C(O)] formed on the char surface is relatively stable and favours the recombination of active sites i.e. [C(O)] (R 5-2) or favours the combination of C(O) with H_2O (R 5-10). Therefore, the step $C(O) + C(O) = CO_2(g) + C$ or $C(O) + H_2O(g) = CO_2(g) + H_2(g)$ dominate over the step $C(O) = CO(g)$, during the gasification in 15% H_2O-Ar. At

higher char conversion, [C(O)] formed on the char surface might be less stable than [C(O)] at lower char conversion and detaches from the char surface easily and results in higher CO/CO_2 ratios.

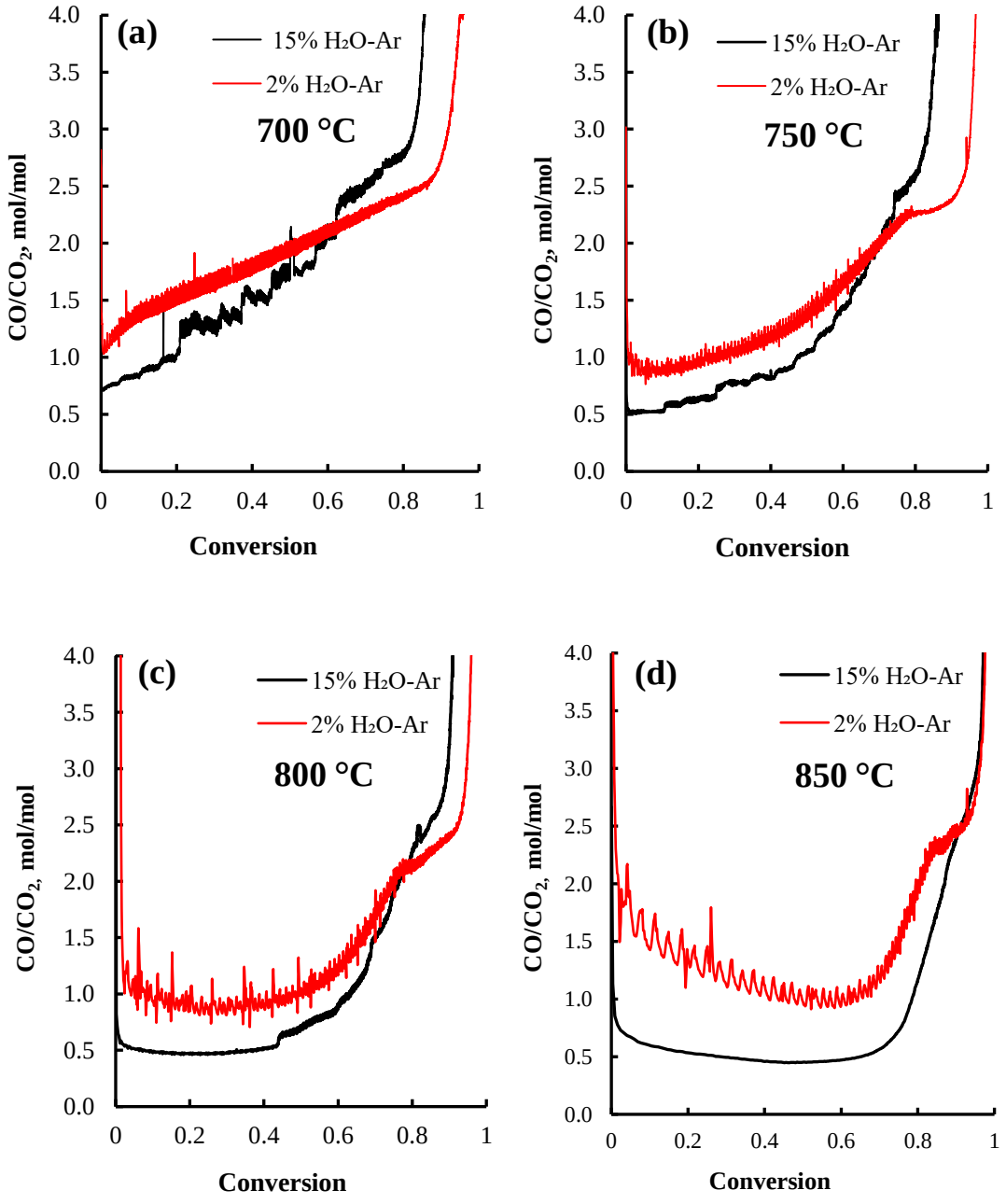

Figure 5-4 The effects of H_2O partial pressure on CO/CO_2 (mol/mol) ratio during the gasification of 2.0-3.3 mm particle sizes in 15% H_2O-Ar and 2% H_2O-Ar at (a) 700 °C, (b) 750 °C, (c) 800 °C and (d) 850 °C.

On the contrary, during the gasification in 2% H_2O-Ar, the relative concentration of [C(O)] is lower than in 15% H_2O-Ar and, therefore, the rate of the release of CO(g) from carbon-oxygen complex [C(O)] is more favourable than the formation of CO_2. This implies that decreasing the concentration of H_2O favours the formation of CO (first-order reaction) over CO_2 formation and results in a higher CO/CO_2 ratio at lower char conversion. Therefore, the step C(O) = CO(g) dominates over the step C(O) + C(O) = CO_2(g) + C or C(O) + H_2O(g) = CO_2(g) + H_2(g) during the gasification in 2% H_2O-Ar. In conclusion, the local gasifying agent concentration surrounding the char particle significantly affects the relative rates of CO and CO_2 formation and, consequently, CO/CO_2 ratio during the gasification in 15% H_2O-Ar and 2% H_2O-Ar.

5.4.5 Effects of the steam partial pressure on the kinetic compensation effects (KCEs)

Figure 5-5 illustrates the KCEs during the gasification in 15% H_2O-Ar and 2% H_2O-Ar. For this purpose, the apparent kinetic parameters i.e. lnA_{app} and E_{app} of char gasification and formation of CO, CO_2, and H_2 were plotted to calculate extents ('m' and 'c' values) of the KCEs. The distinctive attributes of the KCE are summarised below (Figure 5-5):

a. The apparent kinetic parameters of char gasification and formation of CO, CO_2, and H_2 demonstrated strong linear relationships between lnA_{app} and E_{app} in 15% H_2O-Ar and 2% H_2O-Ar.

b. The apparent activation energy and the slopes 'm' values in the KCE of char gasification and formation of CO, CO_2, and H_2 lowered in 2% H_2O-Ar relative to 15% H_2O-Ar. This indicates the lower extent of the KCE of char gasification and formation of CO, CO_2, and H_2 during the gasification in 2% H_2O-Ar than 15% H_2O-Ar. The relative ratio of $I_D/(I_{(Gr + Vl+ Vr)}$ increased with increasing steam partial pressure from 2% H_2O-Ar to 15% H_2O-Ar, which suggests that increasing steam partial pressure favours the aromatic ring condensation, increasing the relative concentration of large aromatic rings. The activation of

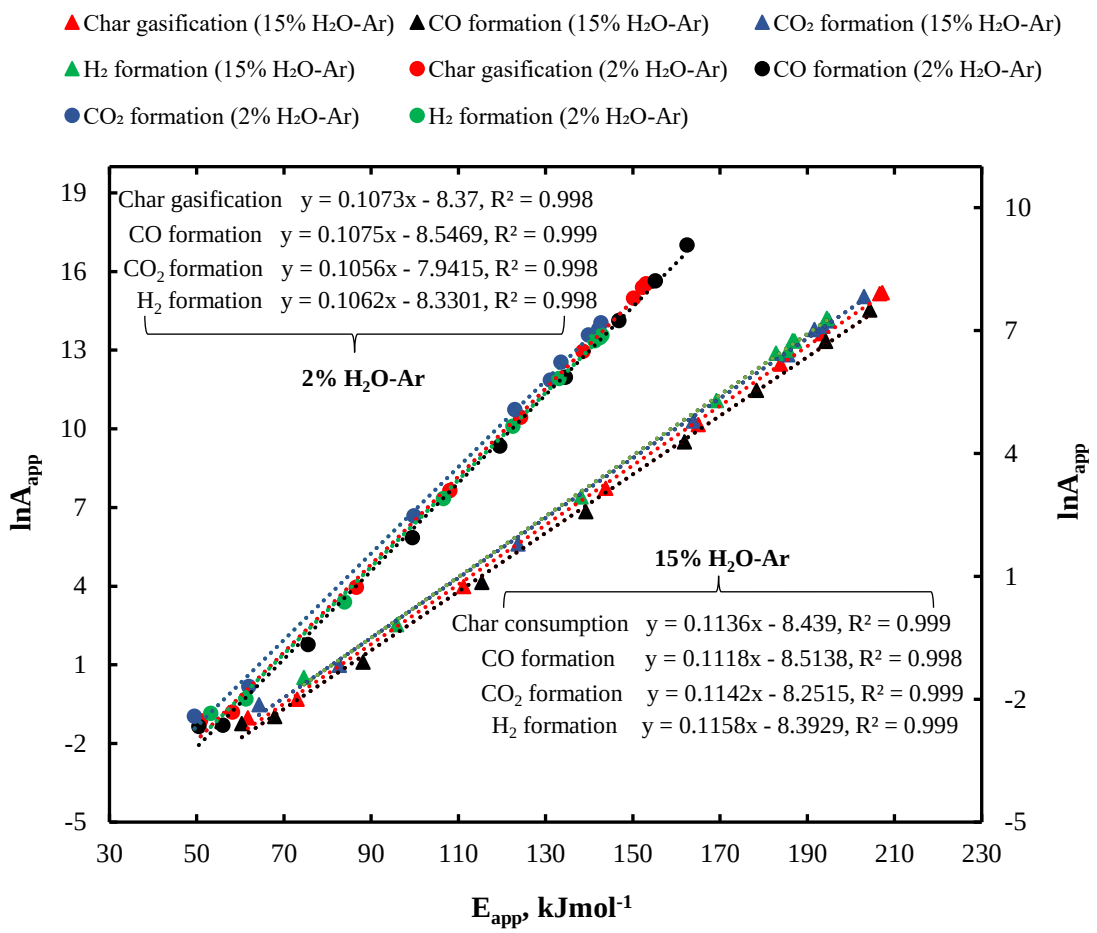

Figure 5-5 The KCE of char gasification and CO, CO_2 and H_2 formation during the gasification of 2.0-3.3 mm particle size range in 15% H_2O-Ar and 2% H_2O-Ar. The data of lnA_{app} for 2% H_2O-Ar are displayed on the secondary vertical axis. The data of 15% H_2O-Ar have been published elsewhere [1].

a large aromatic ring can create multiple active sites with similar properties. It is believed that the presence of bigger aromatic rings requires higher energy of activation during gasification. This also increases the relative concentration of active sites on the activation of aromatic rings and results in higher pre-exponential factors during the gasification in 15% H_2O-Ar than in 2% H_2O-Ar. This has been reflected in the higher extent of the KCE of char gasification, CO, CO_2, and H_2 formation in 15% H_2O-Ar than in 2% H_2O-Ar.

c. During the biochar-H_2O reaction, the H_2O molecule dissociates (in the presence of the certain active sites) to transfer oxygen to the char matrix and

forms a carbon-oxygen surface complex [C(O)]. The similar activation energies and similar extent of KCE for the CO and CO_2 formation imply that the formation of CO and CO_2 involves a common intermediate [C(O)], which is formed on the char surface [1]. The similar values of E_{CO_2} and $E_{H_2}$and the extent of the KCEs also suggest that CO_2 and H_2 can be formed simultaneously through a common carbon-oxygen surface intermediate i.e. [C(O)] (R 5-10). Further, a continuous decrease in E_{CO_2} and A_{CO_2} with char conversion for CO_2 formation suggests that CO_2 is formed largely by the biochar-H_2O surface reaction under both partial pressures of H_2O.

d. The H_2 formation follows the KCE similar to the char gasification. Additionally, E_{app} and A_{app} of char gasification and H_2 formation are quite close to each other, implying that the formation of H_2 includes largely the carbon active sites (R 5-9) during the gasification under both conditions i.e. 15% H_2O-Ar and 2% H_2O-Ar.

5.5 Conclusions

The biochar-H_2O reaction demonstrates a higher extent of the KCE of char gasification and formation of CO, CO_2, and H_2 in 15% H_2O-Ar than in 2% H_2O-Ar. The relative ratio of $I_D/(I_{(Gr\ +\ Vl+\ Vr)}$ indicates the higher rates of aromatic ring recombination/condensation during the gasification in 15% H_2O-Ar than in 2% H_2O-Ar. The increased partial pressure of steam increases the relative concentration of O-containing functional groups [C(O)] on the char external surface and also in the interior pores of the char. It is believed that the relative abundance of oxygen-containing surface species increases the recombination of carbon active sites [C(O)] and/or the combination of [C(O)] with H_2O and results in a lower CO/CO_2 ratio (at lower char conversions) during the gasification of biochar in 15% H_2O-Ar than in 2% H_2O-Ar. The relative ratio of $I_D/(I_{(Gr\ +\ Vl+\ Vr)}$ and the extent of the KCE reveal that the relative concentration of active sites (with similar properties) is higher in 15% H_2O-Ar than in 2% H_2O-Ar.

5.6 References

[1] Akhtar M.A., Zhang S, Li C.-Z. Mechanistic insights into the kinetic compensation effects during the gasification of biochar in H_2O. Fuel 2019;255:115839. doi:10.1016/j.fuel.2019.115839.

[2] Akhtar M.A., Zhang S, Shao X, Dang H, Liu Y, Li T, et al. Kinetic compensation effects in the chemical reaction-controlled regime and mass transfer-controlled regime during the gasification of biochar in O_2. Fuel Process Technol 2018;181:25–32. doi:10.1016/j.fuproc.2018.09.009.

[3] Dhupe AP, Gokarn AN, Doraiswamy LK. Investigations into the compensation effect at catalytic gasification of active charcoal by carbon dioxide. Fuel 1991;70:839–44. doi:10.1016/0016-2361(91)90192-D.

[4] Kwon TW, Kim JR, Kim SD, Park WH. Catalytic steam gasification of lignite char. Fuel 1989;68:416–21. doi:10.1016/0016-2361(89)90261-5.

[5] Shufen Li and Yuanlin Cheng. Catalytic gasification of gas-coal char in CO_2. Fuel 1995;74:456–8.

[6] Bligaard T, Honkala K, Logadottir A, Norskov JK, Dahl S, Jacobsen CJH. On the Compensation Effect in Heterogeneous Catalysis. J Phys Chem B 2003;107:9325–31. doi:10.1021/jp034447g.

[7] Bond GC, Keane MA, Kral H, Lercher JA. Compensation phenomena in heterogeneous catalysis: general principles and a possible explanation. Catal Rev 2000;42:323–83. doi:10.1081/CR-100100264.

[8] Koga N. A review of the mutual dependence of Arrhenius parameters evaluated by the thermoanalytical study of solid-state reactions: The kinetic compensation effect. Thermochim Acta 1994;244:1–20. doi:10.1016/0040-6031(94)80202-5.

[9] Wu H, Li X, Hayashi JI, Chiba T, Li C.-Z. Effects of volatile-char interactions on the reactivity of chars from NaCl-loaded Loy Yang brown coal. Fuel 2005;84:1221–8. doi:10.1016/j.fuel.2004.06.037.

[10] Tay HL, Li C.-Z. Changes in char reactivity and structure during the gasification of a Victorian brown coal: Comparison between gasification in O_2 and CO_2. Fuel Process Technol 2010;91:800–4. doi:10.1016/j.fuproc.2019.10.0 016.

[11] Fushimi C, Araki K, Yamaguchi Y, Tsutsumi A. Effect of heating rate on steam gasification of biomass. 2. Thermogravimetric-mass spectrometric (TG-MS) analysis of gas evolution. Ind Eng Chem Res 2003;42:3929–36. doi:10.1021/ie0300575.

[12] Li J, van Heiningen ARP. Kinetics of gasification of black liquor char by steam. Ind Eng Chem Res 1991;30:1594–601. doi:10.1021/ie00055a027.

[13] Pereira P, Somorjai GA, Heinemann H. Catalytic steam gasification of coals. Energy and Fuels 1992;6:407–10. doi:10.1021/ef00034a009.

[14] Wang J, Jiang M, Yao Y, Zhang Y, Cao J. Steam gasification of coal char catalyzed by K_2CO_3 for enhanced production of hydrogen without formation of methane. Fuel 2009;88:1572–9. doi:10.1016/j.fuel.2008.12.017.

[15] Wigmans T, Elfring R, Moulijn JA. On the mechanism of the potassium carbonate catalysed gasification of activated carbon: the influence of the catalyst concentration on the reactivity and selectivity at low steam pressures. Carbon 1983;21:1–12. doi:10.1016/0008-6223(83)90150-1.

[16] Yip K, Tian F, Hayashi JI, Wu H. Effect of alkali and alkaline earth metallic species on biochar reactivity and syngas compositions during steam gasification. Energy and Fuels 2010;24:173–81. doi:10.1021/ef900534n.

[17] Asadullah M, Zhang S, Min Z, Yimsiri P, Li C.-Z. Importance of biomass particle size in structural evolution and reactivity of char in steam gasification. Ind Eng Chem Res 2009;48:9858–63. doi:10.1021/ie901214z.

[18] Wang S, Wu L, Hu X, Zhang L, Li T, Li C.-Z. Effects of the particle size and gasification atmosphere on the changes in the char structure during the gasification of mallee biomass. Energy and Fuels 2018;32:7678–84. doi:10.1021/acs.energyfuels.8b01309.

[19] Asadullah M, Zhang S, Min Z, Yimsiri P, Li C.-Z. Effects of biomass char structure on its gasification reactivity. Bioresour Technol 2010;101:7935–43. doi:10.1016/j.biortech.2010.05.048.

[20] Li X, Hayashi J, Li C.-Z. FT-Raman spectroscopic study of the evolution of char structure during the pyrolysis of a Victorian brown coal. Fuel 2006;85:1700–7. doi:10.1016/j.fuel.2006.03.008.

[21] Guo X, Tay HL, Zhang S, Li C.-Z. Changes in char structure during the gasification of a Victorian brown coal in steam and oxygen at 800 °C. Energy and Fuels 2008;22:4034–8. doi:10.1021/ef800528c.

[22] Li C.-Z. Importance of volatile-char interactions during the pyrolysis and gasification of low-rank fuels - A review. Fuel 2013;112:609–23. doi:10.1016/j.fuel.2013.01.031.

[23] Li T, Zhang L, Dong L, Li C.-Z. Effects of gasification atmosphere and temperature on char structural evolution during the gasification of Collie sub-bituminous coal. Fuel 2014;117:1190–5. doi:10.1016/j.fuel.2013.08.040.

[24] Tay HL, Kajitani S, Zhang S, Li C.-Z. Effects of gasifying agent on the evolution of char structure during the gasification of Victorian brown coal. Fuel 2013;103:22–8. doi:10.1016/j.fuel.2011.02.044.

[25] Quyn DM, Wu H, Li C.-Z. Volatilisation and catalytic effects of alkali and alkaline earth metallic species during the pyrolysis and gasification of Victorian brown coal. Part I. Volatilisation of Na and Cl from a set of NaCl-loaded samples. Fuel 2002;81:143–9. doi:10.1016/S0016-2361(01)00127-2.

[26] Quyn DM, Wu H, Hayashi J, Li C.-Z. Volatilisation and catalytic effects of alkali and alkaline earth metallic species during the pyrolysis and gasification of Victorian brown coal. Part IV. Catalytic effects of NaCl and ion-exchangeable Na in coal on char reactivity☆. Fuel 2003;82:587–93. doi:10.1016/S0016-2361(02)00323-X.

[27] Li X, Hayashi J ichiro, Li C.-Z. Volatilisation and catalytic effects of alkali and

alkaline earth metallic species during the pyrolysis and gasification of Victorian brown coal. Part VII. Raman spectroscopic study on the changes in char structure during the catalytic gasification in air. Fuel 2006;85:1509–17. doi:10.1016/j.fuel.2006.01.011.

[28] Bayarsaikhan B, Hayashi J, Shimada T, Sathe C, Li C, Tsutsumi a, et al. Kinetics of steam gasification of nascent char from rapid pyrolysis of a Victorian brown coal. Fuel 2005;84:1612–21. doi:10.1016/j.fuel.2005.02.008.

[29] Keown DM, Hayashi J-I, Li C.-Z. Drastic changes in biomass char structure and reactivity upon contact with steam. Fuel 2008;87:1127–32. doi:10.1016/j.fuel.2007.05.057.

[30] Tay HL, Kajitani S, Zhang S, Li C.-Z. Inhibiting and other effects of hydrogen during gasification: Further insights from FT-Raman spectroscopy. Fuel 2014;116:1–6. doi:10.1016/j.fuel.2013.07.066.

[31] Tay HL, Kajitani S, Wang S, Li C.-Z. A preliminary Raman spectroscopic perspective for the roles of catalysts during char gasification. Fuel 2014;121:165–72. doi:10.1016/j.fuel.2013.12.030.

[32] Zhang S, Hayashi JI, Li C.-Z. Volatilisation and catalytic effects of alkali and alkaline earth metallic species during the pyrolysis and gasification of Victorian brown coal. Part IX. Effects of volatile-char interactions on char-H_2O and char-O_2 reactivities. Fuel 2011;90:1655–61. doi:10.1016/j.fuel.2010.11.008.

[33] Zhang S, Min Z, Tay HL, Wang Y, Dong L, Li C.-Z. Changes in char structure during the gasification of mallee wood: effects of particle size and steam supply. Energy & Fuels 2012;26:193–8. doi:10.1021/ef2011589.

[34] Hermann G, Huttinger KJ. Mechanism of water vapour gasification of carbon-A new model. Carbon 1986;24:705–13. doi:10.1016/0008-6223(86)90178-8.

[35] Walker PL, Rusinko F, Austin LG. Gas reactions of carbon. Adv Catal 1959;Volume 11:133–221. doi:doi.org/10.1016/S0360-0564(08)60418-6.

[36] Li C.-Z. Some recent advances in the understanding of the pyrolysis and

gasification behaviour of Victorian brown coal. Fuel 2007;86:1664–83. doi:10.1016/j.fuel.2007.01.008.

[37] Li X, Li C.-Z. Volatilisation and catalytic effects of alkali and alkaline earth metallic species during the pyrolysis and gasification of Victorian brown coal. Part VIII. Catalysis and changes in char structure during gasification in steam. Fuel 2006;85:1518–25. doi:10.1016/j.fuel.2006.01.007.

6.0 Chapter

Some discussions into the reaction mechanisms from the kinetic compensation effects of the gasification of biochar in O_2, H_2O, and their mixtures

6.1 Abstract

This study has investigated the biochar-O_2 and biochar-H_2O reactions in 0.4% O_2-Ar, 15% H_2O-Ar, 0.4% O_2 + 15% H_2O-Ar and 0.4% O_2 + 2% H_2O-Ar using a fluidised-bed reactor. The FT-Raman and XPS spectroscopies were used to investigate the structural features during gasification. Our results confirm that the biochar-O_2 reaction and biochar-H_2O reactions followed different reaction pathways as indicated by the extents of the kinetic compensation effects. The biochar-O_2 and biochar-H_2O reactions cooperate so as to increase the O-containing functional groups on the biochar external surface leading to synergistic effects during the gasification in 0.4% O_2 + 15% H_2O-Ar. The presence of O-containing carbon active sites [C(O)] is found to be the key factor, which leads to synergy most likely on the char external surface in 0.4% O_2 + 15% H_2O-Ar. During the gasification in 0.4% O_2 + 2% H_2O-Ar, the char-O_2 and char-H_2O reactions proceed in parallel on the biochar external surface and inside the char bulk respectively without any synergistic effects. It is believed that the relative increase in the concentration of carbon active sites [C(O)] on the biochar external surface also leads to a drastic increase in the formation rate of H_2 in 0.4% O_2 + 15% H_2O-Ar relative to 15% H_2O-Ar.

Keywords: Mallee wood; Synergistic effects; Carbon active sites; Kinetic compensation effects; Gasification.

6.2 Introduction

The biochar-O_2 and biochar-H_2O reactions are fundamental reactions in the gasification process. The biochar-O_2 reaction oxidises biochar carbon by exothermic reactions and the biochar-H_2O reaction can produce synthesis gas through endothermic reactions [1–4].

The kinetic compensation effects (KCEs) are very useful in understanding the biochar-gas reactions during gasification [5–9]. Our previous study [10] reported the KCE during the char-O_2 reaction at a lower temperature range and its plausible explanation. The biochar-O_2 reaction was investigated further from 400 to 900 °C using a fluidised-bed reactor and it was observed [5] that the extents of the KCEs are different in the kinetics-controlled, mixed and the diffusion-controlled regimes during the biochar-O_2 reaction. The KCEs have also been reported during the biochar gasification in 15% H_2O-Ar [6]. During the biochar gasification in 15% H_2O-Ar, the gasification products i.e. CO, CO_2, and H_2 are formed mainly on the char surface and exhibit similar extents of the KCEs. Our recent study [11] has reported that the extents of the KCEs during steam gasification are also dependant on the partial pressure of H_2O. The H_2O partial pressure changes the surface coverage of the O-containing carbon active sites [C(O)] and, consequently, affects the extents and the relative rates of CO and CO_2 formation. The partial pressure of H_2O also increases the extents of the KCEs in 15% H_2O-Ar in comparison to 2% H_2O-Ar.

Many studies [12–21] have been conducted on carbon-O_2 and carbon-H_2O reactions to understand the nature of carbon active sites. It is commonly believed [22] that edge carbon atoms are more reactive than basal plan carbon atoms and can readily form bonds with the chemisorbed oxygen due to the presence of unpaired sp^2 electrons. However, the concept of edge carbon and basal carbon refers to graphitic structures and has little meaning to biochar. XPS studies [23–28] on carbon oxidation have revealed the presence of oxygen-containing functional groups on the carbon surfaces such as C-O, C=O, and O-C=O. The temperature-programmed desorption (TPD) of gas-phase oxidation of carbon surfaces has also indicated an increase in the oxygen-containing surface complexes (carboxylic, lactone, carbonyl, or carboxylic anhydride etc.), which are formed on dangling carbon sites [29–31]. FT-Raman spectroscopy has

also confirmed the formation of dangling structures during the oxidation of biochar in O_2 [32]. The TPD spectra of carbon materials suggest that CO_2 originates from carboxylic acid groups at low temperatures or from lactone type groups at higher temperatures [29,31,33,34]. It is also proposed [29,31,33] that adjacent carboxylic groups condense together to form a carboxylic anhydride. These carboxylic anhydrides present on dangling carbon sites yield both CO and CO_2. The char-O_2 reaction also changes the inner structure of the char as revealed by the FT-Raman spectroscopy [14,18,20]. Bigger aromatic ring clusters are formed during the oxidation of char as indicated by FT-Raman and ^{13}C NMR spectroscopies [14,35,36].

Further, it is believed [37] that carbon-oxygen complexes formed during the carbon-H_2O reaction are more stable than the carbon-oxygen complexes during the carbon-O_2 reaction. The H_2O vapour dissociates on the carbon surface by the formation of hydroxyl groups and ethers are formed presumably by the condensation of hydroxyl groups, which decompose to CO and new active sites [38]. XPS studies [39] have revealed the increase of such C-O structures (phenol and ethers type) on the char surface during the gasification of char in H_2O. The FT-Raman spectroscopy has also indicated the increase in the oxygen-containing functional groups in the char matrix as well as aromatic rings condensation during steam gasification [15,16,21].

The distribution of the energy levels of active sites is important and gives rise to the KCEs during the biochar gasification. However, the past studies mentioned above have not considered in situ monitoring of O-containing gaseous species (i.e. CO and CO_2) during the progress of biochar-O_2 and biochar-H_2O reactions. The formation kinetics of these key gasification products i.e. CO, CO_2 and H_2 (in the case of biochar-H_2O reaction) and char consumption can be very useful to investigate the distribution of energy levels during the biochar-O_2 and biochar-H_2O reactions. Further, the KCEs in the kinetics-controlled regime are found to be a key indicator of the reaction pathways during the gasification of biochar. During steam gasification, the carbon active sites are also occupied by C(H) or C(H_2). It is not clear how the presence of oxidising atmosphere i.e. O_2 would affect the KCEs of char gasification and formation of CO, CO_2, and H_2 during the biochar-H_2O gasification. The partial pressure of steam also effects the relative concentration of O-containing functional groups i.e. [C(O)] on the biochar external surface and inside the pores of the char matrix, which leads to

different relative rates of CO and CO_2 release during the gasification in 15% H_2O-Ar than those in 2% H_2O-Ar [11]. It is still unclear how the distribution of energy levels of active sites and the extent of the KCEs would change when partial pressure of steam is changed in the binary mixture of O_2 and H_2O. There is also no definite conclusion if the active sites formed from the biochar-O_2 reaction and the biochar-H_2O reaction would have the same energy distribution.

Therefore, this study will investigate the distribution of energy levels during the biochar gasification in O_2, H_2O, and their mixtures. The study will also provide mechanistic insight into the formations of CO, CO_2, and H_2 when the partial pressure of H_2O is changed in the mixture of O_2 and H_2O. The KCEs will be discussed to gain mechanistic insights during the biochar-O_2, biochar-H_2O reactions and in their mixtures.

6.3 Experimental

6.3.1 Experimental procedure

The wood of Australian mallee tree was used to prepare biomass samples in this study. The details of sample preparation can be found in a previous study [12]. Around 2.0 g of mallee wood sample was oven-dried overnight at 105 °C and was pyrolysed in ultra-high purity (UHP) argon in the fluidised-bed reactor so that $U \approx 10\ U_{mf}$, where U_{mf} represents the minimum fluidisation velocity. The reactor was firstly heated by an external electric furnace to the selected temperature until the temperature inside the reactor was stabilised. The feeding of the biomass was accomplished by the use of an electric vibrator. After holding for 5 minutes in UHP argon, the biochar samples were gasified in situ using the mixture of 0.4% O_2 balanced with argon (0.4% O_2-Ar), 15% H_2O balanced with argon (15% H_2O-Ar), 0.4% O_2 + 15% H_2O balanced with argon (0.4% O_2 + 15% H_2O-Ar), or 0.4% O_2 + 2% H_2O balanced with argon (0.4% O_2 + 2% H_2O-Ar). The data of 0.4% O_2-Ar, 2% H_2O-Ar and 15% H_2O-Ar have been published in references [5,6,11].

The product gas mixture was cooled before it was introduced into a quadrupole mass spectrometer (QMS Prisma^{TM} 200). The key gasification products i.e. CO, CO_2, CH_4, and H_2 were continuously monitored during gasification. The mass spectrometer was calibrated using the standard gas mixtures. The contribution of CO_2 to CO at m/z = 28 was calculated and subtracted. The mixing effects, as well as atmospheric air, were avoided by keeping the product sampling line short to the best possible extent. Further details of the experimental procedure can be found in Chapter 2.

For fixed partial pressures (p) of the gasifying agents, the rate of char gasification (r_c), rate of CO formation (r_c), rate of CO_2 formation (r_{CO2}), and the rate of H_2 formation (r_{H2}), at a given conversion x, can be calculated using the following equation [10]:

$$r_i = \frac{1}{W_i}\frac{dW_i}{dt} = f(x)g(p)A\exp\left(-\frac{E_{app}}{RT}\right) = A_i\, exp\left(-\frac{E_i}{RT}\right) \qquad (\text{Eq. } 6-1)$$

Where $i =$ char gasification, CO, CO_2, or H_2 formation. $f(x)$ in Eq. 6-1 represents the changes in char properties, which change with conversion 'x'. Further details of Eq. 6-1 have been outlined in Chapter 2.

6.3.2 Char characterisation

The FT-Raman and X-ray photoelectron spectroscopies (XPS) were used to characterise the biochar samples. The biochar samples were prepared in 0.4% O_2-Ar, 15% H_2O-Ar, 0.4% O_2 + 15% H_2O-Ar or 0.4% O_2 + 2% H_2O-Ar at 800 °C and 850 °C at a biochar conversion of 0.1. The biochar conversion was calculated by taking the ratio of $W_{char\ carbon\ released}$ to that of $W_{Total\ char\ carbon}$ and the reaction was stopped (by switching the flow of the given gasification atmosphere medium to UHP argon) and the reactor was lifted out of the furnace corresponding to the time when this ratio became equal to 0.1.

The Raman spectra in the range of 800 cm^{-1} to 1800 cm^{-1} were deconvoluted into 10 Gaussian bands by following the procedure outlined before [40]. The band intensity ratios of $I_D/(I_{(Gr + Vl+ Vr)}$ and the total Raman area have been used to investigate biochar structural features. The $I_D/(I_{(Gr + Vl+ Vr)}$ ratio represents the relative ratio of the

concentration of large aromatic rings (at least 6 or larger than 6 fused benzene rings) to that of the small aromatic rings (3-5 fused benzene rings). The total Raman area is a measure of O-containing Raman active species in the bulk of the biochar. Further, XPS was used to determine the O/C ratio on the biochar external surface. More details of these procedures can be found in Chapter 2.

6.4 Results and discussion

6.4.1 Char Reactivity

Figure 6-1 show the rate data in the kinetics-controlled regime during the gasification of biochar in 0.4% O_2-Ar, 15% H_2O-Ar, 0.4% O_2 + 15% H_2O-Ar and 0.4% O_2 + 2% H_2O-Ar. It has already been demonstrated elsewhere that kinetics-controlled regime lies in the temperature range of 700 to 850 °C for the biochar-H_2O reaction [6] whereas, for the biochar-O_2 reaction [5], in the temperature range of 400 to 500 °C.

Our results indicate that the shapes of the biochar reactivity curves were quite different during the gasification in 15% H_2O-Ar from 0.4% O_2-Ar (Figure 6-1 a and b). During the biochar-O_2 gasification, the char gasification rate increased monotonically with increasing temperature and char conversion. However, during the gasification in 15%

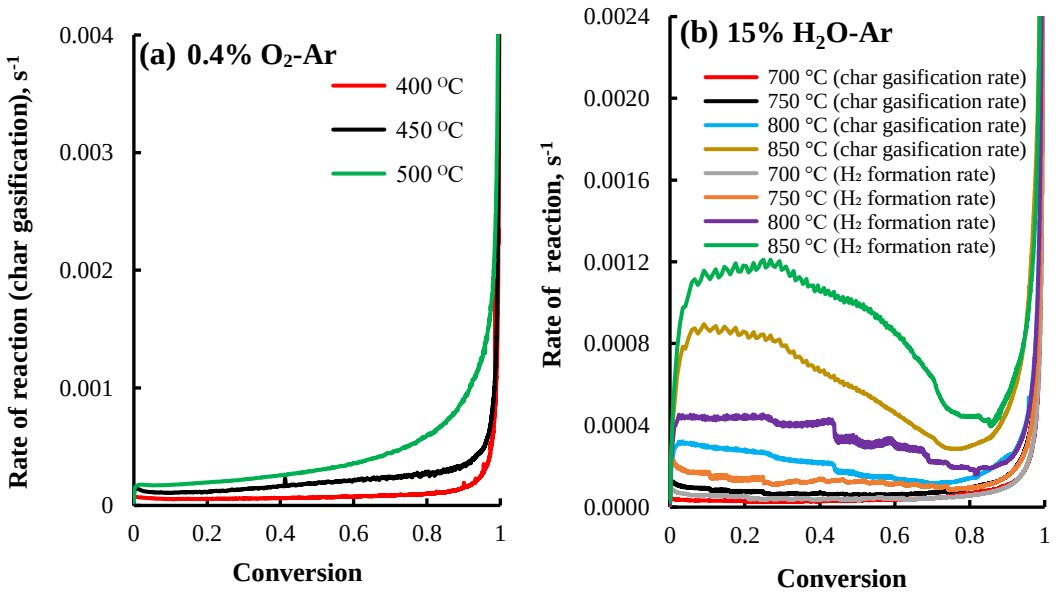

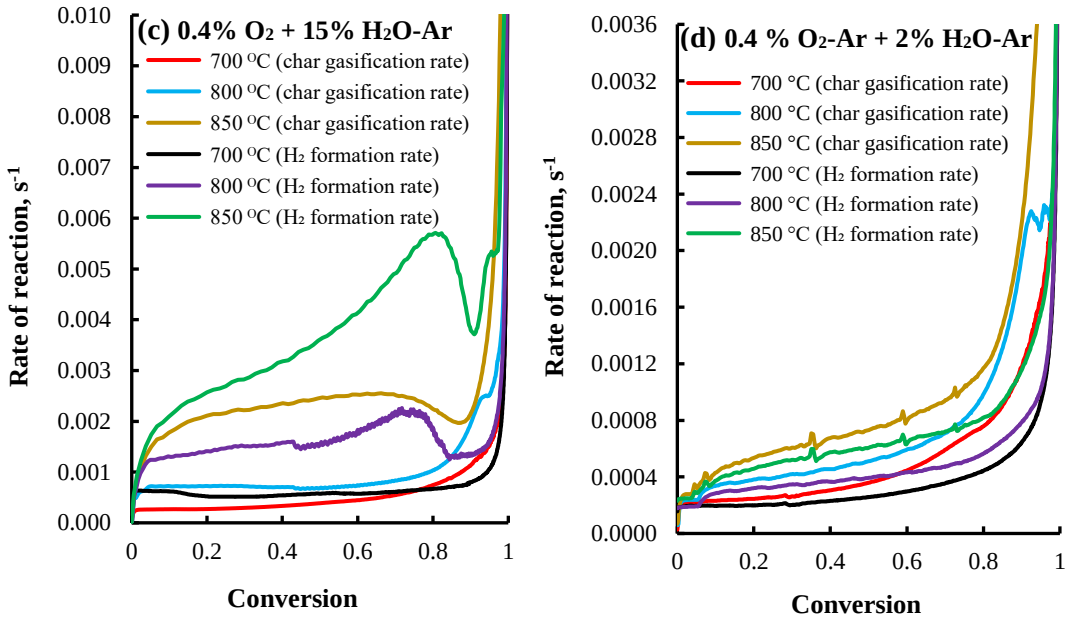

Figure 6-1 Rate vs. char conversion during the gasification of biochar in (a) 0.4% O_2-Ar, (b) 15% H_2O-Ar, (c) 0.4% O_2 + 15% H_2O-Ar and (d) 0.4% O_2 + 2% H_2O-Ar. The data on Figure 6-1 (a-b) have been published in references [5, 6].

H_2O-Ar, the rate of char gasification acquired an initial maximum (particularly at higher temperatures i.e. 800 °C and 850 °C) at very low char conversion followed by decreasing trend and finally exhibited a sharp rise at higher char conversions.

6.4.2 The presence and absence of synergistic effects during gasification in the mixture of O_2 and H_2O

It can be observed clearly (Figure 6-2 a and c) that the rate of char gasification in the mixture of 0.4% O_2 + 2% H_2O-Ar is equal to the sum of the rates in 0.4% O_2-Ar and 2% H_2O-Ar separately. This implies that char gasification rates in the mixture of 0.4% O_2 + 2% H_2O-Ar are addition of the individual rates without any inhibitive or synergistic effects. However, the char gasification rates increased significantly, and synergistic effects were observed during the gasification in the mixture of 0.4% O_2 + 15% H_2O-Ar. Further, it is also obvious (Figure 6-2 b and d) that the rate of H_2 formation increased during the gasification in 0.4% O_2 + 15% H_2O-Ar in comparison

to 15% H_2O-Ar. Similarly, it can be observed clearly that H_2 formation rates increased during the gasification in 0.4 % O_2 + 2% H_2O-Ar relative to 2% H_2O-Ar. This increase is more pronounced during the gasification in 0.4% O_2 + 15% H_2O-Ar relative to 0.4 % O_2 + 2% H_2O-Ar. This implies that the presence of O_2 during the gasification of biochar in H_2O (i.e. 2% H_2O and 15% H_2O) promotes the H_2 formation rate.

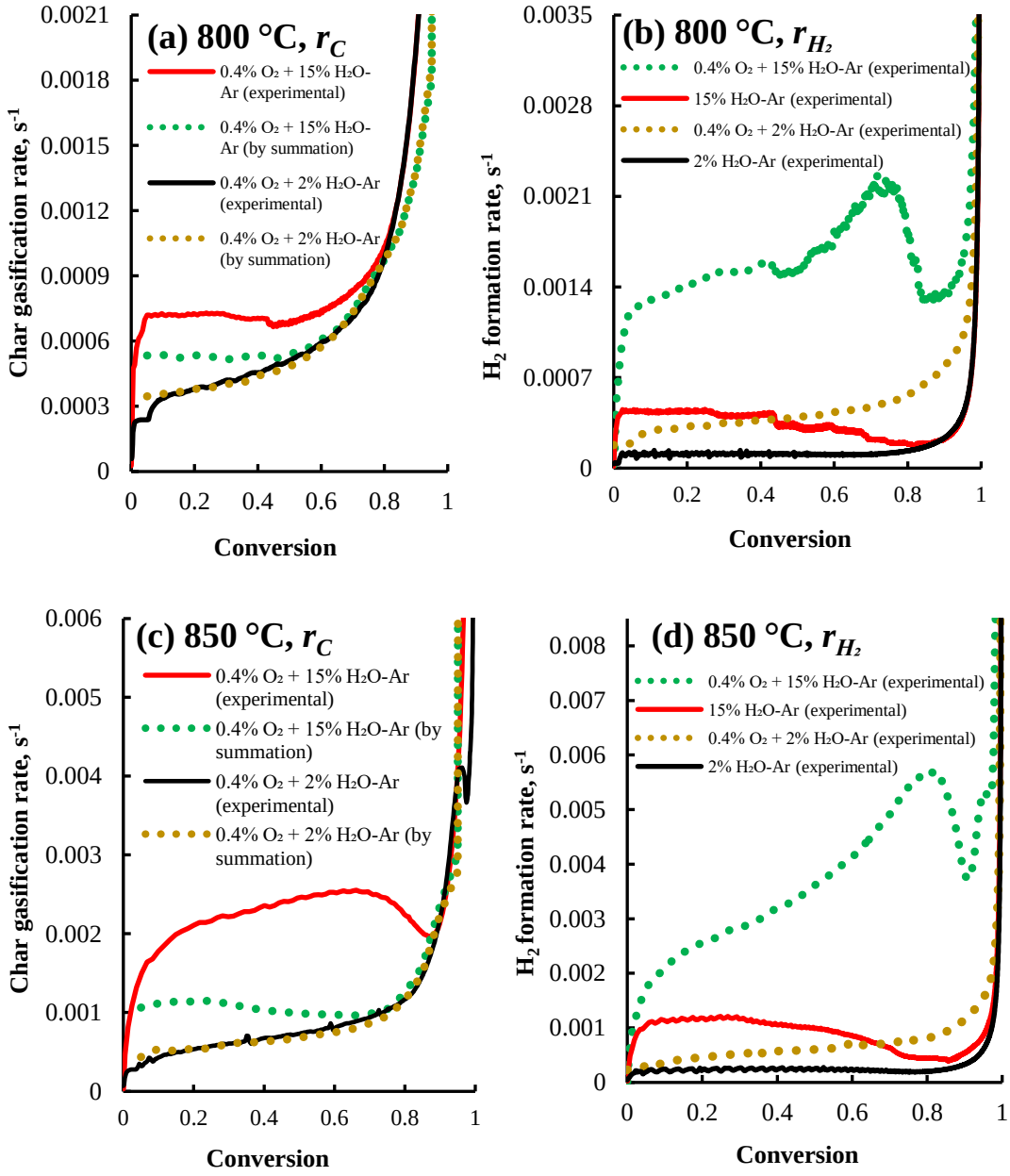

Figure 6-2 Effects of steam concentration on (a) char gasification rate at 800 °C, (b) H_2 formation rate at 800 °C, (c) char gasification rate at 850 °C and (d) H_2 formation rate at 850 °C during the gasification of biochar in a binary mixture of O_2 and H_2O. The data during the gasification in 15% H_2O-Ar and 2% H_2O-Ar have been published in references [6, 11].

6.4.3 Effects of gasification atmospheres on the kinetic parameters

Figure 6-3 (a-d) represent the data of apparent activation energy and apparent pre-exponential factors of char gasification and the formation of CO, CO_2 and H_2 (in case of steam gasification) during the biochar gasification in 0.4% O_2-Ar, 15% H_2O-Ar, 0.4% O_2 + 15% H_2O-Ar or 0.4% O_2 + 2% H_2O-Ar respectively. Our results indicate that the apparent activation energy and the apparent pre-exponential factors exhibited different trends in different gasification atmospheres.

During the biochar gasification in 15% H_2O-Ar [6], the apparent activation energy and the apparent pre-exponential factor of char gasification, CO, CO_2, and H_2 formations appeared to decrease with increasing conversions. During the gasification in 15% H_2O-Ar, the concentration of the oxygen-containing carbon species [C(O)] become increasingly abundant in the char matrix as revealed by the increase in total Raman intensity with increasing conversion for low-rank fuels [2,14,16,18,41]. The concentration of alkali and alkaline earth metallic (AAEM) species also increases with

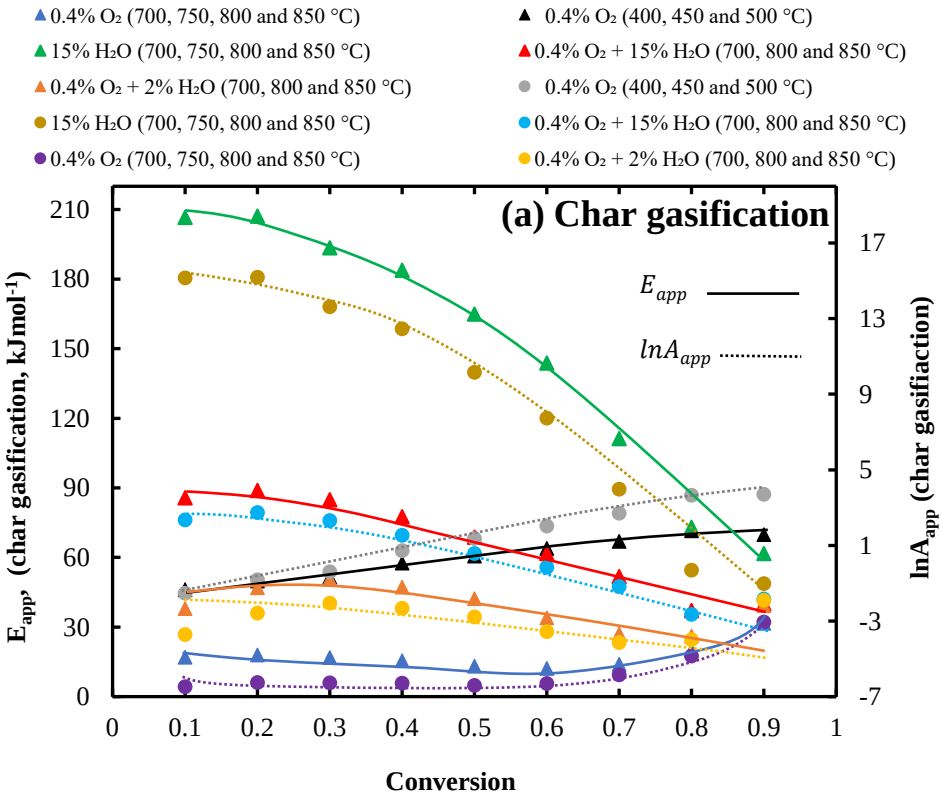

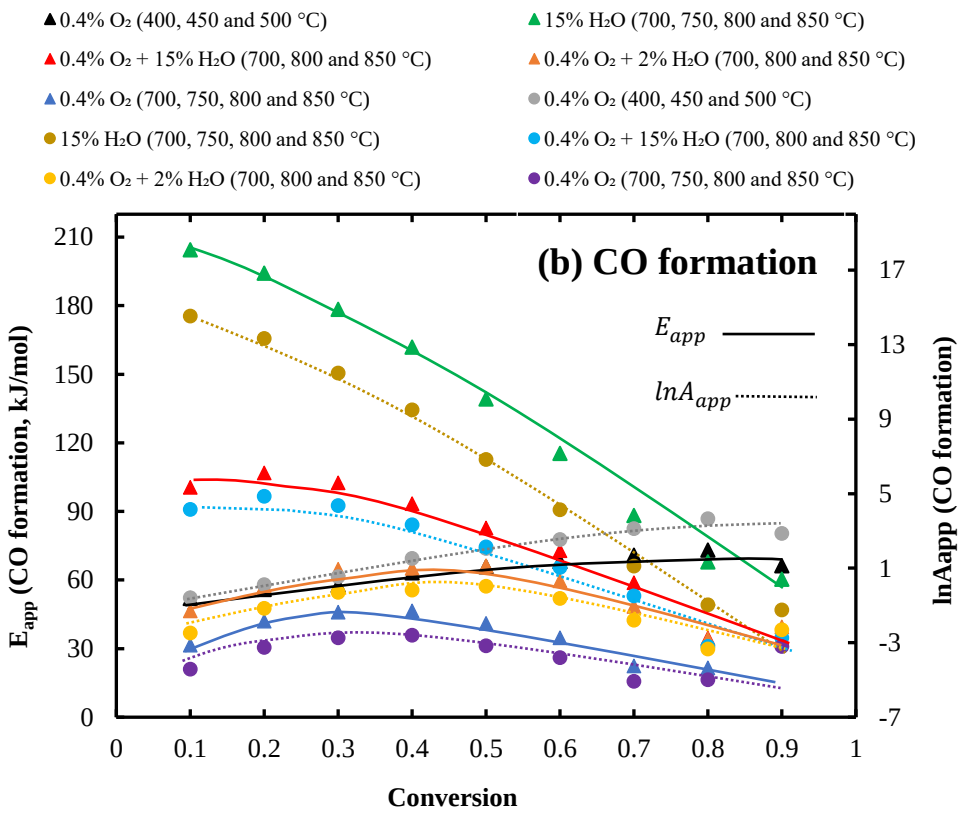
0.4% O2 (400, 450 and 500 °C)
15% H2O (700, 750, 800 and 850 °C)
0.4% O2 + 15% H2O (700, 800 and 850 °C)
0.4% O2 + 2% H2O (700, 800 and 850 °C)
0.4% O2 (700, 750, 800 and 850 °C)
0.4% O2 (400, 450 and 500 °C)
15% H2O (700, 750, 800 and 850 °C)
0.4% O2 + 15% H2O (700, 800 and 850 °C)
0.4% O2 + 2% H2O (700, 800 and 850 °C)
0.4% O2 (700, 750, 800 and 850 °C)
(b) CO formation
Eapp
lnAapp
Eapp (CO formation, kJ/mol)
lnAapp (CO formation)
Conversion

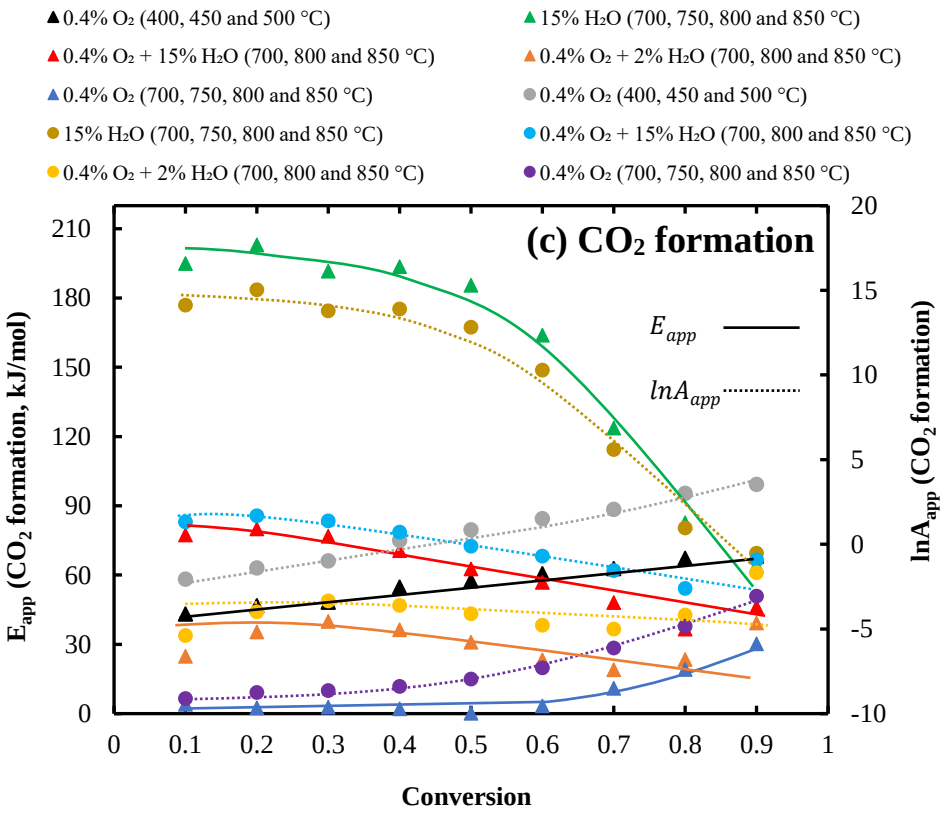
0.4% O2 (400, 450 and 500 °C)
15% H2O (700, 750, 800 and 850 °C)
0.4% O2 + 15% H2O (700, 800 and 850 °C)
0.4% O2 + 2% H2O (700, 800 and 850 °C)
0.4% O2 (700, 750, 800 and 850 °C)
0.4% O2 (400, 450 and 500 °C)
15% H2O (700, 750, 800 and 850 °C)
0.4% O2 + 15% H2O (700, 800 and 850 °C)
0.4% O2 + 2% H2O (700, 800 and 850 °C)
0.4% O2 (700, 750, 800 and 850 °C)
(c) CO2 formation
Eapp
lnAapp
Eapp (CO2 formation, kJ/mol)
lnAapp (CO2 formation)
Conversion

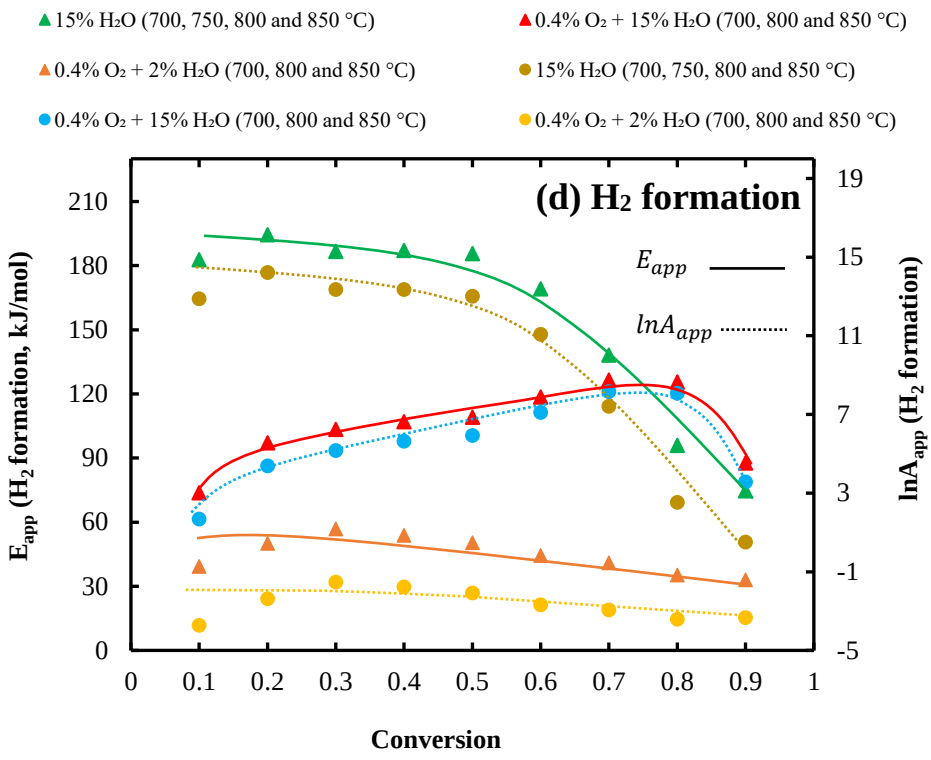

Figure 6-3 The apparent activation energy (E_{app}) and apparent pre-exponential factors (lnA_{app}) of (a) char gasification vs. biochar conversion, (b) CO formation vs. biochar conversion, (c) CO_2 formation vs. biochar conversion and (d) H_2 formation vs. biochar conversion during the gasification in 0.4% O_2-Ar, 15% H_2O-Ar, 0.4% O_2 + 15% H_2O-Ar and 0.4% O_2 + 2% H_2O-Ar. Symbols ▲ and ● are used to represent the apparent activation energy and the apparent pre-exponential factors respectively. The data of the pre-exponential factors have been shown on the secondary vertical axis. The data during the gasification in 0.4% O_2-Ar, 15% H_2O-Ar have been published in references [5, 6].

increasing char conversions [42–44]. It is believed [18] that these AAEM species are bonded to O-containing carbon active sites, thereby increasing the catalytic effects in the residual char with increasing char conversion, which is considered to be responsible for the decrease in the apparent activation energy levels with conversion during the biochar gasification in 15% H_2O-Ar. While, during the gasification in 0.4% O_2-Ar in the kinetics-controlled regime (400 to 500 °C), the apparent activation energy and the apparent pre-exponential factor of char gasification, CO and CO_2 formations increased monotonically with increasing char conversion. The comparison at any

given conversion reveals that activation energy levels of char gasification, CO and CO_2 formations are significantly different during the gasification in 0.4% O_2-Ar from those for 15% H_2O-Ar. This implies that biochar gasification in 0.4% O_2-Ar and 15% H_2O-Ar follows different reaction pathways.

The steam gasification forms O-containing carbon active sites [C(O)] and H-containing carbon active sites [C(H)] on the char surface by the dissociation of the H_2O. During steam gasification, the aromatic rings would open up. In the presence of [C(O)] and [C(H)], these broken aromatic rings can either be gasified or recombine to become bigger aromatic rings. The steam gasification involves the preferential consumption and/or conversion of the smaller aromatic rings present in the biochar into larger aromatic rings and, consequently, the aromatic rings system grows with the biochar conversion during steam gasification [1,14,15,17,45].

The gasification in O_2 forms aliphatic or sp^3-rich structures by the breakage of the aromatic rings, which are transformed into the dangling structures [32]. These dangling structures attached to the aromatic rings are considered to be the active sites on the char surface, which can further be released/gasified during the biochar-O_2 reaction. It is believed that these dangling structures are formed preferentially on smaller aromatic rings system at lower char conversion requiring lower apparent activation energy and lower pre-exponential factors [10]. As conversion is progressed, the active sites on larger aromatic rings become the dominant sites of reaction requiring higher apparent activation energy and higher pre-exponential factors [10].

The activation energy levels and the pre-exponential factors reduced significantly during the biochar gasification in 0.4% O_2 + 15% H_2O-Ar in comparison to 15% H_2O-Ar. The biochar-O_2 reaction is controlled by the diffusion limitations from 700 to 850 °C as indicated by the apparent activation energy values in this temperature range and the mass transport of oxygen to the biochar external surface and to the interior pores near the external surface is the rate-controlling step. This also suggests that char gasification in the mixture of 0.4% O_2 + 15% H_2O-Ar is affected by mass transfer limitations in terms of the char-O_2 reaction.

However, biochar-H_2O reaction is mainly controlled by the intrinsic kinetics in the temperature range of 700 to 850 °C and corresponding CO and CO_2 would be formed from the bulk of biochar because of the char-H_2O reaction. Therefore, in the mixture of 0.4% O_2 + 15% H_2O-Ar, the observed apparent activation energy of char gasification, CO and CO_2 formations are controlled by the intrinsic kinetics of the biochar-H_2O gasification. However, due to the presence of mass-transfer effects of biochar-O_2 surface reaction, the apparent activation energy values of char gasification, CO and CO_2 formations are reduced in the mixture of 0.4% O_2 + 15% H_2O-Ar relative to 15% H_2O-Ar. Further, to investigate the structural changes in the char bulk surface and on the char external surface, we performed the FT-Raman and XPS analysis respectively, which are included in the subsequent section.

As, the partial pressure of H_2O was reduced i.e. from 15% to 2% in the mixture of O_2 and H_2O, the apparent activation energy and the apparent pre-exponential factors of char gasification, CO and CO_2 formations appeared to decrease with biochar conversions and remained between the values of 0.4% O_2-Ar and 0.4% O_2 + 15% H_2O-Ar. The partial pressure of H_2O affects the relative concentration of O-containing carbon active species [C(O)] on the char surface [11]. Therefore, during the char gasification in the mixture of 0.4% O_2 + 2% H_2O-Ar, the extent of biochar-H_2O gasification is reduced. In other words, the importance of the char-O_2 reaction (i.e. in the diffusion-controlled regime in the range of 700-850 °C) increases relative to the char-H_2O reaction. This results in lowering the apparent activation energy values and the apparent pre-exponential factors in 0.4% O_2 + 2% H_2O-Ar relative to 0.4% O_2 + 15% H_2O-Ar.

6.4.4 Biochar characterisation by FT-Raman and XPS

Figure 6-4 (a-c) illustrate the total Raman area and $I_D/(I_{(Gr + Vl+ Vr)}$ ratio determined by Raman spectroscopy and O/C ratio determined by XPS at 800 °C and 850 °C at a char conversion of 10%. The data show that the total Raman area and $I_D/(I_{(Gr + Vl+ Vr)}$ ratio are higher during the gasification in 15% H_2O-Ar than 0.4% O_2-Ar. The total Raman area is affected by the Raman scattering and light absorptivity of char [40,42,45]. The

electron-rich structures such as O-containing functional groups, when connected to aromatic rings, give a resonance effect and increase the Raman scattering ability and, therefore, the observed total Raman area [42,45]. The presence of large aromatic rings in the biochar has the tendency to increase the light absorptivity of char, thereby decreasing the total Raman area or the Raman active O-containing groups.

As the FT-Raman gives the bulk property analysis, therefore, increase in total Raman area indicates that the relative formation of O-containing functional groups is higher in the bulk of char during the gasification in 15% H_2O-Ar than 0.4% O_2-Ar. On the contrary, the O/C ratio determined by the XPS shows that the oxygen bound on the biochar external surface is higher during the gasification in 0.4% O_2-Ar than 15% H_2O-Ar. This shows the presence of more O-containing functional groups on the char external surface during the gasification in 0.4% O_2-Ar relative to 15% H_2O-Ar. This also implies that the char-O_2 reaction is in the diffusion-controlled regime at 800 °C and 850 °C and oxygenates char external surface relative to the char bulk surface. Further, $I_D/(I_{(Gr + Vl+ Vr)}$ ratio indicates that the preferential consumption and/or conversion of the smaller aromatic rings into larger aromatic rings is higher during the gasification in 15% H_2O-Ar than 0.4% O_2-Ar. This reflects that the char-H_2O reaction is intrinsic in nature at 800 °C and 850 °C and causes more structural changes (as reflected by total Raman area and $I_D/(I_{(Gr + Vl+ Vr)}$ ratio) in the bulk surface of biochar relative to the char-O_2 reaction.

Further, the closeness in the total Raman area and $I_D/(I_{(Gr + Vl+ Vr)}$ ratio during the gasification in 0.4% O_2 + 15% H_2O-Ar to that of 15% H_2O-Ar indicates that changes in the char structure are mainly because of the char-H_2O reaction in the char bulk. Whereas, a drastic increase in O/C ratio in 0.4% O_2 + 15% H_2O-Ar relative to either 0.4% O_2-Ar or 15% H_2O-Ar shows a significant increase in the O-containing functional groups on the char external surface. It is believed that gasification in 0.4% O_2 + 15% H_2O-Ar creates additional active sites, particularly on the external char surface as a result of breaking off the aromatic rings. As the aromatic rings would break off during the biochar-O_2 and biochar-H_2O reactions, the accessibility of O_2 and H_2O to these newly created active sites would increase the oxygenation rate, as reflected by the O/C ratio on the external char surface and, consequently, the char

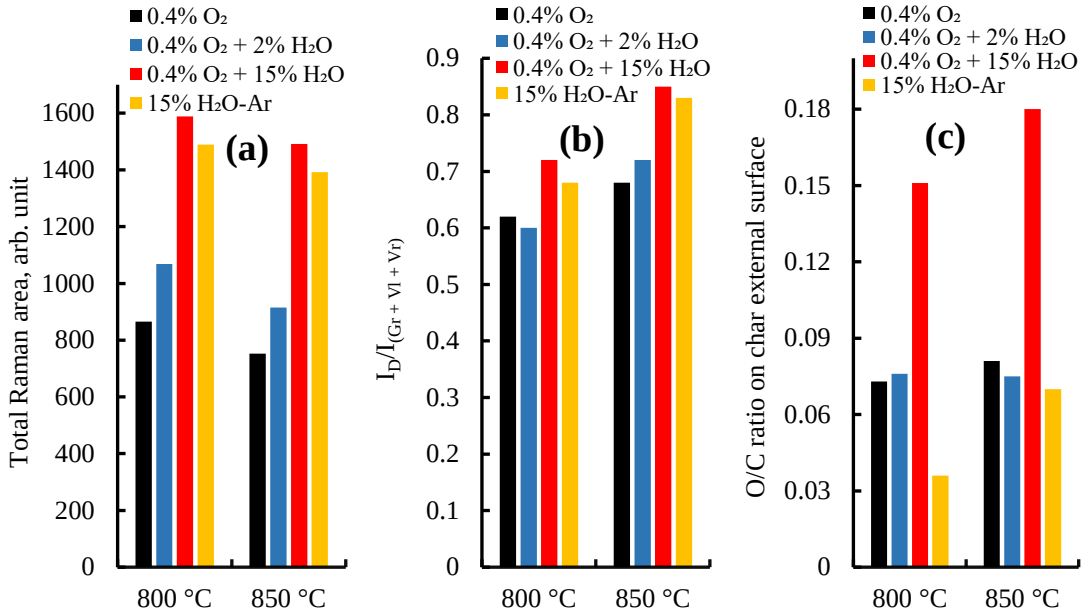

Figure 6-4 (a) Total Raman area, (b) ratio of $I_D/(I_{(Gr + Vl+ Vr)}$ (c) ratio of oxygen to carbon on the biochar external surface during the gasification of biochar in 0.4% O_2-Ar, 0.4% O_2 + 2% H_2O-Ar, 0.4% O_2 + 15% H_2O-Ar and 15% H_2O-Ar at 800 °C and 850 °C for char conversion i.e. x = 0.1

gasification rate as indicated by the synergistic effects (Figure 6-2 a and c). The relative increase in the total Raman area, $I_D/(I_{(Gr + Vl+ Vr)}$ ratio and O/C ratio during gasification in 0.4% O_2 + 15% H_2O-Ar to that of 15% H_2O-Ar also suggests that the presence of O_2 would promote the reaction of C(O) with H_2O and this leads to higher rates of char gasification and would increase the rates more than merely the sum of the rates in 0.4% O_2 and 15% H_2O.

Whereas, during the gasification in 0.4% O_2 + 2% H_2O-Ar, a slight increase in the total Raman area relative to 0.4% O_2-Ar without any significant changes in $I_D/(I_{(Gr + Vl+ Vr)}$ ratio and O/C ratio (on the char external surface) reveals that the carbon active sites on the biochar external surface or close to the external surface are oxygenated mainly by the O_2 (diffusion-controlled) and the active sites in the char bulk are oxygenated predominantly by the H_2O (kinetics-controlled). As a result, the relative concentration of O-containing carbon active sites [C(O)] only increases inside the char bulk surface, which is reflected in the increased total Raman area during the gasification in 0.4% O_2 + 2% H_2O-Ar in comparison to 0.4% O_2-Ar. Further, the biochar-H_2O reaction would

be much slower than biochar-O_2 reaction and the biochar-O_2 reaction (on the external char surface or on the neighbouring active sites) and the biochar-H_2O reaction (inside the char bulk) take place in parallel without any synergistic effects in 0.4% O_2 + 2% H_2O-Ar.

Furthermore, the increase in the total Raman area and O/C ratio during the gasification in 0.4% O_2 + 15% H_2O-Ar relative to 0.4% O_2 + 2% H_2O-Ar indicates that the relative concentration of O-containing carbon surface species [C(O)] is higher in 0.4% O_2 + 15% H_2O-Ar than 0.4% O_2 + 2% H_2O-Ar. A sharp rise in the O/C ratio or [C(O)] in 0.4% O_2 + 15% H_2O-Ar relative to 0.4% O_2 + 2% H_2O-Ar also suggests that the nature/type of [C(O)] formed on the char external surface in 0.4% O_2 + 15% H_2O-Ar can be different in comparison to 0.4% O_2 + 2% H_2O-Ar.

Additionally, the lower relative ratio of $I_D/(I_{(Gr + Vl+ Vr)}$, as well as the lower relative concentration of O-containing functional groups, suggest that gasification in 0.4% O_2 + 2% H_2O-Ar decreases the relative rates of aromatic rings gasification and condensation in comparison to 0.4% O_2 + 15% H_2O-Ar. The lower relative ratio of $I_D/(I_{(Gr + Vl+ Vr)}$ indicates the lower concentration of larger aromatic rings and, consequently, the growth of the aromatic rings system is reduced, which leaves the char less condensed during the char gasification in the mixture of 0.4% O_2 + 2% H_2O-Ar relative to 0.4% O_2 + 15% H_2O-Ar at same char conversion.

Moreover, the formation of H_2 mainly involves the carbon active sites on the char surface during steam gasification [10]. The drastic increase in the formation rate of H_2 during the gasification in 0.4% O_2 + 15% H_2O-Ar suggests that such increase is also from those O-containing carbon active sites present on the biochar external surface or from the active sites close by. The gasification in 0.4% O_2 + 15% H_2O-Ar would also increase the concentration of H-radicals [C(H)] on the char external surface and, consequently, H_2 formation rate relative to 0.4% O_2 + 2% H_2O-Ar.

6.4.5 Effects of gasification atmospheres on the formation of CO and CO_2

The data in Figure 6-5 (a-d) display the molar flux of CO and CO_2 during the biochar gasification in the mixtures of 0.4% O_2 + 15% H_2O-Ar, 0.4% O_2 + 2% H_2O-Ar and 0.4% O_2-Ar. The molar flux of CO and CO_2 increased relative to 0.4% O_2-Ar as the

biochar undergoes gasification in the mixture of 0.4% O_2 + 2% H_2O-Ar. Similarly, the molar flux of CO and CO_2 became higher during the gasification in the mixture of 0.4% O_2 + 15% H_2O-Ar in comparison to 0.4% O_2 + 2% H_2O-Ar. It has also been found that the relative formation of O-containing functional groups, as reflected by the total Raman area, increased during the gasification in 0.4% O_2 + 2% H_2O-Ar in comparison to 0.4% O_2-Ar. Similarly, the total Raman area became higher during the biochar gasification in the mixtures of 0.4% O_2 + 15% H_2O-Ar relative to 0.4% O_2 + 2% H_2O-Ar. This reveals that the molar flux of CO and CO_2 from the char surface is correlated with the concentration of oxygen-containing active species [C(O)] formed on the biochar surface during the gasification. This can be represented as:

$$r_{co} = g[C(O)] \quad \text{(Eq. 6-2)}$$

$$r_{co_2} = z[C(O)] \quad \text{(Eq. 6-3)}$$

where r_{co} and r_{co_2} represent the molar flux of CO and CO_2 and [C(O)] indicates the concentration of O-containing carbon actives sites. Further, the char reactivity is higher during the gasification in 0.4% O_2 + 2% H_2O-Ar relative to 0.4% O_2-Ar and, similarly, during the gasification in 0.4% O_2 + 15% H_2O-Ar relative to 0.4% O_2 + 2% H_2O-Ar, which infers that the concentration of [C(O)] formed on the char surface is at least partly responsible for the higher biochar reactivity during the gasification.

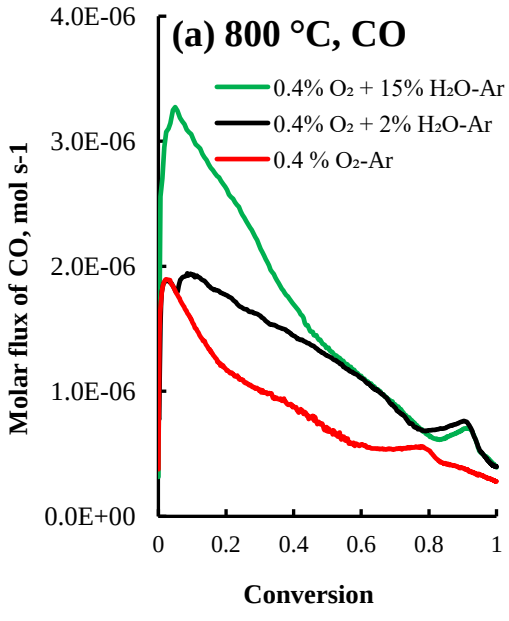

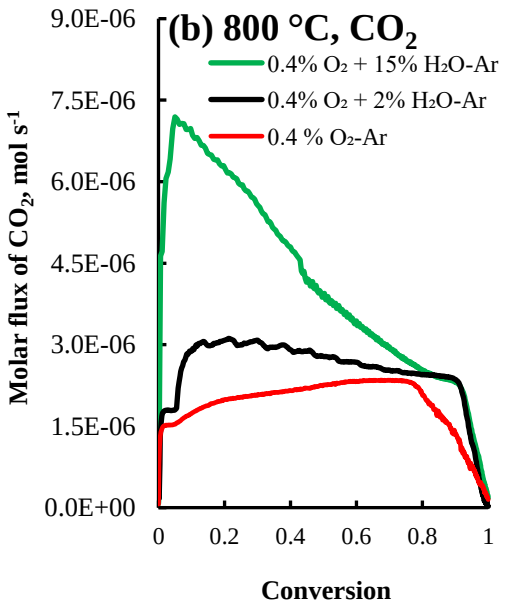

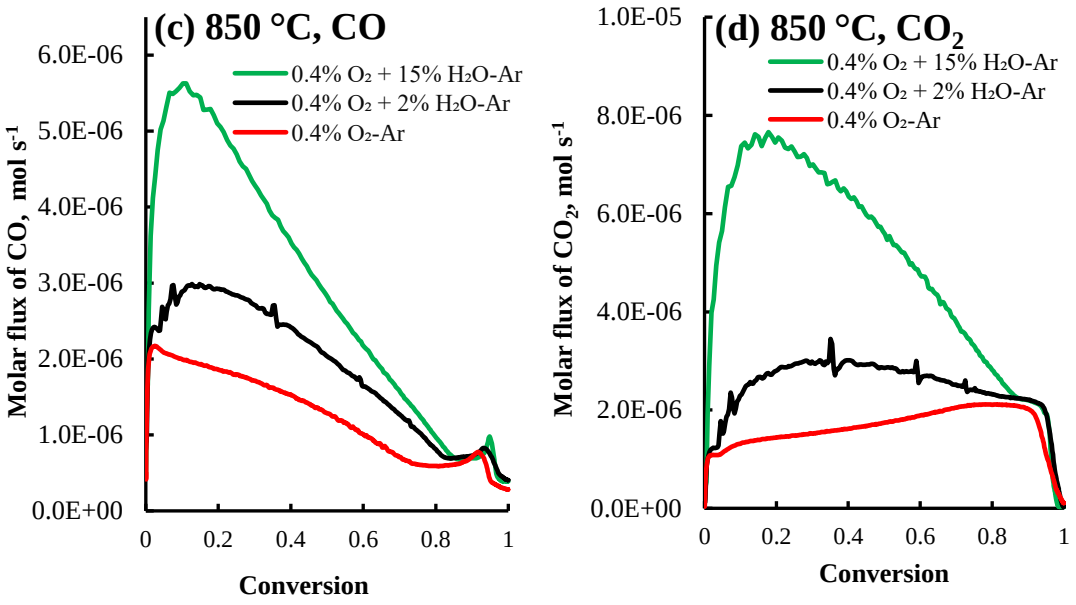

Figure 6-5 The molar flux of (a) CO and (b) CO_2 as a function of biochar conversion at 800 °C and the molar flux of (c) CO and (d) CO_2 as a function of biochar conversion at 850 °C during the gasification of biochar in 0.4% O_2 + 15% H_2O-Ar, 0.4% O_2 + 2% H_2O-Ar and 0.4% O_2-Ar.

6.4.6 Effects of gasification atmospheres on the kinetic compensation effects (KCEs)

The char gasification demonstrated different activation energy levels and demonstrated different slopes '*m*' and the intercepts '*c*' values in the KCEs during the char gasification in 0.4% O_2-Ar from 15% H_2O-Ar (Figure 6-6). This indicates that the char undergoes different extents of the KCEs in 0.4% O_2-Ar and 15% H_2O-Ar. Further, the activation energy values and the extents of the KCEs (indicated by different '*m*' and '*c*' values) of CO and CO_2 formations are also different during the gasification in 0.4% O_2-Ar from 15% H_2O-Ar. This confirms that gasification in 0.4% O_2-Ar and 15% H_2O-Ar follows different reaction pathways, which has been discussed in the earlier section.

As the char undergoes gasification in a binary mixture of 0.4% O_2 + 15% H_2O-Ar, the extents of the KCEs of the char gasification, CO, CO_2, and H_2 formations are found to be different either from 0.4% O_2-Ar or 15% H_2O-Ar. Further, the '*m*' and '*c*' values

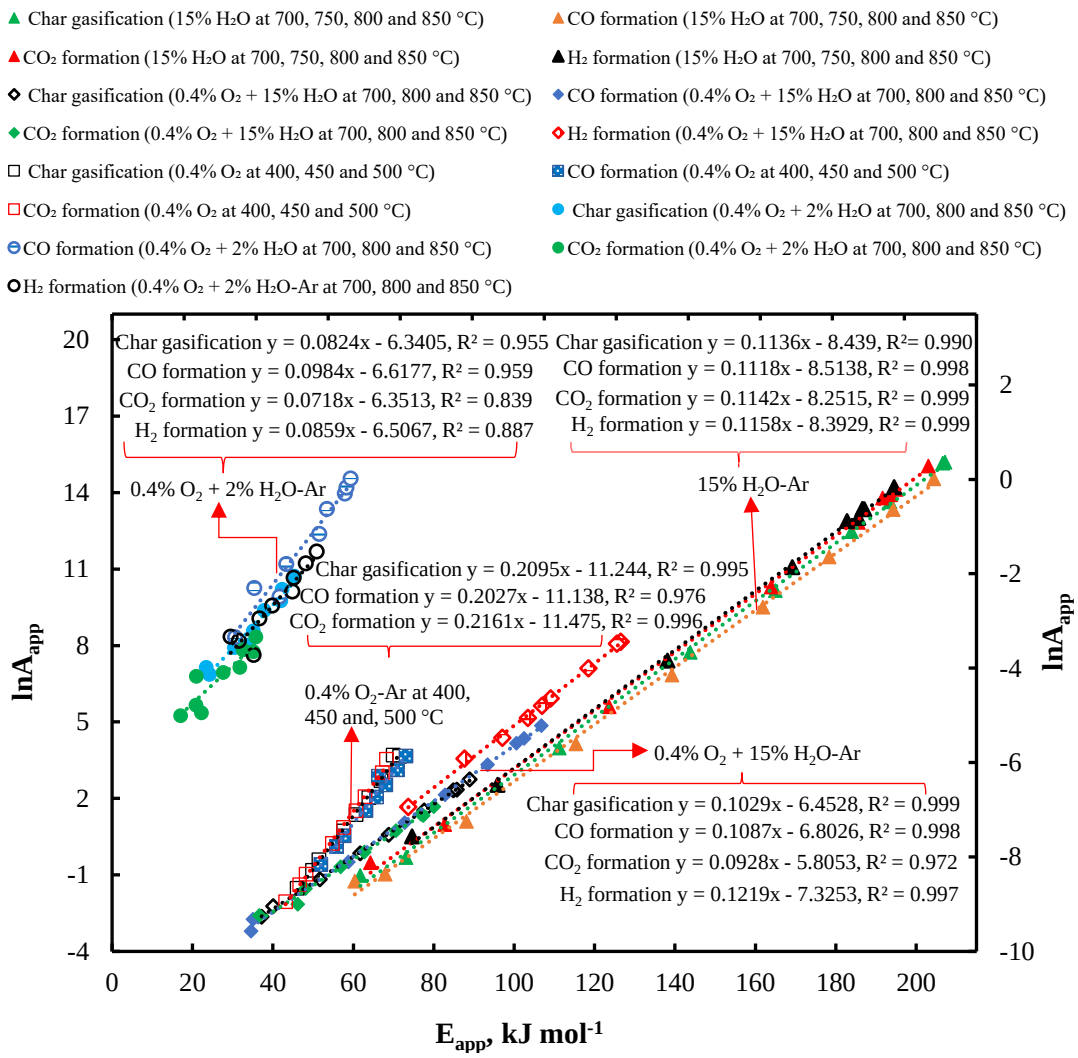

Figure 6-6 Effects of gasification atmospheres on the kinetic compensation effects of char gasification and the formation of CO, CO_2 and H_2 during the gasification of biochar in 15% H_2O-Ar, 0.4% O_2 + 15% H_2O-Ar, 0.4% O_2-Ar and 0.4% O_2 + 2% H_2O-Ar. The data of lnA_{app} during the gasification in 0.4% O_2 + 2% H_2O-Ar have been shown on the secondary vertical axis. The data during the gasification in 0.4% O_2-Ar and 15% H_2O-Ar have been published in references [5, 6].

in the KCEs of char gasification, CO, CO_2 and H_2 formations in 0.4% O_2 + 15% H_2O-Ar found to be close to the values in 15% H_2O-Ar (Figure 6-6). This confirms that during the char gasification in the mixture of 0.4% O_2 + 15% H_2O-Ar, the intrinsic kinetics of biochar-H_2O reaction dominates relative to biochar-O_2 reaction. Further, it is believed that the reaction of C(O) with H_2O is the rate-limiting step during gasification in the mixture of O_2 and H_2O. During the steam gasification in the presence of O_2, a lot of oxygen-containing species C(O) are formed particularly on the

char external surface as indicated by the O/C ratio in comparison to either 0.4% O_2-Ar or 15% H_2O-Ar. As a result of this, the reaction of C(O) with steam would be promoted. The closeness in the total Raman area and $I_D/(I_{(Gr + Vl+ Vr)}$ ratio, which represent the changes in the chemical structure in the char bulk, during the gasification in 0.4% O_2 + 15% H_2O-Ar and 15% H_2O-Ar also confirms that the reaction of C(O) with steam is dominant inside the char bulk relative to char-O_2 reaction.

Further, the activation energy values and the slopes i.e. '*m*' values in KCEs of char gasification, CO, CO_2, and H_2 formations reduced during the gasification in the mixture of 0.4% O_2 + 2% H_2O-Ar relative to 0.4% O_2 + 15% H_2O-Ar (Figure 6-6). The higher partial pressure of H_2O increases the extent of steam gasification during the gasification in the O_2 and H_2O mixture particularly in the char bulk. Whereas, lower partial pressure of the H_2O reduces the relative concentration of [C(O)] and [C(H)] on the char surface and lowers the char gasification and H_2 formation rates (Figure 6-1 c and d) from the char surface. This suggests that due to lower relative concentration of [C(O)] during gasification in 0.4% and 2% H_2O mixture, the reaction of C(O) with steam is not promoted even in the presence of O_2. This also mean that the char-O_2 reaction would be dominant relative to char-H_2O reaction, which results in reducing the activation energies and '*m*' values in the KCEs during the gasification in the mixture of 0.4% O_2 + 2% H_2O-Ar relative to 0.4% O_2 + 15% H_2O-Ar.

In addition to this, the apparent activation energies and '*m*' values in the KCEs of char gasification and H_2 formation also lowered in the binary mixture of 0.4% O_2 + 2% H_2O-Ar relative to 2% H_2O-Ar. For char gasification $m = 0.1073$ and for H_2 formation $m = 0.1062$ during the gasification in 2% H_2O-Ar, which has been reported before [11]. These values reduced from '0.1073' to '0.0824' for char gasification and from '0.1062' to '0.0859' for H_2 formation during the gasification in 0.4% O_2 + 2% H_2O-Ar. This also suggests that as the extent of biochar-H_2O reaction is reduced, the apparent activation energies and '*m*' values in the KCEs of char gasification and H_2 formation decrease during the gasification in 0.4% O_2 + 2% H_2O-Ar relative to 2% H_2O-Ar.

6.5 Conclusions

The biochar-O_2 and biochar-H_2O reactions demonstrate different extents of the kinetic compensation effects of char gasification, and the formation of CO and CO_2. The kinetics of char gasification, as well as FT-Raman and XPS results, show that during the gasification in 0.4% O_2 + 2% H_2O-Ar, the biochar-O_2 reaction and the biochar-H_2O reactions take place in parallel on the biochar external surface (or on the active sites close to the external surface) and inside the char bulk surface respectively without any synergistic effects. Whereas, the O/C ratio determined by XPS reveals the increasing O-containing carbon active sites [C(O)] on the char external surface during the gasification in 0.4% O_2 + 15% H_2O-Ar relative to either 0.4% O_2 or 15% H_2O-Ar. The values of E_{app}, $I_D/(I_{(Gr + Vl+ Vr)}$ ratios as well as O/C ratios suggest that the relative concentration and type/nature of [C(O)] is different in 0.4% O_2 + 15% H_2O-Ar in comparison to 0.4% + 2% H_2O-Ar, which leads to synergistic effects in 0.4% O_2 + 15% H_2O-Ar.

6.6 References

[1] Li C.-Z. Some recent advances in the understanding of the pyrolysis and gasification behaviour of Victorian brown coal. Fuel 2007;86:1664–83. doi:10.1016/j.fuel.2007.01.008.

[2] Li C.-Z. Importance of volatile-char interactions during the pyrolysis and gasification of low-rank fuels - A review. Fuel 2013;112:609–23. doi:10.1016/j.fuel.2013.01.031.

[3] Li C.-Z. Advances in the science of Victorian Brown Coal. 2004. doi:10.1016/B978-0-08-044269-3.X5000-6.

[4] Li C.-Z. Special issue - Gasification: A route to clean energy. Process Saf Environ Prot 2006;84:407–8. doi:10.1205/psep.ed.0606.

[5] Akhtar M.A., Zhang S, Shao X, Dang H, Liu Y, Li T, et al. Kinetic compensation effects in the chemical reaction-controlled regime and mass transfer-controlled regime during the gasification of biochar in O_2. Fuel Process Technol 2018;181:25–32. doi:10.1016/j.fuproc.2018.09.009.

[6] Akhtar M.A., Zhang S, Li C.-Z. Mechanistic insights into the kinetic compensation effects during the gasification of biochar in H_2O. Fuel 2019;255:115839. doi:10.1016/j.fuel.2019.115839.

[7] Dhupe AP, Gokarn AN, Doraiswamy LK. Investigations into the compensation effect at catalytic gasification of active charcoal by carbon dioxide. Fuel 1991;70:839–44. doi:10.1016/0016-2361(91)90192-D.

[8] Kwon TW, Kim JR, Kim SD, Park WH. Catalytic steam gasification of lignite char. Fuel 1989;68:416–21. doi:10.1016/0016-2361(89)90261-5.

[9] Shufen Li and Yuanlin Cheng. Catalytic gasification of gas-coal char in CO_2. Fuel 1995;74:456–8.

[10] Wu H, Li X, Hayashi JI, Chiba T, Li C.-Z. Effects of volatile-char interactions on the reactivity of chars from NaCl-loaded Loy Yang brown coal. Fuel

2005;84:1221–8. doi:10.1016/j.fuel.2004.06.037.

[11] Akhtar M.A., Li C.-Z. Mechanistic insights into the kinetic compensation effects during the gasification of biochar : Effects of the partial pressure of H_2O.Fuel 2020;263:116632. doi:10.1016/j.fuel.2019.116632

[12] Asadullah M, Zhang S, Min Z, Yimsiri P, Li C.-Z. Importance of biomass particle size in structural evolution and reactivity of char in steam gasification. Ind Eng Chem Res 2009;48:9858–63. doi:10.1021/ie901214z.

[13] Bayarsaikhan B, Hayashi J, Shimada T, Sathe C, Li C, Tsutsumi a, et al. Kinetics of steam gasification of nascent char from rapid pyrolysis of a Victorian brown coal. Fuel 2005;84:1612–21. doi:10.1016/j.fuel.2005.02.008.

[14] Guo X, Tay HL, Zhang S, Li C.-Z. Changes in char structure during the gasification of a Victorian brown coal in steam and oxygen at 800 °C. Energy and Fuels 2008;22:4034–8. doi:10.1021/ef800528c.

[15] Keown DM, Hayashi J-I, Li C.-Z. Drastic changes in biomass char structure and reactivity upon contact with steam. Fuel 2008;87:1127–32. doi:10.1016/j.fuel.2007.05.057.

[16] Li T, Zhang L, Dong L, Li C.-Z. Effects of gasification atmosphere and temperature on char structural evolution during the gasification of Collie sub-bituminous coal. Fuel 2014;117:1190–5. doi:10.1016/j.fuel.2013.08.040.

[17] Tay HL, Kajitani S, Zhang S, Li C.-Z. Inhibiting and other effects of hydrogen during gasification: Further insights from FT-Raman spectroscopy. Fuel 2014;116:1–6. doi:10.1016/j.fuel.2013.07.066.

[18] Tay HL, Kajitani S, Zhang S, Li C.-Z. Effects of gasifying agent on the evolution of char structure during the gasification of Victorian brown coal. Fuel 2013;103:22–8. doi:10.1016/j.fuel.2011.02.044.

[19] Tay H-L, Kajitani S, Wang S, Li C.-Z. A preliminary Raman spectroscopic perspective for the roles of catalysts during char gasification. Fuel 2014;121:165–72. doi:10.1016/j.fuel.2013.12.030.

[20] Zhang S, Hayashi JI, Li C.-Z. Volatilisation and catalytic effects of alkali and alkaline earth metallic species during the pyrolysis and gasification of Victorian brown coal. Part IX. Effects of volatile-char interactions on char-H_2O and char-O 2 reactivities. Fuel 2011;90:1655–61. doi:10.1016/j.fuel.2010.11.008.

[21] Zhang S, Min Z, Tay HL, Wang Y, Dong L, Li C.-Z. Changes in char structure during the gasification of mallee wood: Effects of particle size and steam supply. Energy and Fuels 2012;26:193–8. doi:10.1021/ef2011589.

[22] Marsh H, Kuo K. Introduction to Carbon Science. Butterworth & Co. (Publishers) Ltd; doi:10.1016/b978-0-408-03837-9.50009-9.

[23] Boehm H-P. Surface chemical characterization of carbons from adsorption studies. Adsorpt by Carbons 2008:301–27. doi:10.1016/b978-008044464-2.50017-1.

[24] Da Youxian, Wang Dianxun, Sun Mujin, Chen Chuanzheng, Yue Jin. A study of the surface of carbon fiber by means of X-ray photoelectron spectroscopy-III. Compos Sci Technol 1987;30:119–26. doi:10.1016/0266-3538(87)90044-3.

[25] Lee WH, Lee JG, Reucroft PJ. XPS study of carbon fiber surfaces treated by thermal oxidation in a gas mixture of $O_2/(O_2+N_2)$. Appl Surf Sci 2001;171:136–42. doi:10.1016/S0169-4332(00)00558-4.

[26] Levi G, Senneca O, Causà M, Salatino P, Lacovig P, Lizzit S. Probing the chemical nature of surface oxides during coal char oxidation by high-resolution XPS. Carbon 2015;90:181–96. doi:10.1016/j.carbon.2015.04.003.

[27] Perry DL, Grint A. Application of XPS to coal characterization. Fuel 1983;62:1024–33. doi:10.1016/0016-2361(83)90135-7.

[28] Wang S, Wu L, Hu X, Zhang L, Li T, Jiang S, et al. Changes in the biochar chemical structure during the low-temperature gasification of mallee biochar in air as revealed with fourier transform infrared/raman and x-ray photoelectron spectroscopies. Energy and Fuels 2018;32:12545–53.

doi:10.1021/acs.energyfuels.8b02870.

[29] Otake Y, Jenkins RG. Characterization of oxygen-containing surface complexes created on a microporous carbon by air and nitric acid treatment. Carbon 1993;31:109–21. doi:10.1016/0008-6223(93)90163-5.

[30] Figueiredo JL, Pereira MFR, Freitas MMA, Orfao JJM. Modification of the surface chemistry of activated carbons 1999;37:1379–89.

[31] Boehm HP. Surface oxides on carbon and their analysis: A critical assessment. Carbon 2002;40:145–9. doi:10.1016/S0008-6223(01)00165-8.

[32] Zhang L, Li T, Wang S, Song Y, Dong L, Zhang S, et al. Changes in char structure during the thermal treatment of nascent chars in N_2 and subsequent gasification in O_2. Fuel 2017;199:264–71. doi:10.1016/j.fuel.2017.02.097.

[33] Belhachemi M, Khiari B, Jeguirim M, Sepulveda-Escribano A. Characterization of biomass-derived chars. 2019. doi:10.1016/B978-0-12-814893-8.00003-1.

[34] Boehm HP. Some aspects of the surface chemistry of carbon blacks and other carbons. Carbon 1994;32:759–69. doi:10.1016/0008-6223(94)90031-0.

[35] Park J, Yoo S, Lim KH, Rojas OJ, Hubbe MA, Park S. Impact of oxidative carbonization on structure development of loblolly pine-derived biochar investigated by nuclear magnetic resonance spectroscopy and X-ray photoelectron spectroscopy. Diam Relat Mater 2019;96:140–7. doi:10.1016/j.diamond.2019.05.001.

[36] Yip K, Ng E, Li C.-Z., Hayashi JI, Wu H. A mechanistic study on kinetic compensation effect during low-temperature oxidation of coal chars. Proc Combust Inst 2011;33:1755–62. doi:10.1016/j.proci.2010.07.073.

[37] Walker PL, Rusinko F, Austin LG. Gas reactions of carbon. Adv Catal 1959;Volume 11:133–221. doi.org/10.1016/S0360-0564(08)60418-6.

[38] Hermann G, Huttinger KJ. Mechanism of water vapour gasification of carbon-

A new model. Carbon 1986;24:705–13. doi:10.1016/0008-6223(86)90178-8.

[39] Wang S, Wu L, Hu X, Zhang L, O'Donnell KM, Buckley CE, et al. An X-ray photoelectron spectroscopic perspective for the evolution of O-containing structures in char during gasification. Fuel Process Technol 2018;172:209–15. doi:10.1016/j.fuproc.2017.12.019.

[40] Li X, Hayashi J, Li C.-Z. FT-Raman spectroscopic study of the evolution of char structure during the pyrolysis of a Victorian brown coal. Fuel 2006;85:1700–7. doi:10.1016/j.fuel.2006.03.008.

[41] Wang S, Wu L, Hu X, Zhang L, Li T, Li C.-Z. Effects of the particle size and gasification atmosphere on the changes in the char structure during the gasification of mallee biomass. Energy and Fuels 2018;32:7678–84. doi:10.1021/acs.energyfuels.8b01309.

[42] Li X, Hayashi J ichiro, Li C.-Z. Volatilisation and catalytic effects of alkali and alkaline earth metallic species during the pyrolysis and gasification of Victorian brown coal. Part VII. Raman spectroscopic study on the changes in char structure during the catalytic gasification in air. Fuel 2006;85:1509–17. doi:10.1016/j.fuel.2006.01.011.

[43] Quyn DM, Wu H, Hayashi J, Li C.-Z. Volatilisation and catalytic effects of alkali and alkaline earth metallic species during the pyrolysis and gasification of Victorian brown coal. Part IV. Catalytic effects of NaCl and ion-exchangeable Na in coal on char reactivity☆. Fuel 2003;82:587–93. doi:10.1016/S0016-2361(02)00323-X.

[44] Quyn DM, Wu H, Li C.-Z. Volatilisation and catalytic effects of alkali and alkaline earth metallic species during the pyrolysis and gasification of Victorian brown coal. Part I. Volatilisation of Na and Cl from a set of NaCl-loaded samples. Fuel 2002;81:143–9. doi:10.1016/S0016-2361(01)00127-2.

[45] Li X, Li C.-Z. Volatilisation and catalytic effects of alkali and alkaline earth metallic species during the pyrolysis and gasification of Victorian brown coal. Part VIII. Catalysis and changes in char structure during gasification in steam.

Fuel 2006;85:1518–25. doi:10.1016/j.fuel.2006.01.007.

7.0 Chapter

Conclusions and Recommendations

7.1 Conclusions

This study aimed to gain insight into the mechanism and kinetics of biochar gasification in oxygen, steam and their mixtures. For this purpose, gasifying agents consisting of 0.4% O_2-Ar, 15% H_2O-Ar, 2% H_2O-Ar, 0.4% O_2 + 15% H_2O-Ar and 0.4% O_2 + 2% H_2O-Ar were used for the gasification of biochar. The biochar was produced in situ from the pyrolysis of mallee wood in two particle size ranges of 0.80-1.0 mm and 2.0-3.3 mm in a fluidised-bed reactor in UHP argon. A quadrupole mass spectrometer was used to monitor the product gas composition continuously. The kinetic parameters i.e. the apparent activation energy (E_{app}) and the apparent pre-exponential factors (lnA_{app}) of char consumption and the formation of CO, CO_2, and H_2 were calculated by the Arrhenius plots. The FT-Raman and XPS spectroscopies were used to investigate the structural features of biochar. The phenomenon of kinetic compensation was observed. The results from this study contribute to a better understanding of the biochar gasification mechanisms. The main conclusions/findings of this study will be summarised below.

7.1.1 Biochar-O_2 reaction

- The biochar-O_2 reaction exhibited different extents of the KCEs in different temperature regimes i.e. kinetics-controlled, mixed and diffusion-controlled regimes. The apparent activation energies during the char-O_2 reaction can be explained with the activation of the aromatic ring sizes.
- The extent of diffusion limitation was found to be correlated with the extent of the KCEs in the mixed regime. The higher diffusion limitations led to higher 'm' and 'c' values in the KCEs i.e. $lnA_{app} = mE_{app} + c$
- The 'm' and 'c' values in the mixed regime can serve as a criterion for the extent of the mass-transfer effects during the char-O_2 reaction.
- The weak and/or negative KCE were observed in the diffusion-controlled regime unlike the kinetics-controlled regime.

- The extent of the KCEs varied with char conversion in the kinetics-controlled regime. This change in the extent of the KCEs indicated that the char properties changed significantly at higher conversions where the reaction rates were also high in comparison to lower conversions.

7.1.2 Biochar-H_2O reaction

- The gasification in 15% H_2O-Ar also demonstrated the KCEs. The demonstration of the KCE of CO and CO_2 formation in the kinetics-controlled and mixed regime revealed that the formation of CO_2 was mainly from the biochar-H_2O surface reaction instead of gas-phase water-gas-shift reaction.

- Additionally, E_{app} and lnA_{app} of CO and CO_2 formation, which were found to be very close to each other suggested that the formation of CO and CO_2 involves the same types of O-containing carbon species [C(O)] on the biochar surface (R 7-1 to R 7-3) or CO_2 is formed by the surface-catalysed water-gas-shift reaction. This can be expressed as:

$$C(O) \longrightarrow CO(g) \qquad \text{(R 7-1)}$$

$$C(O) + C(O) \longrightarrow CO_2(g) + C \qquad \text{(R 7-2)}$$

$$C(CO) + H_2O(g) \longrightarrow CO_2(g) + H_2(g) + C \qquad \text{(R 7-3)}$$

- The extent of the KCE didn't change considerably both in the kinetic-controlled and mixed regime with particle size i.e. 0.80-1.0 mm vs 2.0-3.3 mm. The KCEs of H_2 formation and biochar consumption were also found to be similar for both particle sizes. The formation of H_2 largely involves the carbon species on the biochar surface instead of the gas-phase water-gas-shift reaction.

- The reduction in the partial pressure of H_2O (from 15% to 2%) decreased the apparent activation energies, the apparent pre-exponential factors, as well as '*m*' values in the KCEs of char gasification and formation of CO, CO_2, and H_2. The higher partial pressure of H_2O increased the concentration of O-containing

functional groups on the biochar external surface and inside the char bulk as reflected by FT-Raman and XPS data.

- The relative concentration of these O-containing carbon species [C(O)] affected the relative rates of the CO and CO_2 release resulting in a lower CO/CO_2 ratio (at lower char conversions) during the gasification in 15% H_2O-Ar than those in 2% H_2O-Ar. The step, $C(O) + C(O) = CO_2(g) + C$ or $C(O) + H_2O(g) = CO_2(g) + H_2(g)$ was dominating over the step i.e. $C(O) = CO(g)$ during the gasification in 15% H_2O-Ar. Whereas the step, $C(O) = CO(g)$ was dominating over $C(O) + C(O) = CO_2(g) + C$ or $C(O) + H_2O(g) = CO_2(g) + H_2(g)$ during the gasification in 2% H_2O-Ar.
- The gasification in 15% H_2O-Ar favoured the aromatic ring condensation and increased the relative concentration of larger aromatic rings in 15% H_2O-Ar in comparison to 2% H_2O-Ar as indicated by the $I_D/(I_{(Gr + Vl+ Vr)}$ ratio.
- The higher relative concentration of larger aromatic rings was requiring higher energy of activation and increased the relative concentration of active sites (with similar properties) on the activation of bigger aromatic rings, which resulted in the higher pre-exponential factors. Due to this, the biochar-H_2O reaction demonstrated higher extents of the KCE of char gasification and formation of CO, CO_2, and H_2 in 15% H_2O-Ar relative to 2% H_2O-Ar.

7.1.3 Biochar gasification in O_2 and H_2O mixtures

- During the gasification in the mixture 0.4% O_2 + 2% H_2O-Ar, the char-O_2 reaction and char-H_2O reaction proceeded in parallel on the biochar external surface and inside the char bulk respectively without any synergistic effects. This was confirmed by the kinetics of char gasification and by the FT-Raman and XPS spectroscopies.
- XPS and FT-Raman data confirmed that the biochar gasification in 0.4% O_2 + 15% H_2O-Ar enhanced the formation of O-containing functional groups [C(O)] on the biochar external surface. The relative abundance of

[C(O)] during steam gasification in the presence of O_2 also promoted the reaction of C(O) with H_2O which led to the synergistic effects in 0.4% O_2 + 15% H_2O-Ar.

- The molar flux of CO and CO_2 from the char surface, which was determined by the mass spectrometer, was found to be correlated with the concentration of oxygen-containing Raman active species [C(O)] on the biochar surface during the gasification. This can be represented as:

$$r_{co} = g[C(O)] \quad \text{(Eq. 7-1)}$$

$$r_{co_2} = \mathrm{z}[C(O)] \quad \text{(Eq. 7-2)}$$

where r_{co} and r_{co_2} represent the molar flux of CO and CO_2 and [C(O)] indicates the concentration of carbon actives sites with surface bound O_2.

- The H_2 formation rate also increased sharply along with the char gasification rate in 0.4% O_2 + 15% H_2O-Ar relative to 15% H_2O-Ar and involved the O-containing carbon species [C(O)] most likely on the biochar external surface.

7.2 Recommendations for future work

- This study focused on the wood from the mallee tree. The other low-grade fuels e.g. brown coal, lignite and sub-bituminous coal that are excellent gasification feedstocks can be selected to extend the present work. These low-grade fuels have different chemical structures and feed composition from the mallee wood. For instance, brown coal and biomass are quite different in their inherent oxygen contents. The char formed after the pyrolysis of these fuels would also have different structures, which would change the nature of the carbon active sites and the KCE as well as their reactivity during gasification. Understanding the fundamental nature of the carbon active sites from these fuels in relation to the char reactivity can greatly help to understand the gasification behaviour of char.

- In the present study, the char has been characterised by FT-Raman and XPS at ambient conditions whereas, the char is produced at a higher temperature during the gasification. It could be very useful and meaningful if these analyses are performed either in situ or at a similar temperature at which char is produced. This can help to understand if the char has different structural features at ambient temperature from its preparation temperature.

- The present work aimed at the biochar gasification in O_2, H_2O, and their mixtures. The char gasification in 0.4% O_2 + 15% H_2O-Ar has synergistic effects whereas, the char gasification in 0.4% O_2 + 2% H_2O-Ar is only additive. This shows that synergistic effects during the char gasification also depend on the partial pressure of H_2O in the binary mixture of O_2 and H_2O. This finding can be further explored using the binary mixtures of CO_2 + H_2O as well as CO_2 + O_2 using different partial pressure of CO_2. The presence of CO_2 with steam or CO_2 with O_2 can also form active sites similar to those in 0.4% O_2 + 15% H_2O-Ar, which can lead to synergistic effects during gasification.

- This study investigated char chemical properties using FT-Raman and XPS spectroscopies. As the active site on the char surface is consumed, it could change the pore structure and size distribution along with the char structural changes. Therefore, it can also be important to analyse these physical properties. This can aid to investigate the effects of these physical properties on the char reactivity and to correlate these properties to the char structural changes, and thus the KCEs, during gasification.

- This work used O_2 gas as an oxidising atmosphere. The use of oxygen carriers e.g. solids can also be investigated as an alternate for partial oxidation instead of gas-phase oxygen. The use of solid adsorbents would eliminate the need to use pure oxygen.

Appendix-I

(Supplementary Data)

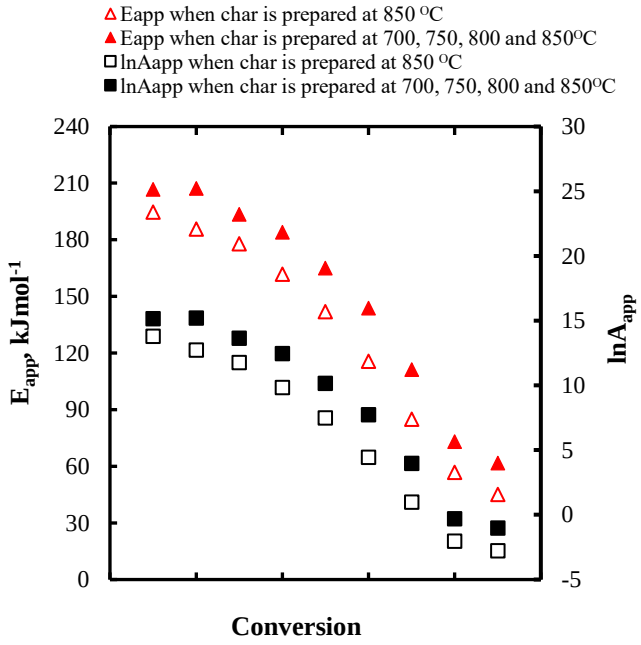

Figure S1 Effects of pyrolysis temperature on the apparent activation energy (E_{app}) and the apparent pre-exponential factors (lnA_{app}) for 2.0-3.3 mm particle size.

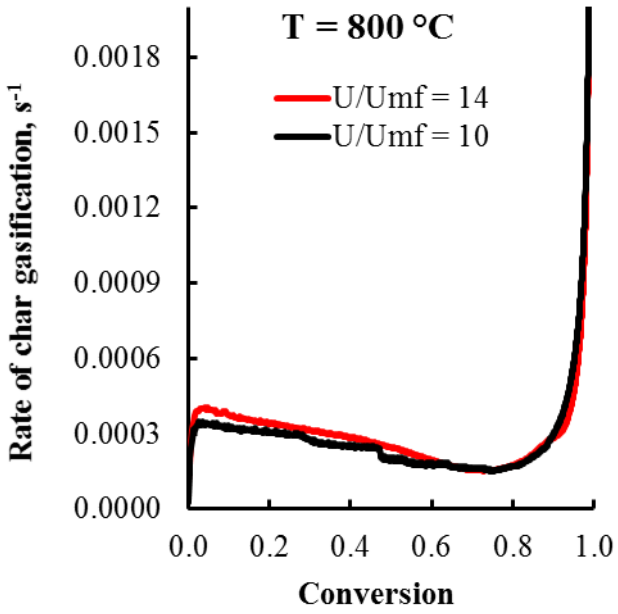

Figure S2 Rate of char gasification vs. conversion using particle sizes of 2.0-3.3 mm mallee wood in 15% H_2O-Ar. U and Umf represent the superficial gas velocity and the velocity of the minimum fluidisation respectively.

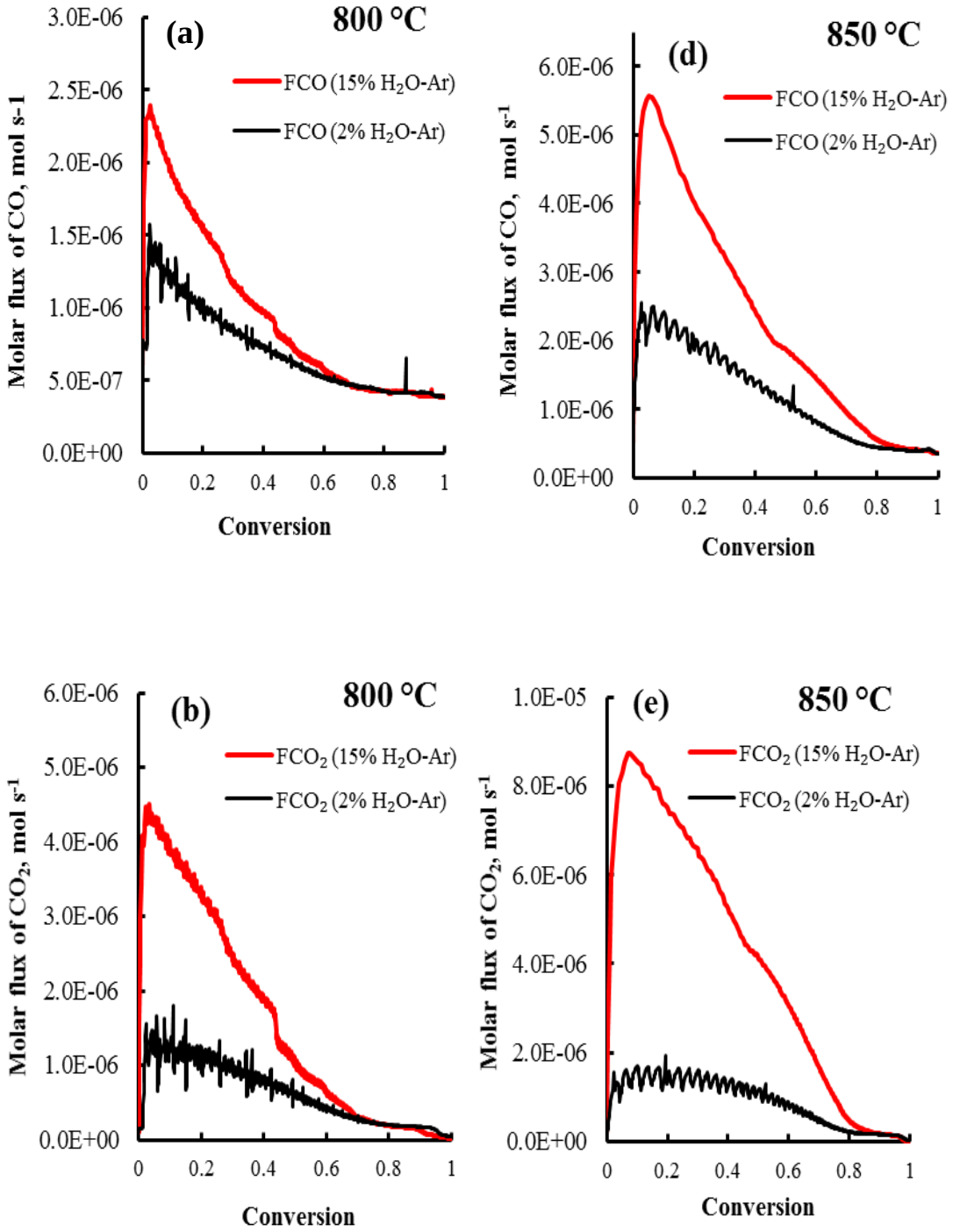
(a)
800 °C
FCO (15% H2O-Ar)
FCO (2% H2O-Ar)
Molar flux of CO, mol s-1
Conversion
(d)
850 °C
FCO (15% H2O-Ar)
FCO (2% H2O-Ar)
Molar flux of CO, mol s-1
Conversion
(b)
800 °C
FCO2 (15% H2O-Ar)
FCO2 (2% H2O-Ar)
Molar flux of CO2, mol s-1
Conversion
(e)
850 °C
FCO2 (15% H2O-Ar)
FCO2 (2% H2O-Ar)
Molar flux of CO2, mol s-1
Conversion

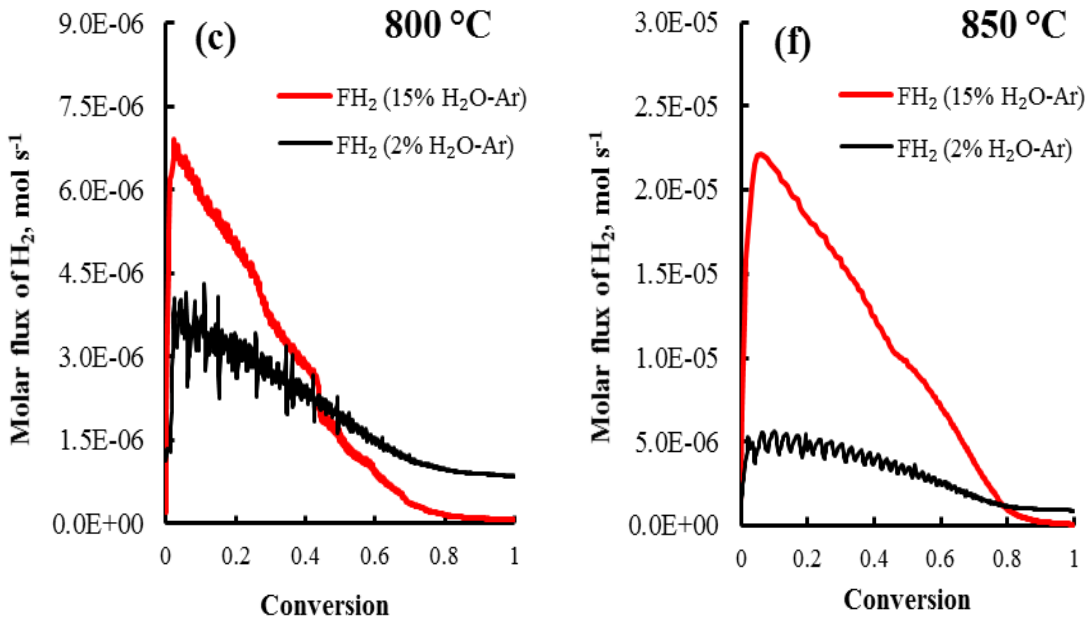

Figure S3 The molar flux of (a) CO, (b) CO_2 and (c) H_2 as a function of biochar conversion at 800 °C and the molar flux of (d) CO, (e) CO_2 and (f) H_2 as a function of biochar conversion at 850 °C during the gasification of biochar in 15% H_2O-Ar and 2% H_2O-Ar.

Appendix-II

(Permission of Reproduction from

the Copyright Owner)

Title: FT-Raman spectroscopic study of the evolution of char structure during the pyrolysis of a Victorian brown coal
Author: Xiaojiang Li,Jun-ichiro Hayashi,Chun-Zhu Li
Publication: Fuel
Publisher: Elsevier
Date: September 2006

Order Completed

Thank you for your order.

This Agreement between Fuels and Energy Technology Institute ("You") and Elsevier ("Elsevier") consists of your license details and the terms and conditions provided by Elsevier and Copyright Clearance Center.

Your confirmation email will contain your order number for future reference.

printable details

License Number	4658760699264
License date	Aug 30, 2019
Licensed Content Publisher	Elsevier
Licensed Content Publication	Fuel
Licensed Content Title	FT-Raman spectroscopic study of the evolution of char structure during the pyrolysis of a Victorian brown coal
Licensed Content Author	Xiaojiang Li,Jun-ichiro Hayashi,Chun-Zhu Li
Licensed Content Date	Sep 1, 2006
Licensed Content Volume	85
Licensed Content Issue	12-13
Licensed Content Pages	8
Type of Use	reuse in a thesis/dissertation
Portion	figures/tables/illustrations
Number of figures/tables/illustrations	1
Format	both print and electronic
Are you the author of this Elsevier article?	No
Will you be translating?	No
Original figure numbers	Table 1
Title of your thesis/dissertation	Biochar Gasification Mechanism
Expected completion date	Jun 2020
Estimated size (number of pages)	150
Requestor Location	Fuels and Energy Technology Institute Bentley WA 6102, Australia Perth, WA 6152 Australia Attn: Fuels and Energy Technology Institute
Publisher Tax ID	GB 494 6272 12
Total	0.00 USD

ORDER MORE | CLOSE WINDOW

Chapter 3, Article: “Kinetic compensation effects in the chemical reaction-controlled regime and mass transfer-controlled regime during the gasification of biochar in O_2”. Fuel Process Technol 2018;181:25–32. **https://doi.org/10.1016/j.fuproc.2018.09.009**

Chapter 4, Article: “Mechanistic insights into the kinetic compensation effects during the gasification of biochar in H_2O”. Fuel 2019;255:115839. **https://doi.org/10.1016/j.fuel.2019.115839**

Chapter 5, Article: “Mechanistic insights into the kinetic compensation effects during the gasification of biochar: Effects of the partial pressure of H_2O”. Fuel 2020;263:116632. **https://doi.org/10.1016/j.fuel.2019.116632**

Appendix-III

(Attribution Statements)

To Whom It May Concern

I, Muhammad Asif Akhtar, contributed in terms of conceptualization, methodology, experimental investigations, formal analysis of data, writing-original draft and revising to the publication entitled:

"Akhtar M.A., Zhang S, Shao X, Dang H, Liu Y, Li T, Zhang L, Li C.-Z. Kinetic compensation effects in the chemical reaction-controlled regime and mass transfer-controlled regime during the gasification of biochar in O_2. Fuel Process Technol 2018; 181:25–32. doi:10.1016/j.fuproc.2018.09.009".

The second co-author also contributed to methodology and reviewed the manuscript. The third, fourth and fifth co-authors provided assistance in some experimental investigation and reviewed the manuscript. The sixth and seventh co-authors reviewed the manusoript. The eighth co-author contributed to the paper in terms of conceptualization, methodology, formal analysis of data, review and editing of the manuscript and supervision of the study.

I, as a Co-Author, endorse that this level of contribution by the candidate indicated above is appropriate.

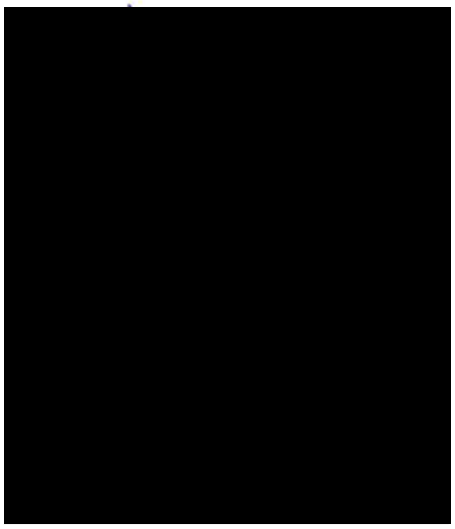

Muhammad Asif Akhtar

Shu Zhang

Xin Shao

Huu Dang

Yurong Liu

Tingting Li

Lei Zhang

Chun-Zhu Li

To Whom It May Concern

I, Muhammad Asif Akhtar, contributed in terms of conceptualization, methodology, experimental investigations, formal analysis of data, writing-original draft and revising to the publication entitled:

"Akhtar M.A., Zhang S, Li C.-Z. Mechanistic insights into the kinetic compensation effects during the gasification of biochar in H_2O. Fuel 2019;255:115839. doi:10.1016/j.fuel.2019.115839".

The second co-author contributed to methodology and reviewed the manuscript. The third co-author contributed to the paper in terms of conceptualization, methodology, formal analysis of data, review and editing of the manuscript and supervision of the study.

I, as a Co-Author, endorse that this level of contribution by the candidate indicated above is appropriate.

Muhammad Asif Akhtar

Shu Zhang

Chun-Zhu Li

To Whom It May Concern

I, Muhammad Asif Akhtar, contributed in terms of conceptualization, methodology, experimental investigations, formal analysis of data, writing-original draft and revising to the publication entitled:

"Akhtar M.A., Li C.-Z. Mechanistic investigation into the kinetic compensation effects during the gasification of biochar: Effects of the partial pressure of H_2O Fuel 2020; 263:116632. https://doi.org/10.1016/j.fuel.2019.116632".

The second co-author contributed to the paper in terms of conceptualization, methodology, formal analysis of data, review and editing of the manuscript and supervision of the study.

I, as a Co-Author, endorse that this level of contribution by the candidate indicated above is appropriate.

Muhammad Asif Akhtar

Chun-Zhu Li

To Whom It May Concern

I, Muhammad Asif Akhtar, contributed in terms of conceptualization, methodology, experimental investigations, formal analysis of data, writing-original draft and revising to the publication entitled:

"Akhtar M.A., Li C.-Z. Some discussions into the reaction mechanisms from the kinetic compensation effects of the gasification of biochar in O_2, H_2O, and their mixtures (plan to submit in Fuel)".

The second co-author contributed to the paper in terms of conceptualization, methodology, formal analysis of data, review and editing of the manuscript and supervision of the study.

I, as a Co-Author, endorse that this level of contribution by the candidate indicated above is appropriate.

Muhammad Asif Akhtar -

Chun-Zhu Li --